universität wien

MASTERARBEIT / MASTER'S THESIS

Titel der Masterarbeit / Title of the Master's Thesis

„Metabolic kinetics of *Alternaria* toxins and potential interspecies differences "

verfasst von / submitted by

Eszter Borsos, B.Sc.

angestrebter akademischer Grad / in partial fulfilment of the requirements for the degree of

Master of Science (MSc)

Wien, 2021 / Vienna, 2021

Studienkennzahl lt. Studienblatt / degree programme code as it appears on the student record sheet:	UA 066 862
Studienrichtung lt. Studienblatt / degree programme as it appears on the student record sheet:	Masterstudium Chemie
Betreut von / Supervisor:	Univ.-Prof. Dr. Doris Marko
Mitbetreut von / Co-Supervisor:	DI Dr. Elisabeth Varga

Acknowledgements

First of all, I would like to thank Univ.-Prof. Dr. Doris Marko for arousing my interest in food toxicology through her exciting and motivating lectures. And more importantly, for allowing me to conduct research and write my master thesis in her working group at the Department of Food Chemistry and Toxicology.

I want to express my special gratitude to Dr. Elisabeth Varga for her competent guidance and supervision. I have learned so much from her about LC-MS measurements, academic writing, teaching activities, laboratory duties, and how to work in a devoted and inspiring way in a research group. She supported me on a professional, organisational, and even on an emotional level. I am grateful to her for appreciating my work and always having an open ear for my scientific opinion.

Additionally, I would like to thank Dr. Georg Aichinger for being practically my second co-supervisor. He provided great support by introducing me to cell culture work and the practice of microsomal incubations. He played an essential role in planning my research project and provided enormous help during data evaluation and interpretation of the acquired quantitative information, for which I am genuinely thankful.

Also, I appreciate the practical help and encouragement I received from my colleagues at the Department of Food Chemistry and Toxicology. In particular, Andrea Betschler and Dino Grgic provided massive assistance in preparing the second biological replicate of porcine liver microsomes. Dr. Julia Beisl and Cornelia Schmutz kindly supported me in maintaining cultured HepG2 cells when I was not allowed to go to the institute because of the Corona pandemic. Moreover, I am thankful to Dr. Francesco Crudo for the microsomal preparation protocol and to the Mass Spectrometry Center at the University of Vienna for the technical support.

Furthermore, I would like to thank my closest friends and boyfriend for always having an open ear and understanding me. Last but not least, a big “köszönöm˝ to my dearest family for giving me emotional and financial support and believing in me throughout my life.

Table of Contents

1. Introduction

Moulds are associated with numerous adverse health effects, such as allergies, fungal infections, and the production of mycotoxins (Borchers *et al*., 2017). As secondary fungal metabolites, mycotoxins can be classified as abiotic hazards deriving from biotic origins (Marin *et al*., 2013). They show an immense structural diversity and are consequently heterogeneous in the modes of affecting animal and human health. However, mycotoxins share the ability to exert their harmful activity on vertebrates even in low concentrations (Taevernier *et al*., 2016).

Species of the genus *Alternaria* occur ubiquitously, infesting various plants, including certain grains, fruits, tomato, sunflower seeds and olives. Since they show high resistance to low temperatures, they might infest foodstuffs even after the harvest – during storage or transport despite cooling (Ostry, 2008). Thus, the mycotoxins produced by *Alternaria* strains can easily enter the food chain either directly through the consumption of contaminated plant products or indirectly from foods originating from exposed animals (Taevernier *et al*., 2016).

The *in vitro* toxicity of the *Alternaria* toxins alternariol (AOH) and alternariol monomethyl ether (AME) is thoroughly studied. They were reported to possess – among others – cytotoxic (Aichinger *et al*., 2017; Bensassi *et al*., 2015; Chiesi *et al*., 2015; Juan-García *et al*., 2015), genotoxic and mutagenic (Brugger *et al*., 2006; Fernández-Blanco *et al*., 2015; Fehr *et al*., 2009; Solhaug *et al*., 2012), immunosuppressive (Grover and Lawrence, 2017; Schmutz *et al*., 2019), as well as hormone-mimicking (Dellafiora *et al*., 2018; Lehmann *et al*., 2016) properties. Although the dietary exposure of AOH and AME frequently exceeds the threshold of toxicological concern, no regulations exist to date for these mycotoxins (EFSA, 2011). Nevertheless, the lack of legally binding guidelines does not indicate the absence of toxicological relevance. In fact, it highlights the urgent need to comprehensively understand the impact of AOH and AME on the human body. In particular, *in vitro*, *in vivo*, and *in silico* toxicokinetic data could contribute to broadening our knowledge about these emerging mycotoxins (Aichinger *et al*., 2021).

2. Theoretical background

2.1. The genus *Alternaria*

Alternaria is a versatile and ubiquitous genus of fungi belonging to the division Ascomycota and family Pleosporaceae (Kustrzeba-Wójcicka *et al.*, 2014). When Nees von Esenbeck firstly described this genus in 1816, he could report only one known species, *A. tenuis* (current term: *A. alternata*). In contrast, according to the currently accepted taxonomic classification, there are more than 250 *Alternaria* species known so far (Pinto and Patriarca, 2017).

These species vary from endophytes through saprophytes to plant or animal pathogens (Freire *et al*., 2017). Their ability to infect various plants – such as cereals, fruit crops and vegetables – in the field or during storage is of particular concern since they cause a reduction of crop yields and consequently economic losses. Moreover, several species can produce mycotoxins, threatening human and animal health when the toxins enter the food or feed chain (Russell *et al*., 2016).

The main similarities among the pathogenic *Alternaria* species are the high resistance to adverse weather, the adaptability in a wide temperature range, and the fact that they produce spores, particularly on necrotic and dead tissue (Rotem, 1994). *A. brassicae* (roses), *A. carotiincultae* (carrots), *A. infectoria* (wheat) and *A. solani* (potatoes and tomatoes) are examples for some host-specific *Alternaria* species (Anuj *et al*., 2013).

A. alternata – which belongs to the most common *Alternaria* species – is classified as a so-called outdoor mould. However, this fungus also appears in buildings lacking sufficient ventilation and is therefore partially responsible for the “sick building syndrome”. Although the preferred temperature for its growth and germination is around 20-21 °C, it survives more extreme temperature conditions, ranging between 2 and 32 °C. This fact leads to the cosmopolitan nature of *A. alternata*: its spores occur not only in tropic and subtropic regions, but even in temperate areas, at least in the warm season (Kustrzeba-Wójcicka *et al*., 2014).

Figure 1: *Alternaria alternata* Scale bar: 10 µm; © Roman Labuda, Ph.D. (roman.labuda@vetmeduni.ac.at)

Due to its melanin content, *A. alternata* forms darkly pigmented, relatively simple, and large conidia (Figure 1). However, the morphology of conidia and spores varies depending on the conditions of growth. After being released from the conidiophore, the spores act as the most important fungal aeroallergens, playing a role in the development and aggravation of asthma (Kustrzeba-Wójcicka *et al*., 2014). Additionally, in immunocompromised patients, *Alternaria* species may cause an infection called alternariosis (Pastor and Guarro, 2008). Besides the listed adverse health effects, these moulds produce a range of mycotoxins. Studies about their occurrence in food and feed are of paramount importance from a toxicological point of view (EFSA, 2016).

2.2. *Alternaria* toxins

2.2.1. Classification

More than 70 secondary metabolites of *Alternaria* species are currently known, mostly acting as phytotoxins. As mentioned, some of them have been reported to potentially cause adverse health effects for humans and animals. These mycotoxins are structurally diverse and were classified by the European Food Safety Authority (EFSA) into five main groups based on their chemical similarities, albeit the last group contains the remaining substances, not belonging to any of the four other classes (EFSA, 2011). Figure 2 summarises this classification and provides examples for each substance group.

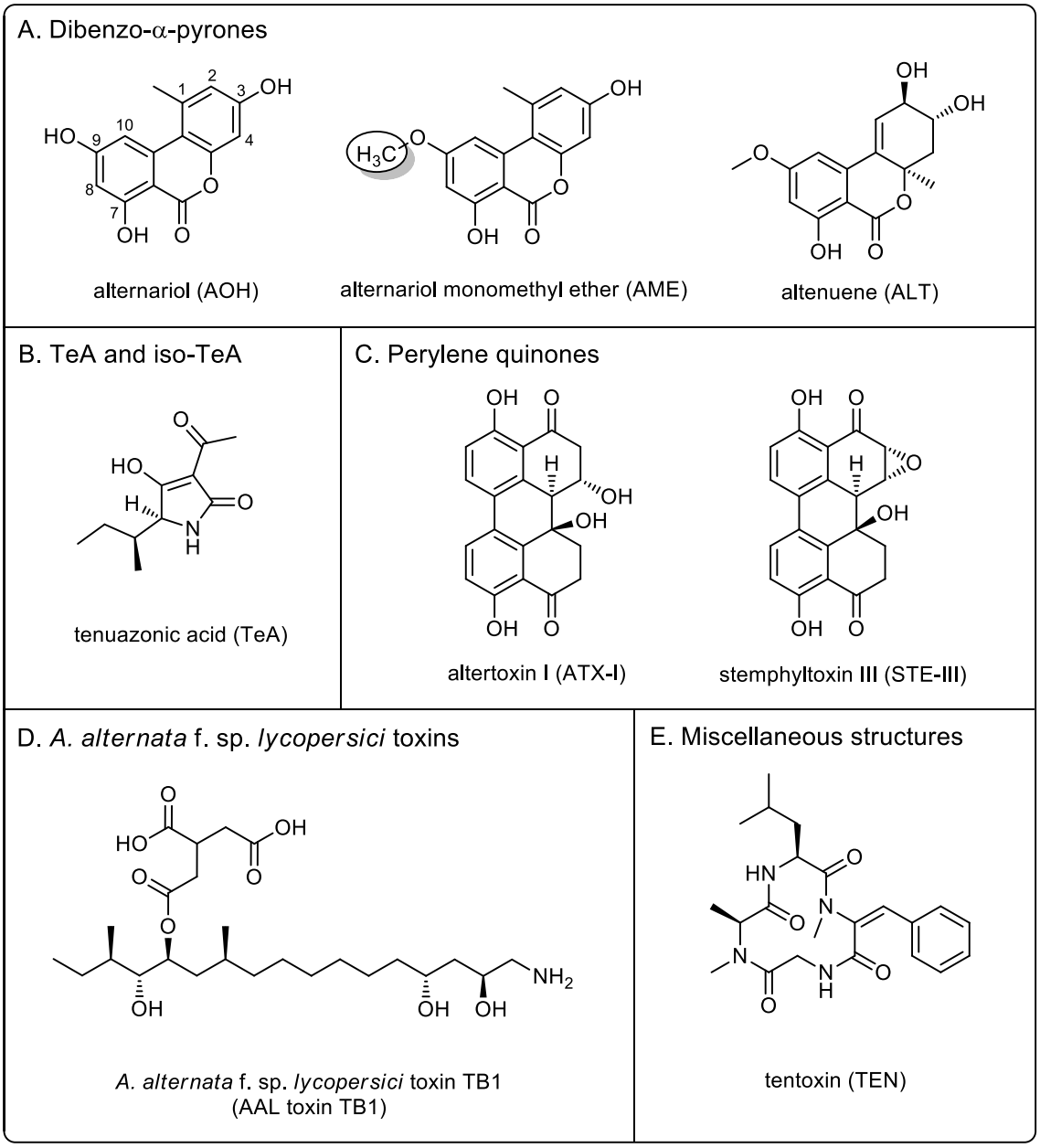

Figure 2: Structural classification of *Alternaria* toxins
Modified from PubChem (https://pubchem.ncbi.nlm.nih.gov), 22.04.2021.

Alternatively, *Alternaria* toxins can be categorised regarding their effect on plants: host-specific and non-host-specific toxins are distinguished. Host-specific toxins (such as AAL toxins, Figure 2/D) target only a narrow range of hosts and are responsible for severe plant diseases, which usually start from triggered cell death. Since their particular selectivity suggests that they might have a lower impact on animal and human health, they are not studied comprehensively in this regard. In contrast, non-host-specific toxins (e.g. alternariol (AOH), alternariol monomethyl ether (AME) or tenuazonic acid) affect a broader range of plant species, but have a milder phytotoxic effect. They are considered as only additional factors and not direct causative agents of plant diseases. Since these toxins can intervene in fundamental cellular processes, they might act noxiously in mammals (EFSA, 2011; Thomma, 2003).

2.2.2. Chemical and physical properties of AOH and AME

AOH and AME differ only in the position 9 with a hydroxy or a methoxy group, respectively (Figure 2/A). They both have a dibenzo-α-pyrone scaffold and belong to the non-host-specific *Alternaria* toxins (EFSA, 2011). By crystallisation from ethanol, AOH and AME form colourless needles, which melt at 350 and 267 °C, respectively (EFSA, 2011). They are soluble in most organic solvents; e.g. 30 mg/mL is the solubility of AOH in dimethyl sulphoxide (Stypuła-Trębas *et al*., 2017).

The presence of three (positions 3, 7, and 9) and two (positions 3 and 7) hydroxy groups in AOH and AME, respectively, suggests that these substances can undergo conjugations (e.g. glucosylation) due to the host plant metabolism, resulting in the so-called “masked mycotoxins” (Berthiller *et al*., 2005). Besides, several other chemical, physical and biological transformations might lead to the formation of “modified” or even “matrix-associated mycotoxins” such as alteration of the structure during food processing or by microorganisms. Such modifications may produce more or less toxic substances compared to their precursors. Furthermore, they might be cleaved in the animal and human gastrointestinal tract, which leads to the regeneration of the original compound, enabling it to exert its adverse health effect. Hence, the detection and quantification of this range of “bound mycotoxins” would be highly desirable (Rychlik *et al*., 2014). However, it represents a significant challenge due to the deficiency of their structural characterisation and lack of standards (EFSA, 2011).

Heat treatment and the change of the pH value are examples of techniques, which may be applied throughout food processing. Modelling these processes, Siegel *et al.* (2010) found AOH and AME to be stable under realistic wet baking conditions. However, during dry baking, degradation was discernible, where AME showed higher stability than AOH. Refluxing the toxins in 0.15 M phosphate buffer (pH 5) for five hours, their structure remained unchanged. In contrast, due to similar treatment with 0.1 M KOH solution and 0.18 M phosphate/citrate buffer (pH 7), degradation products occurred.

2.2.3. Occurrence and exposure assessment of AOH and AME

Due to the omnipresent manner of *Alternaria* moulds and the fact that AOH and AME are non-host-specific toxins, they occur in a wide variety of food samples. Also, the co-occurrence with mycotoxins from other mould strains is no rarity (EFSA, 2011). The “Dietary exposure assessment to *Alternaria* toxins in the European population” is a scientific report of EFSA based on 15,563 analytical results of 4,168 samples

(EFSA, 2016). In this work, the highest mean AOH content was detected in grains, particularly buckwheat and oats, whereas the highest mean AME levels were shown in chestnuts and sesame seeds. These concentration values varied between 10 and 40 µg/kg. Toddlers and other children were reported to be exposed to the greatest extent to AOH and AME per body weight per day. While fruits and fruit products contribute predominantly to the AOH dietary exposure, vegetable oil and pome fruits are the main contributors in case of AME. Overall, the threshold of toxicological concern (TTC value: 2.5 ng/kg body weight per day) was exceeded by the estimated mean chronic dietary exposures at the upper bound and 95th percentile dietary exposures. Consequently, AOH and AME are of great interest from a toxicological perspective (EFSA, 2016).

Another way of estimating human exposure towards mycotoxins is the so-called human biomonitoring (HBM) approach. For this purpose, biomarkers (such as parent mycotoxins, their phase I and II metabolites, DNA or protein adducts) are quantified in human body fluids (Al-Jaal *et al*., 2019; Habschied *et al*., 2021). With this method, not only dietary, but also environmental and occupational exposure can be evaluated (Habschied *et al*., 2021). Martins *et al.* (2019) measured 24 h urine and first-morning urine paired samples from 94 Portuguese participants with this approach. They quantified AOH for the first time in urine samples originating from Europe, whereas AME could not be detected. Of the 24 h urine samples 29 % contained AOH in a detectable amount, with a maximum of 24.6 µg/L. In 13 % of the first-morning urine samples this toxin was quantified and the maximum value was 9.91 µg/L AOH. Braun *et al.* (2020b) reported a longitudinal investigation of 29 mycotoxins and metabolites in breast milk. After the analysis of 87 samples – provided by one volunteer – AME could be quantified in 90 % of the samples, with a concentration mostly below 10 ng/L. This finding should not discourage mothers from breastfeeding but indicates the urgent need for more toxicological and exposure data on this topic.

2.2.4. Bioavailability and metabolism of AOH and AME

Already in 1982, Pollock *et al.* reported that AME – at least in a very lipophilic matrix (olive oil) – was poorly absorbed in the gastrointestinal tract of three Sprague-Dawley rats since faecal excretion exceeded 81-87 % within three days. Besides, 5-9 % of the dose was found in the urine as unknown polar metabolites using ^{14}C tracking (Pollock *et al*., 1982). Puntscher *et al*. (2019) confirmed this finding more recently by feeding 14 rats of the same outbred model with sunflower oil containing an *Alternaria* culture extract (50 mg/kg body weight). The detected faecal excretion was above 89 % for AOH and AME after 24 hours. Less than 2.8 % of the original toxin concentration was recovered *via* the urine. Furthermore, 4-hydroxy and 3-*O*-sulphate metabolites of these mycotoxins were detected partially in urine, faeces, and blood samples. In addition to the substances described in this study, several other metabolites of AOH and AME have been reported in the literature. Table 1 and Table **2** summarise the most important ones for AOH and AME, respectively.

Table 1: Phase I and II metabolites of alternariol

Abbreviation	Name and sum formula	*In vitro* or *in vivo* model	Detection	Reference
2-OH-AOH	2-hydroxy-alternariol $C_{14}H_{10}O_6$	rat, porcine and human liver microsomes with NADPH	HPLC-DAD, GC-MS/MS	Pfeiffer *et al*., 2007b
		male and female NMRI mice[1)]	GC-MS and LC-MS/MS of blood and urine samples	Schuchardt *et al*., 2014
4-OH-AOH	4-hydroxy-alternariol $C_{14}H_{10}O_6$	rat, porcine and human liver microsomes with NADPH	HPLC-DAD, GC-MS/MS	Pfeiffer *et al*., 2007b
		male and female NMRI mice	GC-MS and LC-MS/MS of blood and urine samples	Schuchardt *et al*., 2014
		male Sprague Dawley rats	LC-MS/MS of faeces samples	Puntscher *et al*., 2019
8-OH-AOH	8-hydroxy-alternariol $C_{14}H_{10}O_6$	rat, porcine and human liver microsomes with NADPH	HPLC-DAD, GC-MS/MS	Pfeiffer *et al*., 2007b
		male and female NMRI mice	GC-MS and LC-MS/MS of urine samples	Schuchardt *et al*., 2014
10-OH-AOH	10-hydroxy-alternariol $C_{14}H_{10}O_6$	rat, porcine and human liver microsomes with NADPH	HPLC-DAD, GC-MS/MS	Pfeiffer *et al*., 2007b
		male and female NMRI mice	GC-MS and LC-MS/MS of blood and urine samples	Schuchardt *et al*., 2014
Me-OH-AOH	methyl-hydroxy-alternariol $C_{14}H_{10}O_6$	rat, porcine and human liver microsomes with NADPH	HPLC-DAD, GC-MS/MS	Pfeiffer *et al*., 2007b
AOH-3-GlcA	alternariol-3-*O*-glucuronide $C_{20}H_{19}O_{12}$	Caco-2 cell line	LC-DAD-MS, HPLC-UV	Burkhardt *et al*., 2009
		Hepatic and intestinal microsomes of humans, pigs and rats with UDPGA	LC-MS, GC-MS	Pfeiffer *et al*., 2009
AOH-9-GlcA	alternariol-9-*O*-glucuronide $C_{20}H_{19}O_{12}$	Caco-2 cell line	LC-DAD-MS, HPLC-UV	Burkhardt *et al*., 2009
		Hepatic and intestinal microsomes of humans, pigs and rats with UDPGA	LC-MS, GC-MS	Pfeiffer *et al*., 2009
AOH-3-S	alternariol-3-*O*-sulphate $C_{14}H_{10}O_8S$	Caco-2 cell line	LC-DAD-MS, HPLC-UV	Burkhardt *et al*., 2009
		male Sprague Dawley rats	LC-MS/MS of urine samples	Puntscher *et al*., 2019
AOH-GSH	glutathione conjugate of AOH ($C_{24}H_{25}O_{10}N_3S$) and proposed degradation products	HepG2 cell line	LC-MS/MS	Juan-García *et al*., 2015

1) An outbred mouse model. Its name derives from the Naval Medical Research Institute (Traub, 1975)

Table 2: Phase I and II metabolites of alternariol monomethyl ether

Abbreviation	Name and sum formula	*In vitro* or *in vivo* model	Detection	Reference
AOH	alternariol $C_{14}H_{10}O_5$	rat liver post-mitochondrial supernatant with NADPH[1)]	TLC-autoradiography	Pollock *et al*,1982
		adult male Sprague-Dawley rats	TLC-autoradiography of urine and faeces samples, and tissue residues	
		homogenised liver samples of gilts with NADPH	TLC (UV) and HPLC-UV (determination of AME recovery)	Olsen and Visconti, 1988
		rat, porcine and human liver microsomes with NADPH	HPLC-DAD, GC-MS/MS	Pfeiffer et al., 2007b
4-OH-AME	2-hydroxy-alternariol monomethyl ether $C_{15}H_{12}O_6$	rat, porcine and human liver microsomes with NADPH	HPLC-DAD, GC-MS/MS	Pfeiffer *et al*., 2007b
4-OH-AME	4-hydroxy-alternariol monomethyl ether $C_{15}H_{12}O_6$			
8-OH-AME	8-hydroxy-alternariol monomethyl ether $C_{15}H_{12}O_6$			
10-OH-AME	10-hydroxy-alternariol monomethyl ether $C_{15}H_{12}O_6$			
Me-OH-AME	methyl-hydroxy-alternariol monomethyl ether $C_{15}H_{12}O_6$			
$(OH)_2$-AME	dihydroxy-alternariol monomethyl ether $C_{15}H_{12}O_7$	rat liver microsomes with NADPH	HPLC-DAD, GC-MS/MS	Pfeiffer *et al*., 2007b
AME-x-GlcA	glucuronides in general $C_{21}H_{21}O_{12}$	homogenised liver and intestinal samples of gilts with UDPGA	TLC (UV) and HPLC-UV (determination of AME recovery)	Olsen and Visconti, 1988
AME-3-GlcA	alternariol monomethyl ether-3-*O*-glucuronide $C_{21}H_{21}O_{12}$	Caco-2 cell line	LC-DAD-MS, HPLC-UV	Burkhardt *et al*., 2009
		Hepatic and intestinal microsomes of humans, pigs and rats with UDPGA	LC-MS, GC-MS	Pfeiffer *et al*., 2009
AME-7-GlcA	alternariol monomethyl ether-7-*O*-glucuronide (small amount) $C_{21}H_{21}O_{12}$	Caco-2 cell line	LC-DAD-MS, HPLC-UV	Burkhardt *et al*., 2009
		Liver and intestinal microsomes of humans, pigs and rats with UDPGA	LC-MS, GC-MS	Pfeiffer *et al*., 2009
AME-3-S	alternariol monomethyl ether-3-*O*-sulphate $C_{15}H_{12}O_8S$	Caco-2 cell line	LC-DAD-MS, HPLC-UV	Burkhardt *et al*., 2009
		male Sprague Dawley rats	LC-MS/MS of blood and urine samples	Puntscher *et al*., 2019

1) Obtained after centrifugation at 10,000 *g*, but otherwise similar to S9-mix (centrifugation at 9,000 *g*).

As Table 1 suggests, the phase I metabolism of AOH leads to the hydroxylation in one of the unsubstituted aromatic positions (position 2, 4, 8 or 10) or the carbon atom of the methyl group in the 1st position. The oxidative metabolism of AME shows a similar pattern, although in this case, the detection of a dihydroxy product was also described by incubation with rat liver microsomes (Pfeiffer *et al*., 2007b). Additionally, the demethylation of AME – resulting in the formation of AOH – could be observed (Table 2). Since all four hydroxylated metabolites of both toxins include catechol or hydroquinone moieties, they may undergo redox cycling or be transformed into reactive semiquinones and hydroquinones. Therefore, the inactivation of these compounds by conjugation reactions is toxicologically relevant (Pfeiffer *et al*., 2007b).

The conjugation of AOH and AME with glucuronic acid was described after 2 hours of incubation in differentiated Caco-2 cells (immortalised human colorectal adenocarcinoma cell line). AOH was glucuronidated at the hydroxy groups in position 3 and 9, while AME was mainly conjugated at position 3-*O*, but to a small extent also at position 7-*O* (Burkhardt *et al*., 2009). This finding was in line with the conjugation pattern observed in intestinal and hepatic microsomes of humans, pigs, and rats, fortified with uridine-diphosphate-glucuronic acid (UDPGA); where the incubation times varied up to 2 hours. However, alternariol monomethyl ether-7-*O*-glucuronide could not be detected in human hepatic or porcine microsomes (Pfeiffer *et al*., 2009).

The formation of the 3-*O*-sulphate of AOH and AME was also observed in differentiated Caco-2 cells after incubation with the respective parent toxins (Burkhardt *et al*., 2009). With a targeted LC-MS/MS method, the same metabolites were quantified in one or both urine and faecal samples of Sprague Dawley rats after the consumption of *Alternaria* culture extract in a sunflower oil matrix (Puntscher *et al*., 2019). Only the hydroxy group in position 3 of AOH and AME was not known to be sulphated in these model systems. In contrast, also AOH-7-*O*-sulphate, AOH-9-*O*-sulphate, and AME-7-*O*-sulphate were generated in rat liver cytosol from AOH and AME in the presence of 3′-phosphoadenosine-5′-phosphosulphate (Burkhardt *et al*., 2009).

Juan-García *et al.* (2015) detected the generated AOH metabolites after 24, 48, and 72 hours of exposure in HepG2 cells. The glutathione conjugate of AOH occurred most abundantly. This result is partly in line with the finding regarding the gene expression of HepG2, as a higher mRNA level of *GSTA4* was present in HepG2 cells than in human primary hepatocytes (Hessel-Pras *et al*., 2019; Juan-García *et al*., 2015). However, sulphation products might also be expected based on the current knowledge about the HepG2 cell line (Hessel-Pras *et al*., 2019; Wilkening *et al*., 2003). Thus, more data would be necessary to identify the metabolism products of AOH in HepG2 cells.

The scientific interest has recently shifted towards the formation of di-conjugates, a novel type of mycotoxin metabolites. To the best of my knowledge, no such AOH or AME conjugates have been identified in animal or human model systems so far. However, the formation of sulpho-glucosides in *A. alternata*-inoculated tomato is known. Soukup *et al*. (2016) observed that the parent toxin AME can be sulphated at position 3-*O*, and AOH additionally at the position 9-*O* (Figure 2/A) by the fungus itself. The subsequent glucosylation of the sulphates is carried out by the tomato

tissue during its detoxification processes. Hence the possibility that di-conjugates (such as bi-sulphates or sulpho-glucuronides) occur in the human phase II metabolism – either by consuming foodstuffs contaminated by the parent toxins or their sulphates – should be considered (Puntscher *et al*., 2020).

2.2.5. Toxicity of AOH and AME

Numerous *in vitro* studies were carried out to investigate the cytotoxicity of AOH and AME. Alternariol showed cytotoxic effects in the human hepatoma cell line HepG2, with a half-maximal inhibitory concentration (IC_{50}) varying between 65-96 µM AOH depending on whether the incubation lasted for 24, 48, or 72 hours (Juan-García *et al*., 2015). Similarly, moderate dose-dependent cytotoxicity could be observed in human intestinal cells (HCT 116) after 24 hours of incubation, where the IC_{50} value exceeded 65 µM (Bensassi *et al*., 2015). In contrast, no IC_{50} could be reached, but the induction of cell mortality was reported in Caco-2 cells after incubation with 75 and 100 µM AOH for 24 and 48 hours; as well as in the human colon carcinoma cell line HT-29 after 24 h incubation with at 25-100 µM AOH (Aichinger *et al*., 2017; Chiesi *et al*., 2015).

Unlike AOH, AME only exerted weak cytotoxicity in HCT 116 cells, having an IC_{50} value of 120 µM (Bensassi *et al*., 2015). More importantly, Bensassi and co-workers tested the combinatory effect of these two *Alternaria* toxins, as well. Treating the cells with both 25 µM AOH and AME for at least 24 hours, additive cytotoxicity could be observed. The study concluded that AOH and AME induce apoptosis involving the mitochondrial intrinsic pathway and stimulate the generation of mitochondrial superoxide anion in an additive manner.

Whether the metabolic transformation affects the cytotoxicity of AOH and AME was investigated in a comparative study of two hepatic cell models with different metabolic capacities. In HepG2 cells, AME showed a significant decrease in the cell viability even at the incubation concentration of 10 µM after 24 hours. In contrast to this, in the human hepatoma cell line, HepaRG – which is known to show higher metabolic activity – no significant change of the cell viability could be detected. The incubation with 100 µM AOH exerted cytotoxic effects in both cell lines, however, to a smaller extent in case of HepaRG cells. This observation proves the importance of detoxification processes in cytotoxicity (Hessel-Pras *et al*., 2019).

The mutagenic and genotoxic effects of alternariol and its monomethyl ether have been shown in several *in vitro* studies. Already 10 µM AOH induced mutations after 24 hours of incubation in cultured Chinese hamster V79 and mouse lymphoma cells in a concentration-dependent manner (Brugger *et al*., 2006). Similarly, the exposure of the murine macrophage cell line RAW 264.7 to 30 µM AOH for both 2 and 24 hours caused DNA damage, as well as the incubation of Caco-2 cells with 15-60 µM AOH for 24 hours (Fernández-Blanco *et al*., 2015; Solhaug *et al*., 2012). AOH and AME increased the rate of DNA strand breaks in human colon carcinoma (HT-29) and vulva carcinoma (A431) cells after 1-hour incubation in a concentration of ≥1 µM (Fehr *et al*., 2009).

A review of Solhaug *et al.* (2016) addresses the mechanistic background of the AOH-induced genotoxicity. It suggests that two significant pathways contribute to this effect: the interaction with DNA topoisomerase and the induction of reactive oxygen species (ROS) production. AOH acts as a topoisomerase poison, which leads to the

generation of DNA double-strand breaks. In case of murine macrophages, a consequent cell-cycle arrest, morphological changes, autophagy, and senescence could be observed. On the other hand, during the phase I metabolism of AOH, reactive catechols and hydroquinone can be obtained, as described in section 2.2.4. These may lead to the formation of ROS, causing oxidative base damage, apurinic/apyrimidinic sites, and single-strand breaks associated with DNA repair (Solhaug *et al*., 2016). In contrast to this conclusion, some studies suggested that AOH and AME modulate the redox balance of human colon carcinoma cells, but this fact does not play a predominant role in their DNA damaging properties (Tiessen *et al*., 2013). Hence the mode of action of the genotoxicity of AOH and AME should be further examined and potential species differences in this regard should be considered (Tiessen *et al*., 2017).

As the hydroxylated forms of AOH and AME include catechol moiety and may therefore induce ROS production, their genotoxicity and ability to cause oxidative stress was investigated in human oesophageal cells KYSE510 (Tiessen *et al*., 2017). Although the treatment with 4-OH-AOH leads to a fourfold increase of ROS formation, no DNA strand breaks could be observed. The 4-hydroxylated metabolite of AME did not induce the generation of ROS in contrast to the native toxin. A possible explanation of the decrease or lack of (oxidative) DNA-damaging properties of these metabolites compared to the parent molecules could be their poor cellular uptake (Tiessen *et al*., 2017).

To what extent the phase II metabolism affects the DNA damaging ability of AOH and AME was determined in the mammalian cell lines HepG2 and HT-29 (Pfeiffer *et al*., 2007a). The 1-hour incubation of these cells with AOH resulted in concentration-dependent genotoxicity. Analogously, its monomethyl ether elicited similar effects with comparable DNA damaging potency. By longer incubation times (24 hours), a significant induction of the DNA damage could be observed only in HepG2, but not in HT-29 cells. Since remaining unconjugated AOH and AME were absent in HT-29 medium, whereas ca. 75 % of the parent compounds were still detectable in the case of HepG2 cells, a correlation between the metabolism grade and the DNA damaging pattern is reasonable to conclude. Consequently, phase II detoxification seems to abolish the genotoxic activity of these mycotoxins (Pfeiffer *et al*., 2007a).

Although the adverse effects of AOH and AME should not be underestimated, a study carried out in HT-29 cells concluded that these toxins – despite their high occurrence – are not the main contributors to the genotoxicity of complex *A. alternata* extracts (Schwarz *et al*., 2012). Furthermore, AOH appeared to be non-mutagenic in immature bone marrow erythrocytes of male NMRI mice, and no systemic genotoxicity could be observed in the liver tissue of AOH-exposed NMRI mice (Schuchardt *et al*., 2014). The limited bioavailability of AOH, the effective metabolic transformation into non-genotoxic AOH-derivatives, or the actual lack of genotoxicity in systemic tissues might be possible explanations to the apparent contradiction between the *in vitro* and *in vivo* findings. However, further investigations concerning the local genotoxicity of AOH in the gastrointestinal tract and more *in vitro* studies in the presence of a metabolising system may allow a broader view on this topic (Schuchardt *et al*., 2014). Due to the limited amount of available toxicological data, the EFSA Panel on Contaminants in the Food Chain (CONTAM) used the TTC approach to estimate the relative level of concern of the *Alternaria* mycotoxins for human health. The assumed genotoxic properties of AOH and AME led to much

lower TTC values for these toxins than in the case of non-genotoxic *Alternaria* toxins (EFSA, 2016; see also section 2.2.3).

To the complex pattern of physiological alterations caused by AOH and AME belongs immunomodulation, as well. In the human bronchial epithelial cell line BEAS-2B and mouse macrophage cell line RAW 264.7, dose-dependent suppression of the lipopolysaccharide-induced innate immune responses was reported. AOH elicited this effect more potently than AME (Grover and Lawrence, 2017). By investigating the mode of action of the immunosuppressive properties of AOH in THP-1 derived human macrophages, the involvement of the nuclear factor κ B pathway was found with downregulation of pro-inflammatory cytokines and altered microRNA expression. However, relatively high AOH concentrations of 2 and 20 µM exerted these effects, being therefore probably not realistic in physiological conditions (Kollarova *et al*., 2018). Hence the impact of AOH on differentiated Caco-2 cells has been studied as intestinal epithelial cells are particularly exposed to higher amounts of toxins. Immunosuppressive activity of AOH could be demonstrated in an inflamed environment also in these non-immune cells (Schmutz *et al*., 2019).

Furthermore, AOH and AME possess the ability to act as xenoestrogens. Under cell-free conditions, AOH could bind to both human recombinant oestrogen receptors (ER) α and β. However, its affinity to ERα was 10,000-fold and to ERβ 2500-fold lower compared to 17β-estradiol. Additionally, in the human endometrial adenocarcinoma cell line Ishikawa, a pure ER agonistic effect could be detected with the alkaline phosphatase activity assay (Lehmann *et al*., 2006). In a comparable testing system, AME elicited oestrogenic activity, as well, and its interaction with ERs was even more favourable than this of AOH (Dellafiora *et al*., 2018).

Dellafiora *et al.* (2018) also conducted an *in silico*/*in vitro* study to evaluate the oestrogenic potential of the detoxification products of AOH and AME. The 4-hydroxylated metabolites of the parent mycotoxins could not directly bind to the ERs; however, they showed estrogenicity. A possible explanation might be that the further methylation of these substances led to the observed oestrogenic stimulus due to enhanced interaction with the ERs. In contrast, the sulphation and glucuronidation of AOH and AME reduced their oestrogenic properties (Dellafiora *et al*., 2018). This finding is in line with previous results regarding the detoxifying effects of phase II metabolism in the case of AOH and AME (Pfeiffer *et al*., 2007a).

Although for the impact on the endocrine system relatively high concentrations of AOH and AME are necessary, much lower amounts are sufficient to synergistically enhance the activity of other fungal xenoestrogens, such as zearalenone and α-zearalenol (Vejdovszky *et al*., 2017). Moreover, apart from the interaction with ERs, in the yeast reporter androgen bioassay, AOH also induced an androgen response. Its androgenic potency was 0.046 % relative to testosterone (Stypuła-Trębas *et al*., 2017).

Taken together, AOH and AME are of toxicological concern due to their cytotoxic, genotoxic, and oestrogenic properties, based on *in vitro* and *in vivo* findings, even though there are some contradictions in different model systems. Thus, more research projects should address the extent and mechanism of action of the toxicity of these emerging mycotoxins. Nevertheless, even in a scientific consensus, the impact of toxins on health can be affected by various factors. Bodyweight, species, physiological state, and age of the exposed individual, as well as the dose,

co-occurrence with other (myco)toxins, and exposure time are examples of factors playing a role in the final toxicological outcome (Hussein and Brasel, 2001; Richard, 2007).

2.3. *In vitro* models

2.3.1. General introduction

The human liver plays a pivotal role in the metabolism of drugs or other xenobiotics. Therefore, finding an appropriate liver model for each particular research interest is essential and may provide a first insight into the fate of the substance of question in the human body. As Asha and Vidyavathi suggest, perfused liver, liver slices, primary hepatocytes, cytosol, S9 fractions, supersomes, cell lines, transgenic cell lines, and microsomes represent the most widespread *in vitro* models of the liver (Asha and Vidyavathi, 2010).

2.3.2. HepG2 cells

The HepG2 cell line derives from a liver tumour of a 15-year-old Caucasian male from Argentina. Aden and colleagues established this cell line in 1979 and classified the tumour of origin as a well-differentiated hepatocellular carcinoma (Aden *et al*., 1979). Therefore, the scientific literature usually refers to HepG2 as an immortalised human hepatocarcinoma cell line. However, histologic and biologic evidence suggested that in contrast to the common belief, HepG2 originated as a hepatoblastoma (López-Terrada *et al*., 2009).

Regardless of the histologic type, HepG2 represents a well-established tool for the experimental investigation of hepatotoxicity and human biotransformation. A review of cell-based models for liver toxicity highlights that HepG2 has a high reproducibility and proliferation rate, as well as an unlimited life span (Gómez-Lechón *et al*., 2014). Moreover, it provides easy handling, and standardised culture protocols are accessible for this cell line. Due to these benefits, HepG2 is often the *in vitro* model of choice instead of the primary hepatocytes or even the hepatoma cell line HepaRG (Gómez-Lechón *et al*., 2014).

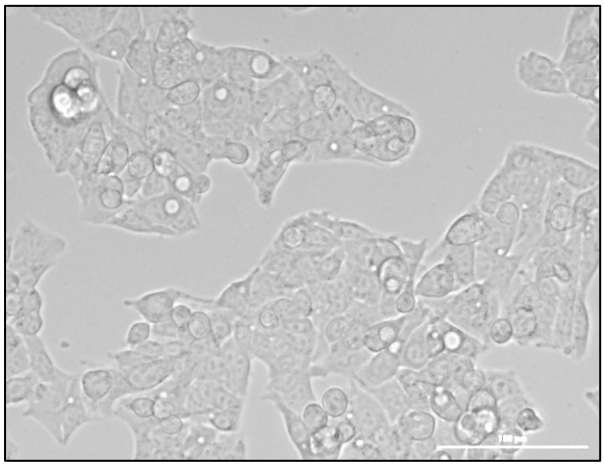

Figure 3: HepG2 cells after 24 hours of incubation subsequent to passaging
Scale bar: 100 µm
© Francesco Crudo, Ph.D. and Chenyifan Hong

Nevertheless, HepG2 also has limitations, especially in terms of biotransformation properties. Wilkening *et al.* (2003) reported low activity and expression of phase I enzymes in this cell line. Furthermore, no mRNA of *CYP3A4* – the most abundant P450 isozyme and the most important in drug metabolism – could be detected in HepG2 cells. In contrast, phase II enzymes were present, especially sulphotransferases and NAD(P)H dehydrogenases of quinone substrates. As phase I metabolism often activates and phase II transformations usually detoxify (food) mutagens, false-negative responses cannot be excluded in genotoxicity studies carried out in HepG2 cells. Also, this cell line seems not to be

optimal to model the general biotransformation in the human liver. However, HepG2 could be a suitable model system to study the regulation of drug-metabolising enzymes or to investigate specifically the phase II reactions, particularly the sulphate conjugation of phenolic compounds (Shwed *et al*., 1992; Wilkening *et al*., 2003). If necessary, an external metabolising system, such as S9 liver homogenate, could amend the insufficient P450 activity (Hessel-Pras *et al*., 2019). The so-called ADV-HepG2 cells could be a beneficial alternative for HepG2. They are an upgraded version of the original cell line created *via* adenoviral transfection. These cells can express the five most relevant phase I enzymes and are therefore more suitable to model human biotransformation (Tolosa *et al*., 2013).

Various publications include assays in HepG2 cells investigating the toxicity and metabolism of AOH and AME. In some studies, the HepG2 cell line represents a possible model for human xenobiotic metabolism. Thus, the time-dependency of cytotoxicity within the same model system demonstrates the impact of biotransformation (Juan-García *et al*., 2015 and 2016). Juan-Garcia *et al.* (2015) found AOH to be cytotoxic in this cell line. Since metabolic activation is not essential for AOH to reduce cell viability, HepG2 may be considered suitable for this approach. The same research group conducted a study addressing the combinatory effects of alternariol with *Fusarium* toxins since the co-occurrence of them is no rarity. The cell line of choice was again HepG2 (Juan-García *et al*., 2016).

In contrast, there is an entirely different approach that labels HepG2 as a cell line with limited metabolic competencies. Therefore, comparison with metabolically more capable cells enables the exploration of the role of metabolic (in)activation in toxicity. Suitable for such investigations might be the human hepatoma cell line HepaRG or the human colon cell line HT-29 (Hessel-Pras *et al*., 2019; Pfeiffer *et al*., 2007a; for the results of these studies, please see section 2.2.5).

An alternative assay setup taking advantage of the insufficient metabolic activity of HepG2 is adding an external metabolising system and monitoring the resulting alteration of toxic effects. Hessel-Pras *et al.* (2019) indirectly detected the DNA damaging properties of AOH and AME in HepG2 cells. When S9 liver homogenate was present in the incubation solution, detoxification took place, resulting in a decrease of the initial DNA damaging effects.

2.3.3. Liver microsomes

The liver microsomal fraction was described already in the 1940s as a component of the liver suspension, which contains “particulate elements of submicroscopic size, but sedimentable under centrifugation at relatively high speed” (Claude, 1946). It is prepared by the homogenisation of the tissue and the subsequent differential centrifugation (Figure 4; Claude, 1946). Since microsomes contain several metabolising enzymes, such as cytochromes P450 (CYP450s) and uridine di-phospho-glucuronosyl transferases (UGT), they are widely applied to assess phase I oxidation or glucuronidation of different xenobiotics. However, in contrast to cell culture model systems, in microsomal incubation tests, the addition of co-factors or their precursors (f. e. NADPH or UDPGA) is essential to initiate the desired enzyme reactions (Asha and Vidyavathi, 2010).

The review of Asha and Vidyavathi labels human liver microsomes (HLM) as the most popular *in vitro* model system. Plausible reasons might be the relatively low

cost, easy usage, and the possibility to preserve their enzyme activity for a long time. If the research question requires, the activity of microsomes deriving from single individuals can be compared. Otherwise, the application of pooled microsomes allows overcoming intra-species variations. Still, the suitability of HLM to represent a qualitative and quantitative model for human biotransformation is somewhat restricted. Lacking cytosolic co-factors and some phase II metabolising enzymes (such as glutathione S-transferases, N-acetyl transferases, or sulphotransferases) cause a different qualitative pattern of the metabolites than in intact hepatic cells. Also, the competitive reactions taking place in the liver cannot be accurately modelled because of the discrepancy in enzyme composition. Notwithstanding the listed limitations, HLM are considered a valuable tool for drug development and enzyme kinetic studies of xenobiotics (Asha and Vidyavathi, 2010). Consequently, the comparison of the results obtained in different *in vitro* models might allow a more profound understanding of the human metabolism of food toxins despite the limited manner of all model systems.

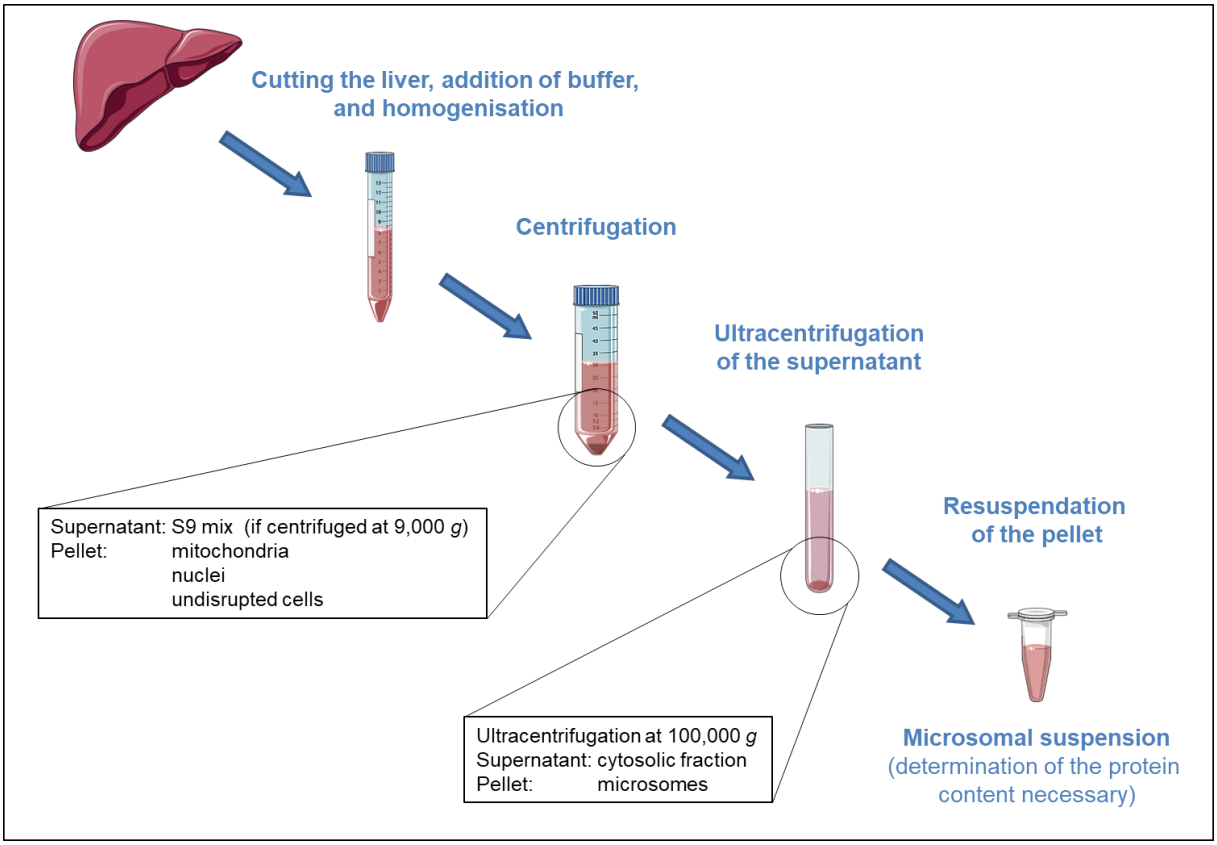

Figure 4: Preparation of the microsomal suspension Captions based on the review of Asha and Vidyavathi, 2010. Illustrations from https://smart.servier.com, accessed online 27/5/2021.

Pfeiffer and co-workers conducted extensive research concerning the biotransformation of AOH and AME in liver microsomes (Pfeiffer *et al*., 2007b, 2008 and 2009). By investigating the phase I metabolism of AME, they detected 2-, 4-, 8- and 10-hydroxy-AME, as well as AOH after incubation with rat, pig, and human liver microsomes (Pfeiffer *et al*., 2007b). The interspecies differences regarding the hydroxylation pattern were also described. The major oxidative metabolite in rat and pig microsomal incubations was 8-hydroxy-AME, whereas 2-hydroxy-AME was the most abundant when incubating with HLM. While carrying out the analogous assay with AOH, 2-, 4-, 8- and 10-hydroxy-AOH could be found in all three species. Rat

liver microsomes generated 10-hydroxy-AOH to the greatest extent, which occurred only in traces after the incubation with HLM. By treating pig hepatic microsomes with AOH, both 2- and 4-hydroxy-AOH appeared in a comparable amount. In human liver microsomes, 2-OH-AOH was formed the most abundantly (Pfeiffer *et al*., 2007b, see also section 2.2.4). The hydroxylation pattern of AOH and AME in HLM was in line with the findings of Simon and colleagues, as well as with the observed activities of human recombinant cytochrome P450 isoforms (Pfeiffer *et al*., 2008; Simon *et al*., 2016). Although this work provided valuable information, the incubations were carried out only with one concentration of each mycotoxin (50 µM) and an incubation time of 40 minutes was chosen. Hence kinetic data about the phase I metabolism of AOH and AME in HLM is still scarce.

In another approach, the extent and position of the glucuronidation of AOH and AME were explored (Pfeiffer *et al*., 2009). The assays were carried out with intestinal and hepatic microsomes of Wistar and Sprague-Dawley rats, pigs, and human donors. The incubation with human microsomes caused the formation of the 3-*O*-glucuronide for both AOH and AME. Interestingly, the species and even the gender of the donor seemed to play a role in the qualitative and quantitative composition of the final product mixture. Moreover, the activity of human UDP-glucuronosyltransferase isoforms suggested a high glucuronidation grade for both toxins (Pfeiffer *et al*., 2009).

2.4. Physiologically-based toxicokinetic modelling (PBTK modelling)

Physiologically-based pharmacokinetic or toxicokinetic models are mathematical simulations aiming to predict the kinetic behaviour of an exogenous compound in an organism of interest. The field of application covers drug development, support of the design of *in vivo* studies, as well as the help for the interpretation of *in vitro* results (d'Yvoire *et al*., 2007). PBTK models are also valuable tools for the risk assessment of toxic compounds as they allow estimating the concentration of a substance in different organs after external exposure (DeWoskin, 2007). This quantitative information is more related to the actual toxic effect in the target organ than exposure data (Krishnan and Peyret, 2009).

The development of a PBTK model relies on a typical workflow. The complex biological system can be simplified by division into so-called compartments, representing tissues and organs linked through the blood flow. A set of mass-balance differential equations expresses the absorption, distribution, metabolism, and excretion of the compound in each relevant compartment (Krishnan and Peyret, 2009). These equations include anatomical parameters of the model species (e.g. tissue volume, enzyme abundance) and substance-specific parameters (e.g. molecular weight, tissue-to-plasma distribution coefficient). They represent available *in vitro* and *in silico* data or known physicochemical properties. Consequently, PBTK models do not rely on *in vivo* experiments and can therefore contribute to the desired elimination of mammalian testing by 2035 (Grimm, 2019). In the last step, suitable modelling software can solve the differential equations leading to the concentration of the compound of interest in each compartment (Krishnan and Peyret, 2009; Zhuang and Lu, 2016).

The development and validation of the first PBTK model for a particular species can be labour-intensive and time-consuming (Schneckener *et al*., 2020). However, if a PBTK model is validated for a species and compound, it can be easily adjusted to

other chemical substances. As available models for various mammals (human, rat, mouse, etc.) already exist, toxicokinetic modelling in these organisms is less strenuous (Schneckener *et al*., 2020). Another facilitation of the method is that the necessary physiological and anatomical parameters are often already incorporated in the modelling software (Zhuang and Lu, 2016). But, due to the high amount of input data, these model systems always carry uncertainty, so the importance of a reliable dataset is especially pronounced (d'Yvoire *et al*., 2007).

No PBTK models have been published to describe the toxicokinetics of AOH and AME. However, such studies on other mycotoxins (e. g. zearalenone and its metabolites) have already been conducted. They enable estimating the adverse health effects over an extended period in humans and determining possibly vulnerable populations towards this fungal metabolite (Mukherjee *et al*., 2014; Shin *et al*., 2009). Therefore, a similar approach addressing the PBTK modelling of AOH and AME might be of scientific interest to gain quantitative information about the toxic effects of these fungal metabolites in the human body.

2.5. Liquid chromatography - mass spectrometry (LC-MS)

2.5.1. Separation of the analytes *via* liquid chromatography (LC)

Although the term ‚chromatography' was already described in the 18th century, meaning a treatise on colour, the scientific community usually associates it with the name of Tswett (Williams and Weil, 1952). He introduced a separation method of plant pigments under this term, using a glass cylinder filled with chalk or sucrose powder as adsorbent and petrol ether-ethanol as a solvent mixture (Tswett, 1906). This application of the word led to the current definition, which describes chromatography as "a physical method of separation in which the components to be separated are distributed between two phases, one of which is stationary (stationary phase) while the other (the mobile phase) moves in a definite direction" (Nič *et al*., 2009).

In high-performance liquid chromatography (HPLC), the stationary phase usually consists of solid sorbents in a column, whereas the mobile phase is liquid. The most fundamental elements of an HPLC system are the mobile phase reservoirs linked to the pumps, the manual injector valve or the more frequently used autosampler, the column in the column oven, as well as the detector of choice. For some applications, even higher efficacy and resolution might be necessary as HPLC systems allow. Ultra-high-performance liquid chromatography (UHPLC) enables higher pressure than HPLC, facilitating the movement of the eluents despite the smaller particle size in the stationary phase (Dong, 2019). Figure 5 depicts the general schema of an LC system on the example of the LC-QqQ instrument used in this work and compares some HPLC and UHPLC parameters.

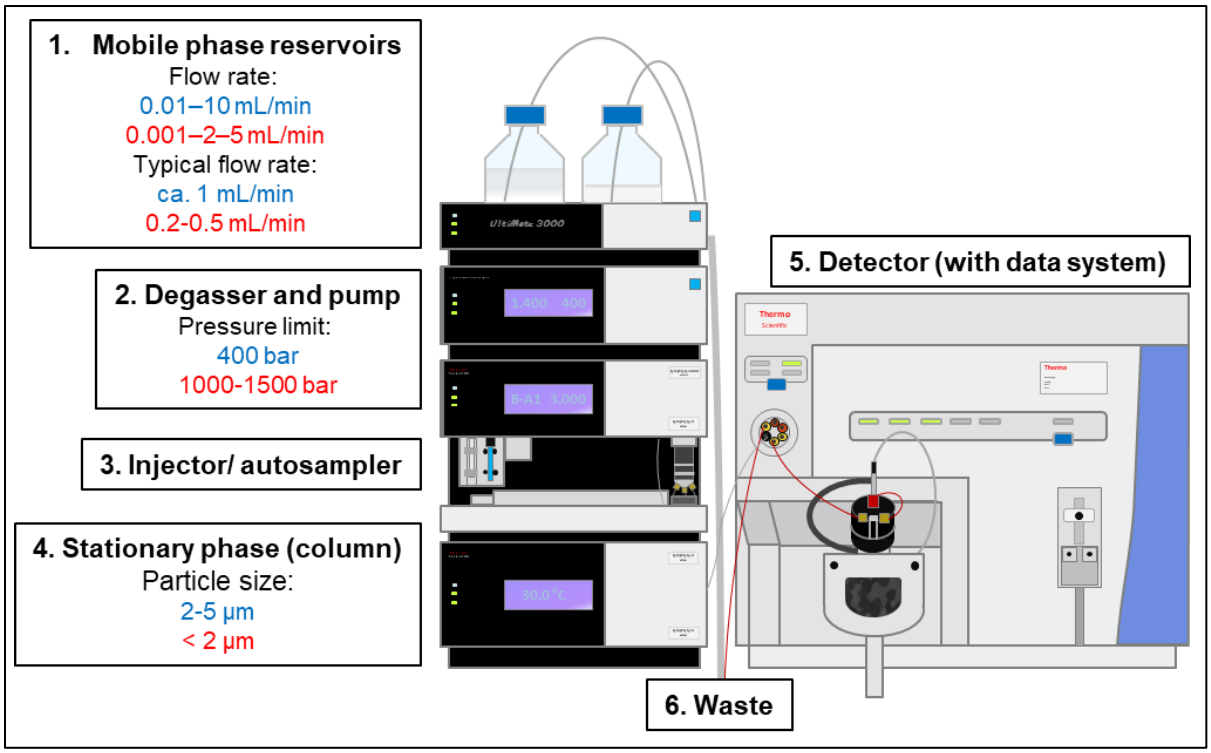

Figure 5: Schematic graphics of an LC-triple quadrupole system, with the most important elements and some characteristic parameters for HPLC (blue) and UHPLC (red) systems Based on Dong, 2019.

Four main separation modes are to distinguish in HPLC approaches: normal- and reversed-phase, ion-exchange, as well as size-exclusion chromatography. Whereas the normal-phase system is the oldest one, reversed-phase (RP) HPLC is currently the most widespread separation mode. This combination of the hydrophobic stationary phase (e. g. octylsylyl or octyldecylsylyl silica gel column) and polar mobile phase (such as methanol-water or acetonitrile-water) enables the analysis of polar, medium-polar, and even some non-polar analytes (Dong, 2019). In addition to its versatility, the robustness, convenience, and high reproducibility of RP-HPLC are also of particular significance in its popularity. However, in the separation and detection of highly polar or chiral analytes, RP-HPLC has some limitations (Snyder *et al*., 2010).

It is important to note that choosing an appropriate HPLC column is one of the main contributors to a successful separation of the analytes. Depending on the application field and the corresponding sample volume, different column dimensions might be reasonable. Capillary columns – having an inner diameter (i. d.) under 0.1 mm – can be used to achieve an efficient separation, despite the small available amounts of a sample (0.05 µg). The other extremes are preparative columns, where the i. d. exceeds 25 mm, and the loading of 30 mg sample is possible. The conventional analytical columns usually have an i. d. of 4.6 mm and allow analysing 100 µg sample (Dong, 2019). Further examples for important column features are the pore diameter, size, qualitative composition, packing density, and type of the particles. Regarding particle type, totally porous, superficially porous (porous shell surrounding a porous core), pellicular (solid spheres covered with very thin surface layer), and perfusion (larger particles, containing network of smaller and larger pores) particles exist (Snyder *et al*., 2010).

Not only the stationary, but also the mobile phase modifies the separation efficacy through the flow rate, composition and consequent viscosity. If an HPLC analysis runs with a constant mobile-phase constitution, we speak about isocratic elution, a simple and convenient form of LC. Nevertheless, some difficulties may occur when analysing multi-component mixtures with this method. The presence of substances with extremely high and low retention times within the same sample causes an unsatisfying separation. Namely, the polar compounds (low retention in RP-LC) may co-elute while the non-polar compounds (having a high affinity to the stationary phase in RP-LC) show undesirable peak broadening under isocratic conditions. If no optimal isocratic separation condition provides overcoming this problem, gradient elution – the continuous change of the mobile-phase composition – might be a considerable alternative. Among other benefits, gradient elution enables the reproducible analysis of high-molecular-weight compounds and helps to avoid unwanted deviation of the peak shape from the Gaussian curve (Snyder *et al*., 2010).

After the separation of the analytes *via* liquid chromatography, the detection takes place. Fluorescent, amperometric, refractive index, mass spectrometry, nuclear magnetic resonance, and ultraviolet-visible detectors are examples of several possibilities to qualify and quantify the compounds of interest. However, all of these methods have specific limitations which are summarised in the fourth chapter of 'HPLC and UHPLC for practicing scientists' (Dong, 2019).

The limit of detection (LOD) is the lowest concentration at which the signal can be distinguished from the noise and is often estimated as the concentration by a signal-to-noise ratio (S/N) of three (Snyder *et al*., 2010). The lowest concentration of analyte which can be quantified with acceptable accuracy is the limit of quantification (LOQ), usually defined as the concentration where S/N is ten. However, the suitable precision and the LOQ depend on the analysis method and research question. The lower and upper limit of quantification values (LLOQ and ULOQ, respectively) offer a more evident designation of the concentration range, where the analytical result is considered reliable. These represent the concentrations of the lowest and highest calibration standards if a certain reproducibility and accuracy in their measurements are given (Vashist and Luong, 2018). The technical development of the state-of-the-art detectors targets lower and lower LOD and LOQ values to enable trace analysis. Coupling a mass spectrometer to a liquid chromatograph may result in the optimal outcome of the LOD and other performance parameters, under favourable circumstances, such as high ion formation yield of the analyte (Kromidas, 2016).

2.5.2. Detection of the analytes *via* mass spectrometry (MS)

The origin of mass spectrometry dates back into the early 1900s, but its development had the first breakthrough during the Second World War within the framework of the Manhattan Project (Smoluch *et al*., 2019). Although the improvement of the MS instruments is still in progress, the fundamentals stayed the same over the years, measuring the mass-to-charge ratio (m/z) of a compound. Since detecting an analyte is only possible in a charged form, the ability to be ionised is the most crucial requirement for a substance to be detectable with MS. When analysing a complex mixture, MS enables the simultaneous measurement of all detectable compounds. On the other hand, if the research interest requires a more sensitive quantification of a selected substance, the so-called single ion monitoring (SIM) allows that (Smoluch *et al*., 2019).

The main elements of an MS are the inlet system, ion source/ interface, mass analyser, and the detector with the data system. Whereas the separation of the analytes happens at (ultra-)high pressure, every type of mass analyser requires a vacuum facilitating the movement of the ions in an electric field. Since most of the ion sources utilised in LC-MS approaches work on atmospheric pressure, they allow a convenient coupling between the two instruments. Moreover, the interface provides the transition between the liquid and gaseous phase and leads to the ionisation of the analytes (Smoluch *et al*., 2019). Electrospray ionisation (ESI), atmospheric pressure chemical (APCI), photo (APPI), and laser (APLI) ionisation are the four commercially available interfaces in the order of the frequency of their use (Kromidas, 2016).

During the ionisation with ESI, the mobile phase – including the analytes – is pumped through a capillary under electric potential. This way, a spray consisting of charged droplets is formed. The counter-current of a heated inert gas facilitates the evaporation of the solvent and its removal from the interface. The consequent shrinkage of the droplets increases the concentration of charge on their surface, resulting in coulombic fission. That leaves the formed analyte ions in a gaseous state, and they can migrate further in the instrument due to the electric field and the vacuum of the analyser (Dong, 2019; Smoluch *et al*., 2019). The electrospray interface is suitable for polar or ionic analytes, but it shows lower ionisation efficiency for less polar and nonpolar substances (Kromidas, 2016). Since the formation of multiply charged ions is no rarity with ESI, it provides a valuable tool for identifying large biomolecules through the detection of m/z. In contrast to other interfaces, an undesirable fragmentation rarely occurs with this method, which is why ESI is considered a so-called soft ionisation technique (Smoluch *et al*., 2019).

Once the ions leave the interface, they arrive in the mass analyser that separates the analytes based on their m/z (Dong, 2019). IonTrap, quadrupole, time of flight (TOF), and Orbitrap are examples of frequently applied analysers (Kromidas, 2016). Quadrupoles (Q) are built from four parallel metal rods, and the opposite rods form pairs, having the same potential in each moment. The combination of radio-frequency voltage and direct current is set on the rods in a way that the superposition of these voltages results in a stable trajectory only for ions with a particular m/z value. Hence, they can reach the detector (e. g. an electron multiplier) while other ions collide with the rods. This leads to the generation of the spectrum. By manipulating the electric field, different m/z values can be quickly scanned in a consecutive manner (Smoluch *et al*., 2019).

When only radio-frequency voltage is set on a quadrupole while no direct current is running, the ions can be focused and transferred, as well as fragmented in the presence of a collision gas. For this purpose, not only quadrupoles, but also hexa- and octupoles are suitable. Triple quadrupole (QqQ, also triple quad) – a type of hybrid mass spectrometers – combines three quadrupoles, taking advantage of their versatile application modes (Smoluch *et al*., 2019). Figure 6 depicts the elements of a QqQ instrument and summarises the possible scan modes with the corresponding analytical purposes.

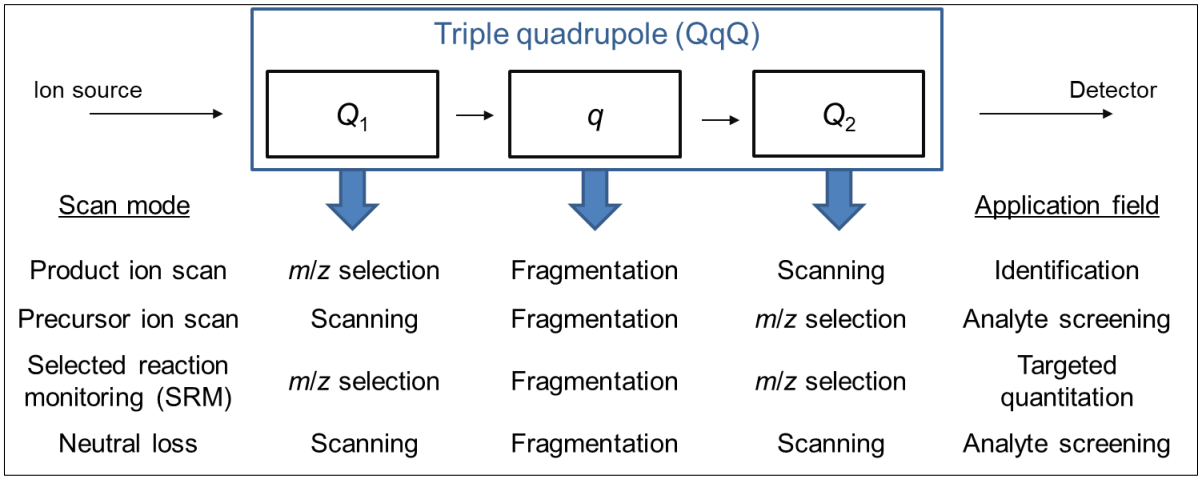

Figure 6: Setup and possible scan modes of a triple quadrupole
Based on Dong, 2019 and Smoluch *et al.*, 2019.

The selected reaction monitoring (SRM) is commonly applied for quantification purposes (Figure 6). In this method, the first analyser (Q_1) acts as a mass filter, selecting the precursor ion(s) with a specific *m*/*z* value. An inert gas in the collision cell (q) facilitates the fragmentation, and finally, the third quadrupole (Q_2) filters for a particular *m*/*z*. The consequent increase in selectivity and sensitivity makes QqQ instruments especially suitable for the quantification of single substances (Smoluch *et al.*, 2019). However, if a comprehensive analysis of a mixture is desired, so-called high-resolution techniques are frequently preferred, such as Orbitrap or quadrupole-time-of-flight (QTOF) instruments (Kromidas, 2016). As they enable the highly accurate determination of the molecular mass of a compound of interest, its elemental composition and chemical formula can be revealed (Smoluch *et al.*, 2019). The benefits and disadvantages of different mass spectrometers described above were considered to select suitable instruments for the analytical questions arising in this work. Hence, the quantification of AOH, AME, and some of their highly represented and known metabolites was realised with a UHPLC-QqQ device, including an ESI interface (for the illustration, see Figure 5). However, to look for a broader range of possible metabolites in the samples collected after incubations with different *in vitro* liver models, a high-resolution mass spectrometer – a linear trap quadrupole Orbitrap coupled to UHPLC, with ESI as one of the possible ion sources – was required.

2.5.3. Previous works using liquid chromatography coupled to mass spectrometry for detecting AOH, AME, and metabolites

As Table 1 and Table 2 already indicate, besides liquid chromatography, gas chromatography (GC) is frequently the separation method of choice in the determination of AOH, AME, and their metabolites (Pfeiffer *et al.*, 2007b; Pfeiffer *et al.*, 2009; Schuchardt *et al.*, 2014). However, since these substances are not volatile, their chemical modification (e. g. the derivatisation with *N*,*O*-bis-(trimethylsilyl)trifluoroacetamide) is required before injecting the sample in the gas chromatograph (Smoluch *et al.*, 2019). Beyond mass spectrometers, ultraviolet (UV) detectors – especially diode-array detectors (DAD) – represent beneficial tools for visualising the elution profile of metabolic mixtures (Burkhardt *et al.*, 2009; Pfeiffer *et al.*, 2007b). Nevertheless, no elucidation of the chemical structure is possible with this detection mode, so it is often applied in addition to mass spectrometry.

Since this work predominantly relies on liquid chromatography-tandem mass spectrometry measurements, already published procedures addressing the detection of AOH and AME with these particular instruments are of special relevance at this point.

Table 3 includes several examples for the LC-MS/MS analysis of alternariol and its derivatives in different matrices, such as blood, faeces, urine, cell lysate, breast milk, and food samples. With no exception, an RP-LC method was developed for this analysis, given that all analytes are relatively polar. Whereas the compared methods showed high diversity in the composition of the mobile phases, nearly all stationary phases were based on silica particles modified with octadecyl-silyl groups (C18). Most of the eluents contained different ammonium salts, considering that they can exert buffer capacity, act as charge carriers, and suppress the formation of potassium and sodium adducts in the ion source (Kromidas, 2016). In some cases, especially in positive ionisation mode, volatile organic acids (e. g. formic and acetic acid) were added to the mobile phase as proton sources. With ESI being the only interface used, the majority of the methods relied on negative ionisation. However, the parent toxins can also be observed in ESI+ mode, as two of the listed publications reported.

Table 3: Some LC-MS/MS methods and their parameters for quantifying AOH, AME and metabolites

Toxin or metabolite	Matrix	Stationary phase	Mobile phase	R. t. (min)	Run time (min)	Ionisation mode	Mass analyser	Precursor mass	Product masses	Publication
alternariol	foodstuffs	Ascentis Express (C18; 2.7 µm, 10 cm × 2.1 mm)	water (5 mM NH_4OAc, pH 8.6) and MeOH	6.6	15.5	ESI-	TSQ Vantage Thermo Scientific	257	215/147	Puntscher *et al.*, 2018
	breast milk	Acquity HSS T3 (C18; 1.8 µm, 10 cm × 2.1 mm)	water (5 mM NH_4OAc, 0.1% HAc) and MeOH	7.2	19	ESI-	TSQ Vantage Thermo Scientific	257.0	215.1/147.1	Braun *et al.*, 2020a
	tomato-based products	Gemini (C18; 3.0 µm, 15 cm × 2.0 mm)	water (5 mM NH_4HCOO, 1 % HCOOH), MeOH (5 mM NH_4HCOO, 1 % HCOOH)	8.3	21	ESI+	SCIEX 3200 QTRAP Applied Biosystems	259	128/184	Rodríguez-Carrasco *et al.*, 2016
	tomato juice and sesame oil	Acquity HSS T3 (C18; 1.8 µm, 10 cm × 2.1 mm)	water (0.01 % TFA) and MeOH	3.9	7	ESI-	Xevo TQ-S Waters	257.1	213.1/215.1	Rico-Yuste *et al.*, 2018
	blood plasma, urine and faeces	Acquity HSS T3 (C18; 1.8 µm, 10 cm × 2.1 mm)	water (0.3 mM NH_4F) and MeOH	14.1	20	ESI-	TSQ Vantage Thermo Scientific	257	215.1/147.1	Puntscher *et al.*, 2019
	cell lysate	Luna (C18; 3.0 µm, 10 cm × 1.0 mm)	water (0.1 % HCOOH) and ACN (0.1 % HCOOH)	3.6	12	ESI-	TSQ Vantage Thermo Scientific	257	213/147	Tiessen *et al.*, 2016
	urine	BEH (C18; 1.7 µm, 10 cm × 2.1 mm)	water (0.15 mM $(NH_4)_2CO_3$) and MeOH (0.15 mM $(NH_4)_2CO_3$)	4.6	7	ESI-	LCMS-8060 Shimadzu	257.1	159.1/212.1	Qiao *et al.*, 2020
	whole blood	Poroshell 120 EC-C18 (2.7 µm, 5 cm × 3.0 mm)	water and methanol		22	ESI-	SCIEX 5500 QTRAP Applied Biosystems	257	213/147	Schuchardt *et al.*, 2014
	cell lysate	Gemini-NX (C18; 3.0 µm, 15 cm × 2.0 mm)	water (5 mM NH_4HCOO, 0.1 % HCOOH), MeOH (5 mM NH_4HCOO, 0.1 % HCOOH)		21	ESI+	SCIEX 3200 QTRAP Applied Biosystems	259	128.0/184.0	Juan-García *et al.*, 2016
4-hydroxy-alternariol	blood plasma, urine and faeces	Acquity HSS T3 (C18; 1.8 µm, 10 cm × 2.1 mm)	water (0.3 mM NH_4F) and MeOH	11.6	20	ESI-	TSQ Vantage Thermo Scientific	273	258.1/214.2	Puntscher *et al.*, 2019
	cell lysate	Luna (C18; 3.0 µm, 10 cm × 1.0 mm)	water (0.1 % HCOOH) and ACN (0.1 % HCOOH)	1.9	12	ESI-	TSQ Vantage Thermo Scientific	273	258/214	Tiessen *et al.*, 2016
alternariol-3*O*-glucuronide	blood plasma, urine and faeces	Acquity HSS T3 (C18; 1.8 µm, 10 cm × 2.1 mm)	water (0.3 mM NH_4F) and MeOH	8.9	20	ESI-	TSQ Vantage Thermo Scientific	419	256.1/227.8	Puntscher *et al.*, 2019
alternariol-9*O*-glucuronide	blood plasma, urine and faeces	Acquity HSS T3 (C18; 1.8 µm, 10 cm × 2.1 mm)	water (0.3 mM NH_4F) and MeOH	8.6	20	ESI-	TSQ Vantage Thermo Scientific	419	256.1/227.8	Puntscher *et al.*, 2019
alternariol-3*O*-sulphate	foodstuffs	Ascentis Express (C18; 2.7 µm, 10 cm × 2.1 mm)	water (5 mM NH_4OAc, pH 8.6) and MeOH	3.7	15.5	ESI-	TSQ Vantage Thermo Scientific	337	257/213	Puntscher *et al.*, 2018
	blood plasma, urine and faeces	Acquity HSS T3 (C18; 1.8 µm, 10 cm × 2.1 mm)	water (0.3 mM NH_4F) and MeOH	10.7	20	ESI-	TSQ Vantage Thermo Scientific	337	257.1/213.1	Puntscher *et al.*, 2019

Toxin or metabolite	Matrix	Stationary phase	Mobile phase	R. t. (min)	Run time (min)	Ionisation mode	Mass analyser	Precursor mass	Product masses	Publication
alternariol monomethyl ether	foodstuffs	Ascentis Express (C18; 2.7 µm, 10 cm × 2.1 mm)	water (5 mM NH_4OAc, pH 8.6) and MeOH	10.0	15.5	ESI-	TSQ Vantage Thermo Scientific	271	256/227	Puntscher *et al.*, 2018
	breast milk	Acquity HSS T3 (C18; 1.8 µm, 10 cm × 2.1 mm)	water (5 mM NH_4OAc, 0.1% HAc) and MeOH	9.0	19	ESI-	TSQ Vantage Thermo Scientific	271.1	256.1/227.1	Braun *et al.*, 2020a
	tomato-based products	Gemini (C18; 3.0 µm, 15 cm × 2.0 mm)	water (5 mM NH_4HCOO, 1 % HCOOH), MeOH (5 mM NH_4HCOO, 1 % HCOOH)	9.1	21	ESI+	SCIEX 3200 QTRAP Applied Biosystems	273	128/228	Rodríguez-Carrasco *et al.*, 2016
	tomato juice and sesame oil	Acquity HSS T3 (C18; 1.8 µm, 10 cm × 2.1 mm)	water (0.01 % TFA) and MeOH	5.2	7	ESI-	Xevo TQ-S Waters	271.2	256.2/228.2	Rico-Yuste *et al.*, 2018
	blood plasma, urine and faeces	Acquity HSS T3 (C18; 1.8 µm, 10 cm × 2.1 mm)	water (0.3 mM NH_4F) and MeOH	15.9	20	ESI-	TSQ Vantage Thermo Scientific	271	256.1/227.1	Puntscher *et al.*, 2019
	cell lysate	Luna (C18; 3.0 µm, 10 cm × 1.0 mm)	water (0.1 % HCOOH) and ACN (0.1 % HCOOH)	9.2	12	ESI-	TSQ Vantage Thermo Scientific	271	256/228	Tiessen *et al.*, 2016
	urine	BEH (C18; 1.7 µm, 10 cm × 2.1 mm)	water (0.15 mM $(NH_4)_2CO_3$) and MeOH (0.15 mM $(NH_4)_2CO_3$)	5.0	7	ESI-	LCMS-8060 Shimadzu	271.1	256.1/228.1	Qiao *et al.*, 2020
4-hydroxy-alternariol monomethyl ether	blood plasma, urine and faeces	Acquity HSS T3 (C18; 1.8 µm, 10 cm × 2.1 mm)	water (0.3 mM NH_4F) and MeOH	15.2	20	ESI-	TSQ Vantage Thermo Scientific	287	188.1/272.1	Puntscher *et al.*, 2019
	cell lysate	Luna (C18; 3.0 µm, 10 cm × 1.0 mm)	water (0.1 % HCOOH) and ACN (0.1 % HCOOH)	5.8	12	ESI-	TSQ Vantage Thermo Scientific	287	272/188	Tiessen *et al.*, 2016
alternariol monomethyl ether-3*O*-glucuronide	blood plasma, urine and faeces	Acquity HSS T3 (C18; 1.8 µm, 10 cm × 2.1 mm)	water (0.3 mM NH_4F) and MeOH	13.2	20	ESI-	TSQ Vantage Thermo Scientific	433	270.0/227.1	Puntscher *et al.*, 2019
alternariol monomethyl ether-3*O*-sulphate	blood plasma, urine and faeces	Acquity HSS T3 (C18; 1.8 µm, 10 cm × 2.1 mm)	water (0.3 mM NH_4F) and MeOH	13.7	20	ESI-	TSQ Vantage Thermo Scientific	351	271.0/256.0	Puntscher *et al.*, 2019
	foodstuffs	Ascentis Express (C18; 2.7 µm, 10 cm × 2.1 mm)	water (5 mM NH_4OAc, pH 8.6) and MeOH	8.0	15.5	ESI-	TSQ Vantage Thermo Scientific	351	256/271	Puntscher *et al.*, 2018

3. Aim of the thesis

Ubiquitously occurring moulds of the genus *Alternaria* produce potentially toxic substances classified as emerging mycotoxins, considering that no legislative regulations have been implemented for them yet (Gruber-Dorninger *et al*., 2017). AOH and AME are among the best-studied *Alternaria* toxins regarding their *in vitro* toxicity. As such, they were claimed to exert cytotoxic, genotoxic, mutagenic, estrogenic, and immunosuppressive effects. In contrast, toxicokinetic data about AOH and AME are scarce.

Thus, this work focused on the metabolic kinetics of these two mycotoxins in *in vitro* liver models. Most importantly, incubation studies were carried out in NADPH-fortified porcine, human, and rat liver microsomes. Subsequently, the parent toxin levels were determined in the drawn samples by HPLC-QqQ measurements. This investigation aimed to gather quantitative data of metabolic processes triggered by AOH or AME treatment. Based on them, potentially occurring interspecies differences were intended to capture. Besides, determining the kinetic parameters of each metabolic reaction was planned as they are essential to develop and utilise computational methods – such as physiologically based toxicokinetic modelling – to estimate the ADME of these toxins in the human body. Noteworthy, the preparation of the porcine hepatic microsomal fraction and the adaptation of an existing, published analytical method was part of this thesis.

The present work also addressed the identification of the phase I metabolites of AOH and AME obtained during the incubation assays. Although a previous study already investigated this topic in comparable assay conditions, analysing pooled incubation samples with an HR-MS system with subsequent comprehensive data evaluation intended to confirm or amend the published findings (Pfeiffer *et al*., 2007b).

Besides the liver microsomes, the human hepatocarcinoma cell line HepG2 was applied as an *in vitro* liver model, as well. The number of publications dealing with the exposure of these cells to AOH is limited, and the available data does not provide a complete picture of its metabolism (Juan-García *et al*., 2016). Therefore, the objective was to gain more qualitative and quantitative information about the detoxification of AOH and AME in HepG2 cells.

4. Materials and methods

4.1. Instruments and software

Analytical balance: Adventurer™, AX224, OHAUS, Greifensee, CH

NewClassic MF, ML204/01, Mettler Toledo, Greifensee, CH

Aspiration system: VACUSAFE, Integra Biosciences AG, Hudson, NY, US

Autoclave: Systec DX-150, Systec GmbH, Wettenberg, DE

Balance: KERN KB 3600-2N, KERN & Sohn GmbH, Balingen, DE

New Classic MF, ML6001/01, Mettler Toledo, Greifensee, CH

Centrifuge: Avanti® J-26 XP, Beckman Coulter GmbH, Vienna, AT

HERMLE Z 326 K, HERMLE Labortechnik GmbH, Wehingen, DE

Hettich Zentrifugen Mikro 220R, Andreas Hettich GmbH & Co. KG, Tuttlingen, DE

ChemDraw: ChemDraw Ultra, Version 12.0.2. 1076. CambridgeSoft, Cambridge, MA, US

Crimper: 11 mm, Supelco, Munich, DE

Decapper: 11 mm, Supelco, Munich, DE

Freezer/Fridge: Liebherr Premium Comfort (4°C, -20°C), Liebherr, Bulle, CH

Homogeniser: FastPrep-24™ 5G, MP Biomedicals, Santa Ana, CA, US

HR-MS system:

- LC unit:
  Vanquish UHPLC, Thermo Fisher Scientific, Waltham, MA, US
- MS unit:
  LTQ Orbitrap Velos ETD, Thermo Fisher Scientific, Waltham, MA, US
- Software:
  Chromeleon, Version 7.2.6., Thermo Fisher Scientific, Waltham, MA, US

  Skyline (64-bit), Version 21.1.0.146, MacCoss Lab, Department of Genome Sciences, University of Washington, Seattle, WA, US

  Thermo XCalibur, Version 2.2SP1.48, Thermo Fisher Scientific, Waltham, MA, US

Incubator: HERACELL 240i CO_2 Incubator, Thermo Fisher Scientific, Waltham, MA, US

Inverse microscope: Zeiss Axiovert 40C, Carl Zeiss Microscopy GmbH, Jena, DE

Ice machine: Scotsman MF 46, Scotsman Ice Systems, Milan, IT

Laminar flow unit: HERASAFE™ KS, Thermo Fisher Scientific, Waltham, MA, US

LC-QqQ system:

- LC unit:
  Dionex UltiMate 3000 UHPLC, Dionex Softron GmbH, Germering, DE
- MS unit:
  TSQ Vantage, Thermo Fisher Scientific, Waltham, MA, US
- Software:
  Thermo XCalibur, Version 4.0.27.42, Thermo Fisher Scientific, Waltham, MA, US

  TraceFinder™, Version 3.3.358.0, Thermo Fisher Scientific, Waltham, MA, US

Microbalance: DeltaRange® XP26, Mettler Toledo, Greifensee, CH

Multichannel pipette: Eppendorf Multipette® Plus 2.5 – 5,000 µL, Eppendorf Research, Hamburg, DE

Origin: OriginPro 2019b, Version 9.6.5.169, OriginLab, Northampton, MA, US

Oven: Binder ED 115, BINDER GmbH, Tuttlingen, DE

pH-meter: PC 8 + DHS, XS Instruments, Carpi, IT

Pipettes: different volumes (10 µL, 20 µL, 100 µL, 200 µL, 1,000 µL, 5 mL), Eppendorf GmbH, Vienna, AT

Pipetting device: Pipetus® Akku, Hirschmann Laborgeräte, Eberstadt, DE

Plate reader: Synergy H1 microplate reader, BioTek, Winooski, VT, US
Software: Gen5, Version 3.08.01

Victor^{3}V, 1420 Multilabel Counter, Perkin Elmer, Waltham, MA, US
Software: Wallac 1420 Workstation Software, Version 3.00

Thermo shaker: Biosan TS-100C, Biosan, Riga, LV

Peqlab Thriller®, VWR International, Radnor, PA, US

Ultracentrifuge: Sorvall WX 80 Ultracentrifuge, Thermo Fisher Scientific, Waltham, MA, US

Sorvall WX + Ultracentrifuge, Thermo Fisher Scientific, Waltham, MA, US

Ultra-Low temperature freezer: Panasonic MDF-DU900V, Panasonic Healthcare Co., Ltd., JP

Ultrasonic bath: VWR Ultrasonic Cleaner, VWR International, Radnor, PA, US

Vortexer: Lab dancer S40, VWR International, Radnor, PA, US

Vortex-Genie 2, Scientific Industries, New York, NY, US

Water bath: Grant GD100, Grant Instruments, Cambridge, UK

4.2. Consumables

Centrifuge tube: 9/16 × 3 3/4 ultracentrifuge tube, Beckman Coulter Inc., Brea, CA, US

12 mL PA tube, Thermo Fisher Scientific, Waltham, MA, US

Crimp vial: 1.5 mL, brown or transparent glass, Bruckner Analysentechnik GmbH, Linz, AT

Crimp vial cap: 11 mm, TEF, Bruckner Analysentechnik GmbH, Linz, AT

Counting chamber: Neubauer, 0.0025 mm^2, depth: 0.100 mm, Paul Marienfeld GmbH & Co. KG, Lauda-Königshofen, DE

Dispenser-tips: 2.5 mL, sterilised, Ratiolab GmbH, Dreieich, DE

Duran bottle – different volumes (100 mL, 250 mL, 500 mL, 1 L, 2 L): Schott AG, Mainz, DE

Boro 3.3, Sigma-Aldrich, St. Louis, MO, US

LC column: Ascentis Express C18 column, 10 cm × 2.1 mm, 2.7 µm, Supelco, Munich, DE

Acquity UPLC HSS T3, 2.1 × 100 mm, 1.8 µm, Waters, Milford, CT, US

LC guard column: Phenomenex SecurityGuard™ C18 Cartridges, 4 × 2.0 mm ID, Phenomenex Ltd. Deutschland, Aschaffenburg, DE

Light-duty tissue wipers: VWR International, Radnor, PA, US

Lysing matrix: “D”, MP Biomedicals, Fountain Parkway Solon, OH, US

Measuring cylinder: 100, 500, and 1,000 mL, Boro 3.3, VWR International, Radnor, PA, US

Micro-insert: flat bottom, 0.3 mL, Macherey-Nagel GmbH & Co. KG, Düren, DE

conical bottom, 0.1 mL, Bruckner Analysentechnik GmbH, Linz, AT

Microscope cover glass: borosilicate glass, 24 x 24 mm, thickness No. 1, VWR International, Radnor, PA, US

Microtest Plate: 96 wells, nonsterile, Sarstedt AG & Co, Nümbrecht, DE

Microtube: 0.5, 1.5, and 5 mL, Sarstedt AG & Co, Nümbrecht, DE

5 mL, Carl Roth GmbH & Co. KG, Karlsruhe, DE

Pasteur pipette: without cotton stopper, 150 mm, Carl Roth GmbH & Co. KG, Karlsruhe, DE

Petri dish: TC dish, sterile, 150 cells+, Sarstedt AG & Co, Nümbrecht, DE

Pipette tip: nonsterile, different volumes (10 µl, 200 µl, 1,000 µl), Sarstedt AG & Co, Nümbrecht, DE

Screw cap: 9 mm, PTFE/RS, Agilent Technologies, Santa Clara, CA, US

Screw vial: 2 mL, brown glass, Agilent Technologies, Santa Clara, CA, US

Serological pipette: 5 and 10 mL, Sarstedt AG & Co, Nümbrecht, DE

TC flask: 25, 75, and 175 cm^2, sterile, vented (red) cap, Sarstedt AG & Co, Nümbrecht, DE

TC plate: 96 wells, sterile, standard, Sarstedt AG & Co, Nümbrecht, DE

Tube: 15 and 50 mL, PP, Sarstedt AG & Co, Nümbrecht, DE

Cellstar® tubes fitting into the homogeniser instrument, 15 mL, PP, sterile, Greiner Bio-One International GmbH, Kremsmünster, AT

4.3. Biological material

Hep G2 cell line: previously purchased from American Type Culture Collection (ATCC number: HB-8065)

Human liver microsomes:
pooled from human males, protein concentration: 20 mg/mL, product number: M0567, lot number: SLCD4391, 0.340 nmol P450 per mg protein, Sigma-Aldrich Co., St. Louis, MO, US

Porcine liver:
purchased on the morning of slaughtering, donor: Edelschwein, female, 3.5-4 months old

Rat liver microsomal suspension:
pooled from 50 Sprague-Dawley rats, protein concentration: 20 mg/mL, catalogue number: RTMCPL, Gibco®, Thermo Fisher Scientific, Waltham, MA, US
Lot no. RT060-B: 0.240 nmol P450 per mg protein
Lot no. RT061-A: 0.399 nmol P450 per mg protein

4.4. Chemicals

Acetonitrile (ACN): CHROMASOLV™ LC-MS, ≥99.9 %, Honeywell Riedel-de Haën™, Seelze, DE

Alternaria reference mixture provided by Dr. Hannes Puntscher

(Puntscher *et al.*, 2019; Tiessen *et al.*, 2017):
Including alternariol, 4-hydroxy-alternariol, 4-hydroxy-alternariol monomethyl ether, alternariol-3-*O*-sulphate, alternariol-3-*O*-glucoside, alternariol-9-*O*-glucoside, alternariol monomethyl ether, alternariol monomethyl ether-3-*O*-sulphate, alternariol monomethyl ether-3-*O*-glucoside and other *Alternaria* toxins

Alternariol (AOH): analytical standard: 100.3 µg/mL (dried out), Biopure™, Romer Labs Diagnostic GmbH, Tulln, AT

for incubations: AOH from *Alternaria* sp., 96 %, Sigma-Aldrich Co., St. Louis, MO, US

Alternariol monomethyl ether (AME):

analytical standard: 101.1 µg/mL (dried out), Biopure™, Romer Diagnostic GmbH, Tulln, AT

for incubations: AME from *Alternaria alternata (tenuis)*, Sigma-Aldrich Co., St. Louis, MO, US

Ammonium acetate solution: 5 M in water, BioUltra, for molecular biology, Sigma-Aldrich Co., St. Louis, MO, US

Ammonium formate: eluent additive for LC-MS, Fluka® Analytical, Sigma-Aldrich Co., St. Louis, MO, US

Ammonium hydroxide solution: ≥ 25 % in water, eluent additive for LC-MS, Fluka® Analytical, Sigma-Aldrich Co., St. Louis, MO, US

Ascorbic acid: Merck, Darmstadt, DE

BCA Protein Assay Kit: Thermo Fisher Scientific, Waltham, MA, US

Buffer solution for the calibration of pH meter:

pH 4.00, 7.00, and 10.00 (20 °C), AppliChem GmbH, Darmstadt, DE

Dimethyl sulphoxide (DMSO): ≥ 99.5 %, bioscience-grade, Carl Roth GmbH & Co. KG, Karlsruhe, DE

Ethanol, 96%: denatured, Brenntag Austria GmbH, Vienna, AT

Ethylenediamine tetraacetic acid (EDTA):
≥ 99 %, for biochemistry, Carl Roth GmbH & Co. KG, Karlsruhe, DE

Foetal bovine serum (FBS): heat-inactivated, EU-approved origin: South America, Gibco®, Thermo Fisher Scientific, Waltham, MA, US

Formic acid: HPLC grade, Carl Roth GmbH & Co. KG, Karlsruhe, DE

Methanol: CHROMASOLV™ LC-MS, ≥ 99.9 %, Honeywell Riedel-de Haën™, Seelze, DE

Mineral oil: for molecular biology, Carl Roth GmbH & Co., Karlsruhe, DE

NADPH: tetrasodium salt, EMD Millipore Corp., Merck, Darmstadt, DE

tetrasodium salt, ~ 98 %, Roche Diagnostics GmbH, Mannheim, DE

Penicillin-Streptomycin (P/S):
10.000 U/mL, 10.000 µg/mL, Gibco®, Thermo Fisher Scientific, Waltham, MA, US

Phosphate-buffered saline solution (PBS): Carl Roth GmbH & Co., Karlsruhe, DE

2-Propanol: CHROMASOLV™ LC-MS, Honeywell Riedel-de Haën™, Seelze, DE

Radioimmunoprecipitation assay (RIPA) lysis buffer:
Roche Diagnostics, Mannheim, DE

Roswell Park Memorial Institute (RPMI) 1640 medium:
(1×), incl. L-glutamine, Gibco®, Thermo Fisher Scientific, Waltham, MA, US

D(+)-sucrose: Carl Roth GmbH & Co., Karlsruhe, DE

Sodium chloride: ≥ 99.8 %, Carl Roth GmbH & Co., Karlsruhe, DE

TRIS hydrochloride: ≥ 99 %, Carl Roth GmbH & Co., Karlsruhe, DE

Trypan blue: for microscopy and cell staining, Carl Roth GmbH & Co., Karlsruhe, DE

Trypsin: 5.000 USP-U/mg, Carl Roth GmbH & Co., Karlsruhe, DE

Water: HiPerSolv CHROMANORM, filtered at 0.2 µm, HPLC LC-MS grade VWR International, Radnor, PA, US

4.5. Methods

4.5.1. HPLC-QqQ measurements

4.5.1.1. Adaptation of an existing method

The quantification of *Alternaria* toxins was conducted on a high-performance liquid chromatography system (UltiMate 3000) coupled to a triple quadrupole mass spectrometer (TSQ Vantage), equipped with a heated electrospray ionisation interface.

To find the best possible method for quantifying AOH, AME, and their metabolites, the suitability of two already published analytical procedures was compared first. The 20-minute method suggested using the Acquity UPLC HSS T3 column, with an aqueous NH_4F solution (0.3 mM) as eluent A and methanol as eluent B (Puntscher *et al*., 2019). The other paper reported using the Supelco Ascentis Express C18 column, with an aqueous NH_4OAc solution (5 mM, pH adjusted to 8.7 with 25 % ammonia solution) as eluent A and methanol as eluent B (Puntscher *et al*., 2018). Overall, the second procedure was preferred and utilised for further measurements. Therefore, the parameters reported in this publication were taken over directly if not indicated otherwise.

Regarding the separation *via* liquid chromatography, a possible change of the overall run time, the gradient profile, and the eluent composition was considered. As Table 3 indicates, both acidic, neutral and alkaline solutions were already used as eluent A while determining alternariol derivatives. Therefore, besides aqueous NH_4OAc (5 mM, pH adjusted to 8.6 with 25 % ammonia solution), distilled water and NH_4HCOO (1 mM, 1 % HCOOH, measured pH: 3.0) were tested as eluent A. Ammonium acetate solution – resulting in the best peak shape – was applied as the aqueous eluent for later analyses.

Due to the high number of samples, the reduction of the original run time – 15.5 minutes – was expedient. Five different methods were generated and compared with a total length of 6, 8, 10, 12, and 15 minutes, while the other parameters remained the same as in the published procedure. During the first minute, the column was kept at 30 % eluent B. Subsequently, the content of eluent B was linearly raised to 100 % within 2, 4, 6, 8, and 10 minutes, respectively. Then the column was washed with 100 % eluent B for 1.5 minutes, except the 15-minute method, in which the purging lasted for 2.5 minutes. Lastly, the column was re-equilibrated at the initial conditions until the end of the run. In this investigation, the goal was to find the shortest possible run time, which still provides a satisfactory separation of the analytes. As a result, the 10-minute method was chosen for further measurements.

The tandem mass spectrometer was operated in multi-reaction monitoring (MRM) mode using negative ionisation, detecting the analytes in their deprotonated forms. As this work focused on the metabolism of AOH and AME in different *in vitro* models, the measurement of other *Alternaria* toxins was not reasonable. Consequently, they were excluded from the method, whereas the remaining analytes are listed in Table 4. By keeping the acquisition time of a targeted transition (dwell time) constant, the reduced amount of measured transitions led to decreasing the overall cycle time per MRM scan (Smoluch *et al*., 2019). Thus, the number of data points per peak was increased, and the peak shape was improved. A potential loss of analytical information due to this decision was not to consider since the HR-MS measurement of the samples provided data regarding the composition of the produced metabolic mixtures. Furthermore, the samples had to be diluted to allow the quantification of AOH and AME and thus formed metabolites were unlikely to be detected.

Table 4: Mass spectrometric parameters of the measured analytes

Analyte	Precursor ion	S-lens	Product ions				Retention time	
			Quantifier		Qualifier			
	(*m/z*)	(V)	(*m/z*)	Collision energy (V)	(*m/z*)	Collision energy (V)	(min)	
AOH	257.1	70	215.1	27	147.1	33	4.6-5.2	
AME	271.1	73	256.1	23	227.1	38	6.2-6.6	
AOH sulphates	337.0	86	257.1	22	213.1	37	2.4-2.6 (AOH-3-S)	3.7-3.8 (AOH-x-S)
AME sulphates	351.0	88	256.0	34	271.0 228.0	22 42	4.9-5.0	

4.5.1.2. Reference solutions and quantification

The absolute quantification of the parent toxins AOH and AME was carried out by injecting and measuring a series of external standard solutions after every 20-30 samples. Both analytical toxin standards were delivered as dried-out solid substances and were dissolved in 1 mL LC-MS grade acetonitrile. Subsequently, the resulting solutions were homogenised *via* vortexing and ultrasonication. The resulting AOH standard had a concentration of 100.3 µg/mL, whereas the AME standard contained 101.1 µg/mL of the toxin. Afterwards, the two standard solutions were combined in a toxin mix by pipetting 75 µL AOH and 15 µL AME standards, as well as 1410 µL dilution mixture into a 2 mL tube. This solution was used for the preparation of the entire calibration set, as summarised in Table 5.

Additionally, a multi-component reference solution stock – formerly prepared by Dr. Hannes Puntscher – was used for quantifying sulphate metabolites and comparing their concentration to that of the parent toxins (Puntscher *et al*., 2018). The stock was diluted according to Table 5, resulting in another standard series. In this, the nominal concentration of alternariol-3-*O*-sulphate and alternariol monomethyl ether-3-*O*-sulphate was the same as for AOH. However, the data obtained with this method should be viewed with caution since the multi-component reference stock was not freshly prepared.

Table 5: Preparation of the LC-MS standard solutions.
Dilution solvent: methanol-water (1:1 or 3:7, v/v)

Name	c_{AOH}	c_{AME}	Original solution		Dilution solvent	Total volume
	(µg/L)	(µg/L)	V (µL)	Name	V (µL)	(µL)
STD 100	100	20	30	AOH + AME toxin mix	1470	1500
			40	multi-component stock	360	400
STD 50	50	10	100	STD 100	100	200
STD 30	30	8	150	STD 100	350	500
STD 10	10	2	60	STD 100	540	600
STD 3	3	0.8	60	STD 30	540	600
STD 1	1	0.2	60	STD 10	540	600
STD 0.3	0.3	0.08	60	STD 3	540	600
STD 0.1	0.1	0.02	60	STD 1	540	600
Blank	0	0	-	-	1000	1000

For the absolute quantification of AOH and AME in the *Alternaria* reference mixture, two calibration sets of the analytical standard mix and the *Alternaria* reference mix were prepared and alternately measured in several replicates. First, the AOH and AME concentration of the analytical standard could be calculated based on the values provided by the manufacturer and the known dilution factors. Using that as an external standard, the mean concentration value of the multi-component reference stock could be determined. Furthermore, by measuring the diluted AOH and AME single-toxin analytical standards, their contamination with the respective other toxin counterpart could be evaluated.

4.5.1.3. Data evaluation, statistics and kinetic calculations

The quantitative data evaluation was performed with the TraceFinder software, whereas the comparison of different analytical methods was enabled by the Skyline software. The concentration data calculated by the software based on external calibration was corrected with the dilution factors and converted into µM units.

The transformation rate values were calculated as following:

$$\mathbf{v} = \frac{\mathbf{c_0 - c}}{\mathbf{t * P}} \qquad \textbf{Equation 1}$$

v: transformation rate
c_0: toxin concentration at the beginning of the incubation
c: toxin concentration after a certain incubation time
t: incubation time
P: protein content of the incubation solution in mg/L

The calculated metabolic rates for AOH and AME between 0 and 10 minutes were fitted to the Michaelis−Menten enzyme-kinetic model, performing a nonlinear regression with OriginPro 2019b. Moreover, a linear regression was applied with the same software.

The statistical analyses of the data were also performed with OriginPro 2019b. The results were tested for normal distribution using the Shapiro-Wilk test and subjected to a Nalimov outlier test. The outliers and the negative concentration or transformation rate values were excluded from the results.

Different groups of datasets were compared with the one-way analysis of variance (ANOVA). If a significant difference could be detected that way ($p < 0.05$), a post-hoc 'Fisher's least significant difference test' (LSD) was applied. In this case, the significance levels were marked in the graphs as follows:

* → $0.01 < p < 0.05$
** → $0.001 < p < 0.01$
*** → $p < 0.001$

4.5.2. HR-MS measurements

4.5.2.1. Analysis method

The analysis of the HR-MS samples was performed on a Vanquish UHPLC system connected to a dual-pressure linear trap-quadrupole-orbitrap mass analyser (Velos), equipped with an ESI interface, in both positive and negative mode. A Supelco Ascentis Express C18 column (10 cm × 2.1 mm, 2.7 µm) was used as the stationary phase. Furthermore, a 2 mm long C18 pre-column was attached to the main column to extend its lifetime. Eluent A was an aqueous ammonium acetate (5 mM, pH adjusted to 8.6 with a 25 % NH_4OH solution), whereas methanol acted as eluent B. A multi-step gradient at a flow rate of 0.4 mL/min was applied. After 1 min at 10 % eluent B, this percentage was linearly raised to 100 % at the 11th minute. Subsequently, the column was purged with 100 % of eluent B for two additional minutes. Finally, the initial eluent composition was reset between minutes 13 and 13.5, followed by a 2-minute re-equilibration under these conditions, resulting in a total run time of 15.5 minutes. The HR-MS measurements were conducted by Dr. Elisabeth Varga.

4.5.2.2. Reference solutions and data evaluation

The data evaluation was carried out with the XCalibur and Skyline software. The transitions of various metabolites were monitored to enable their identification, as further discussed in section 5.6.3. Additionally, the measurement of the *Alternaria* reference mixture allowed an estimated quantification, as well as differentiating between two constitutional isomers of the same metabolite.

4.5.3. Cell culture

4.5.3.1. General remarks

During this work, all cell culture experiments were carried out with the human hepatoma cell line HepG2. The cultivation, passage, seeding, and incubation of the cells with toxins took place in a cell culture laboratory under a sterile laminar flow hood. Several consumables – such as serological pipettes, cell culture flasks, and 96-well plates – were marketed already sterilised and individually packed by the manufacturer. Others – e. g. microtubes, pipette tips, Pasteur pipettes – were treated with pressurised, saturated steam in an autoclave and were consequently dried in an oven to remove the remaining moisture. The sterilisation step of the autoclaving lasted for 20 minutes at 134 °C, followed by 30 minutes of drying at 120 °C. Also, the package of all materials and the nitrile gloves of the operator were sprayed with 70 % aqueous ethanol before working under the laminar flow hood. Prior to coming into contact with the cells, every chemical – such as medium, PBS, trypsin – was pre-heated in a water bath to 37 °C. The incubators worked at the same temperature, with a 5 % CO_2-supplemented atmosphere.

The Roswell Park Memorial Institute (RPMI) 1640 medium was used for cultivating HepG2 cells, facilitating their optimal growth with several nutrients. It contains 20 different L-amino acids, including L-glutamine, 11 vitamins, 6 inorganic salts, as well as reduced glutathione, D-glucose, and phenol red (Moore *et al*., 1967; website of Thermo Fisher Scientific). The latter is used to indicate the change of the initial pH value – approx. 7.2 – due to the production of acidic metabolites, such as lactate. The resulting colour change from red to orange suggests the need for a medium exchange. Another reason for the acidification of the medium might be bacterial contamination (Gstraunthaler and Lindl, 2013). The commercial RPMI 1640 medium was supplemented with 10 % heat-inactivated foetal bovine serum (FBS) since it contains hormones and growth factors. The addition of 1 % penicillin-streptomycin (P/S) aided in avoiding bacterial growth within the cell culture.

4.5.3.2. Thawing of cryopreserved HepG2 cells

HepG2 cell stocks (1 mL in a cryogenic tube) were stored either in liquid nitrogen, or at -80 °C, in a medium containing 10 % dimethyl sulphoxide (DMSO). After thawing up the cell suspension in a water bath, it was critical to work quickly since the cells do not tolerate such high amounts of DMSO in a liquid state. So, 50 mL of the medium was prepared by adding 20 % FBS and 1 % P/S to the pre-heated, commercial RPMI 1640 medium already before thawing the cells. The pipetting of 0.5 mL medium to the cell stock was followed by resuspension of the cells. Then the resulting suspension was split into two aliquots, transferred into 1.5 mL microtubes, and centrifuged for 2 minutes and 300 *g*. The supernatant containing the solvent was carefully removed, whereas the pellet was re-suspended with 1 mL medium. Both aliquots of cell suspension were combined in a T25 cell culture flask. The empty microtubes were rinsed with 1 mL medium each, and these liquids were also

transferred into the flask. Lastly, 6 mL of the medium was added, and the flask was placed into the incubator (37 °C, humidified atmosphere with 5 % CO_2). This process was carried out by Dr. Georg Aichinger. After 2-3 days, the cells were attached, and medium change was reasonable. The old medium was removed, and 10 mL fresh full medium was added to the cells. Further three days of incubation were followed by splitting the cells as described in the following subchapter.

4.5.3.3. Passaging/splitting of HepG2 cells

When the confluence of the cells within the monolayer in the cell culture flask becomes too high, their proliferation rate decreases enormously due to the lack of space. Thus, passaging the cells is essential, and it is recommended to be conducted twice a week in case of HepG2 cells. The following volume measurements concern T75 flasks since they were predominantly used during this work.

Before passaging the cells, they were examined under a light microscope to estimate the confluency (targeted 65-90 %) and detect possible contamination. Then, under a laminar flow hood, the used medium was discarded with a sterile Pasteur pipette attached to a vacuum pump. The remaining cell layer was washed with around 10 mL of phosphate-buffered saline (PBS) to remove the residues of FBS and divalent cations because they might otherwise inhibit the next step. The aspiration of PBS was followed by adding 2.5 mL of trypsin – a pancreas protease, cleaving peptide bonds by the C terminus of arginine and lysine (Gstraunthaler and Lindl, 2013). After the trypsin solution was scattered on the surface of the cells, the cell culture flask was placed back into the incubator until the cell layer was completely detached from the plastic surface (3-7 minutes). Additionally, the cells were removed mechanically by gently tapping the side walls of the flask. The enzyme activity was then terminated by the dilution with 10 mL of the full medium (RPMI 1640, 10 % FBS, 1 % P/S). Subsequently, the cell islands were singularised, and the suspension was homogenised by pipetting up and down in a serological pipette attached to a Pipetus. Then the suspension was transferred into a clean 50 mL tube, and the cell number was determined (subchapter 4.5.3.4). A part of the cell suspension containing 800,000 to 1 million cells was pipetted into a T75 cell culture flask and was combined with approximately 15-20 mL full medium. After gentle homogenisation, the flask was placed into a sterile incubator.

4.5.3.4. Determination of the cell count

When the cell count is calculated, and a constant number of cells is seeded in the TC flask during passaging, the optimal date of the following splitting is easier to predict. Also, seeding a particular number of cells in all wells of a well plate by performing assays is essential to ensure reproducibility and comparability of the results.

After the cell suspension was transferred into a 50 mL tube, it was gently homogenised, and 20 µL of it was mixed in a microtube with 80 µL of Trypan blue. The latter acts as a so-called vital dye, staining the medium and dead cells blue. Contrary, living cells stay unstained since their intact cell membranes exclude the dye (Gstraunthaler and Lindl, 2013). By pipetting the resulting blue suspension between a Neubauer-improved haemocytometer and its cover glass, the number of living (and if necessary, dead) cells can be counted within a precisely determined volume. As Figure 7 depicts, the counting chamber used in this work consists of two identical fields, where 10 µL dyed cell suspension can be filled, respectively. Each part

contains four 1×1 mm fields (highlighted in orange), divided into 16 equal squares, which facilitate tracking the counting process. The depth of the chamber is 0.1 mm, resulting in a total volume of 0.1 mm^3, corresponding to 0.1 µL. As the cell number was determined in all fields, only cells located at two of four edges (marked in red) were counted in case the cells were on the outer lines.

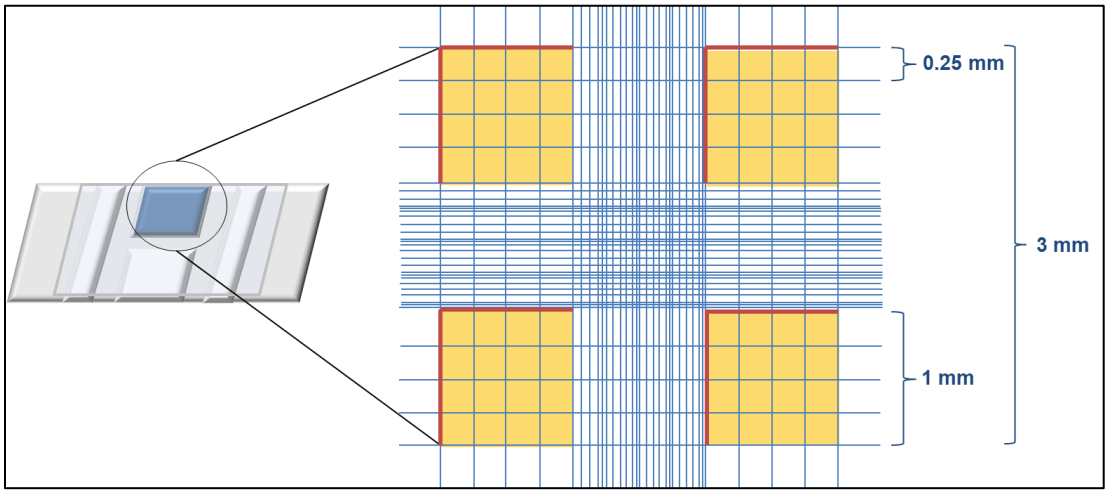

Figure 7: Haemocytometer for the determination of cell count

The mean value of the cell number within the four fields was calculated, as described in the following formula:

$$\text{cell number per mL} = \frac{\text{mean cell number per field} \cdot \text{dilution factor}}{\text{field volume}} = \frac{\text{mean cell number per field} \cdot 5}{0.0001\ \text{mL}} =$$

$$= 50{,}000 \cdot \text{mean cell number per field} \qquad \textbf{Equation 2}$$

As the necessary cell number was specified, the required volume of cell suspension could be calculated (Equation 3). It was then seeded in the TC flask or 96-well plate depending on the further purpose and diluted with the corresponding amount of medium.

$$\text{required volume} = \frac{\text{required cell number} \cdot 1\ \text{mL}}{\text{cell number per mL}} \qquad \textbf{Equation 3}$$

4.5.4. Incubation studies of HepG2 cells

4.5.4.1. Cell seeding for incubation studies

The incubation studies of HepG2 cells with alternariol or alternariol monomethyl ether were conducted in 96-well plates. The position of the samples was changed within the biological replicates to prevent possible systematic errors deriving from minor evaporation differences of the incubation solution in differently located wells. Also, the wells at the edge of the plate were supplied in general with 100 µL PBS, so no cell seeding was required for these wells. Consequently, around 60 wells included HepG2 cells in a plate. Since usually two plates were incubated simultaneously, and 6500 cells in 100 µL medium were seeded, 16,000 µL total medium volumes were prepared, including excess. After determining the cell count (subsection 4.5.3.4), the total necessary cell number was calculated as follows:

$$\text{total cell number} = \frac{\text{cell number per well} \cdot \text{total medium volume}}{\text{medium volume per well}} = \frac{6500 \cdot 16{,}000\ \mu l}{100\ \mu l} = 1{,}040{,}000 \qquad \textbf{Equation 4}$$

Then the required volume of cell suspension for this cell number was defined (Equation 3) and pipetted into a 50 mL tube. It was completed to 16 mL with RPMI 1640 medium, including 10 % FBS and 1 % P/S. The resulting solution was homogenised, and 100 µL of that was distributed into the relevant wells by a multi-stepper pipette. Lastly, the plates were placed into a sterile incubator for 72 hours.

The passage number specifies the number of passages before and after the cryopreservation. After thawing, it is advisable to carry out some subcultivation steps before conducting an assay; however, when a total passage number of 20-30 is reached, the cells should be discarded, otherwise undesired genetic and phenotypic drifts may occur (Gstraunthaler and Lindl, 2013; Vinken and Rogiers, 2015). The passage numbers of the HepG2 cells seeded for incubation studies are listed below.

First biological replicate:	p10+4
Second biological replicate:	p10+11
Third biological replicate:	p10+3

4.5.4.2. Preparation of incubation solutions

The desired concentration of the mycotoxin stock solutions for the HepG2 incubations was 2 mM. For the AOH stock solution, 514 mg toxin was weighed in on a microbalance in a 2 mL tube. Then it was dissolved in 995 µL DMSO and thoroughly homogenised using a vortexer and an ultrasonic bath. Analogously, 818 mg AME was mixed with 1.50 mL DMSO. The stocks were stored at -80 °C when they were not in use. Additionally, the stocks were diluted to fit in the calibration range and measured *via* LC-QqQ in triplicates to determine their actual toxin concentration.

Beyond the general toxin incubations, also four different types of controls were carried out (Table 6). Firstly, for evaporation control (EC), no cells were required since it aimed to indicate the potential change of toxin concentration due to the evaporation of the solvent. Therefore, it was essential to know the intended position of the EC in the 96-well plate while cell seeding and leave it without cultured HepG2 cells. As the presence of the respective toxin was desired, the same incubation mix could be used for EC, as for the general samples. The total volume of the incubation solution was calculated knowing that 100 µL was needed per well. It was advisable to prepare it in a relatively high excess since it tended to foam. To do so, the selected medium (with or without 10 % FBS) was pipetted into a 5 mL microtube, and the respective toxin stock was added in a concentration of 10 µM. The final amount of DMSO was 1 %, inclusive the solvent of the toxin stock.

Table 6: Control incubations of HepG2 cells

Control solution	Abbreviation	Cells	Medium	Toxin
Solvent control	SC	Yes	Yes	No
Evaporation control	EC	No	Yes	Yes
Control before protein precipitation (PP)	BPP	Yes	Yes	Yes, but only before PP
Control after protein precipitation	APP	Yes	Yes	Yes, but only after PP

The solvent control (1 % DMSO) and the two protein precipitation controls (also 1 % DMSO) did not include toxin solutions during incubation, so a different incubation mix was prepared for these controls. In a 2 mL tube, 1 % DMSO was added to the medium (with or without 10 % FBS).

In the main experiment, the incubation times varied between 0-18 hours. Each plate was divided into two theoretical sections to enable exact sampling times despite the broad time range. Wells with 10 hours of incubation time or below formed the so-called first batch of the plate, meaning that the incubation with the respective toxin or control solution started on a morning, 72 hours after cell seeding. The "second batch" described wells with the desired incubation time of 14-18 hours, where the incubation started around 8.5 hours after the first batch, enabling convenient sampling the next day. The incubation plans of all 96-well plates are depicted in Appendix I. The abbreviations used therein correspond to the control solutions described in Table 6, whereas the wells marked with bold font refer to the first batch of incubation within the plate. The preliminary test could be performed by incubating the whole plate at once because of the limited number of incubation times.

4.5.4.3. Incubation and taking samples

When the pre-heated (37 °C) and homogenised incubation solutions were prepared, the old medium of the respective wells was aspirated with a pipette tip connected to a vacuum pump. Then, 100 µL of the incubation mix was added in each well using a multi-stepper pipette, and the plate was returned to the incubator.

After the desired incubation time had passed, 35 µL of the wells' content was pipetted into a labelled 1.5 mL microtube, while its residues were discarded. Then, 50 µL RIPA buffer was added to the well providing the lysis of the cells, enabling the subsequent protein quantification using the BCA assay. The plate was placed into the incubator until the last sample with the longest incubation time was taken, then the plate was stored at -80 °C until the BCA assay was performed.

The so-called 0-minute-samples were taken directly from the respective incubation solution without getting into contact with the cells and the well plate. The following sample preparation steps were performed analogously for all samples.

Immediately after sampling, the protein precipitation took place. For that, 70 µL extraction solvent (ACN/MeOH, 1:1, v/v) was pipetted into the 1.5 mL microtube containing the sample, and everything was homogenised with a vortexer. Lastly, it was stored at -20 °C for at least 1 hour before LC-MS sample preparation.

The toxin content of the BPP and APP controls were compared to detect possible losses of the toxin concentration during the protein precipitation. The appellations of the PP controls refer to the time point of the addition of the respective toxin stock, which – for BPP – happened before protein precipitation. Therefore, not the general extraction solvent was pipetted to this type of samples. The BPP extraction solvent was prepared in a 5 mL tube by pipetting 5 µL AOH or AME stock into 1995 µL of the extraction solution. The later sample preparation steps of BPP were carried out similarly to the other samples. The preparation of the APP samples is described in the following subsection.

4.5.4.4. HepG2 sample preparation for HPLC-QqQ measurements

After protein precipitation, the samples were centrifuged for 15 minutes, at 17,000-18,040 *g* and 4 °C. They were stored on ice, while the supernatant of each sample was diluted with methanol-water (1:1 or 3:7, v/v) in labelled HPLC vials. The remaining non-diluted supernatant of one technical replicate was used for preparing the HR-MS samples, as described in subchapter 4.5.5.6.

The HepG2 samples were incubated with 10 µM toxin solutions. The calibration curve of AOH was linear in the range of 0.1-50 µg/L, whereas that of AME between 0.02 and 20 µg/L. Therefore, 30 µL of the AOH samples were pipetted into 570 µL dilution solvent (dilution factor: 20), allowing the final concentration to be in the linear calibration range. In the case of AME, a higher dilution factor (75) was necessary: 20 µL sample was added to 1480 µL dilution solution.

The APP control was treated differently than other HepG2 samples since the respective toxin solution was added after the protein precipitation (see also subsection 4.5.4.3). First, 20 µL of the 2 mM toxin stocks (preparation described in subchapter 4.5.4.2) were pre-diluted in 980 µL dilution solvent. Then, 18 µL of the resulting AOH solution was added to 4182 µL dilution solvent. In the case of AME, 10 µL of the pre-diluted mixture was pipetted into 9090 µL dilution solvent. The resulting modified dilution solvent was used to prepare the APP control samples as described above.

4.5.4.5. Bicinchoninic acid (BCA) assay

The determination of the total protein content per well was necessary to compare the quantitative results obtained in HepG2 experiments with the data of microsomal incubations. The method of choice was the bicinchoninic acid assay or Smith assay. During this colorimetric reaction, BCA gets deprotonated in an alkaline environment. The consequently formed chelate between two BCA anions and a Cu^{2+} ion has a green colour. In the presence of proteins, this chelate becomes purple due to the reduction of the divalent copper cation to Cu^{+}. Thus, the absorbance measured by around 562 nm is direct proportional to the total protein amount of a sample (Otieno *et al*., 2016).

The BCA assay kit included 1 mL aliquots of a 2 mg/mL bovine serum albumin solution as a protein standard. The standard range was prepared in 1.5 mL tubes by diluting with double-distilled water (ddH_2O), as described in Table 7. For one single plate, 10 mL reagent A (BCA) and 200 µL reagent B ($CuSO_4$ solution) were mixed in a 15 mL tube, and 100 µL of the resulting solution was dispensed into the wells of a clean 96-well plate using a multi-stepper pipette. The other plate – including the cell lysate – was shaken for 300 seconds in a plate reader and brought to room temperature. Then 5 µL of each sample was pipetted into the well at the respective position of the new plate. Since the original TC plate included several wells containing only PBS and no cells, these spots of the new plate could be used for at least three replicates of the standard range. For that, 10 µL of each reference solution was pipetted in the chosen wells. Although the optimal method would have been keeping the volume of the cell lysate and the standards the same, the difference between the pipetted amounts ensured that all the measured results fit into the calibration curve. The accurate and fast operation was essential in this step to ensure the comparability of the data regarding different wells because the reaction the assay begins already at room temperature.

Table 7: Pipetting scheme for the preparation of BCA standard solutions

c_{final} (mg/mL)	1.2	1.0	0.8	0.6	0.4	0.2	0
$V_{standard}$ (µL)	360	200	160	120	80	40	0
V_{water} (µL)	240	200	240	380	320	360	400

The plate was then placed into a pre-heated plate reader, and the following program was started at 37 °C:

Shaking for 60 seconds
Waiting for 30 minutes
Shaking for 10 seconds
Photometric measurement at 570 nm

The original protein content was determined by obtaining the calibration line based on the standard measurements, consequent linear regression, and multiplication with a dilution factor of two. The absorbance value of the blank had to be subtracted from all the results before further calculations.

4.5.5. Incubation studies of liver microsomes

4.5.5.1. Preparation of porcine liver microsomes and determination of the protein content

The liver of a female Edelschwein pig was freshly purchased on the morning of slaughtering and processed based on the microsome preparation procedure kindly provided by Francesco Crudo, PhD. The entire preparation process was carried out on ice as quickly as possible to maintain the enzyme activity of the microsomes. Nevertheless, the incubation studies of the microsomal suspension obtained in the first attempt led to unsatisfying results regarding enzyme activity and reproducibility within different aliquots. Therefore, the preparation procedure was repeated, and the data deriving from the incubation studies of the first batch of microsomes are considered preliminary results, contributing only to the acquisition of the assay, but providing no reliable quantitative information. Besides the microsomes, the S9 mix and cytosolic fraction were also collected and aliquoted for future experiments.

The production of the microsomal suspension and the incubation assays with *Alternaria* toxins were carried out in a non-sterile environment. However, the labware was autoclaved before use to prevent undesired contaminations. All buffers were prepared in advance and were stored at 4 °C. To produce the washing buffer, 9.0 g sodium chloride was weighed in a Duran flask and dissolved in 1 L of distilled water. In total, 2 L of it was used for the temporary storage of the liver during delivery and for washing the whole liver, as well as the liver pieces before homogenisation. For the storage buffer, 15.8 g Tris-HCl was added into a 2 L Duran flask, dissolved in nearly 2 L of distilled water. Then a pH value of 7.4 was set with concentrated sodium hydroxide. Lastly, the flask was filled up to the mark, resulting in the desired 0.05 M Tris-HCl solution. The homogenisation buffer contained 88.2 g sucrose, 0.3 g EDTA, and 1 L of the storage buffer. Hence, its composition was 0.05 M Tris-HCl, 1 mM EDTA, and 0.25 M sucrose.

The steps of the microsome preparation sketched in Figure 4 are depicted in more detail in Figure 8 with pictures. The liver was first cut with clean scissors into small (2-4 cm) parts, which were placed on a Petri dish filled with ice-cold washing buffer. They were thoroughly washed to remove as much blood as possible and then shredded into even smaller pieces (0.5-1 cm).

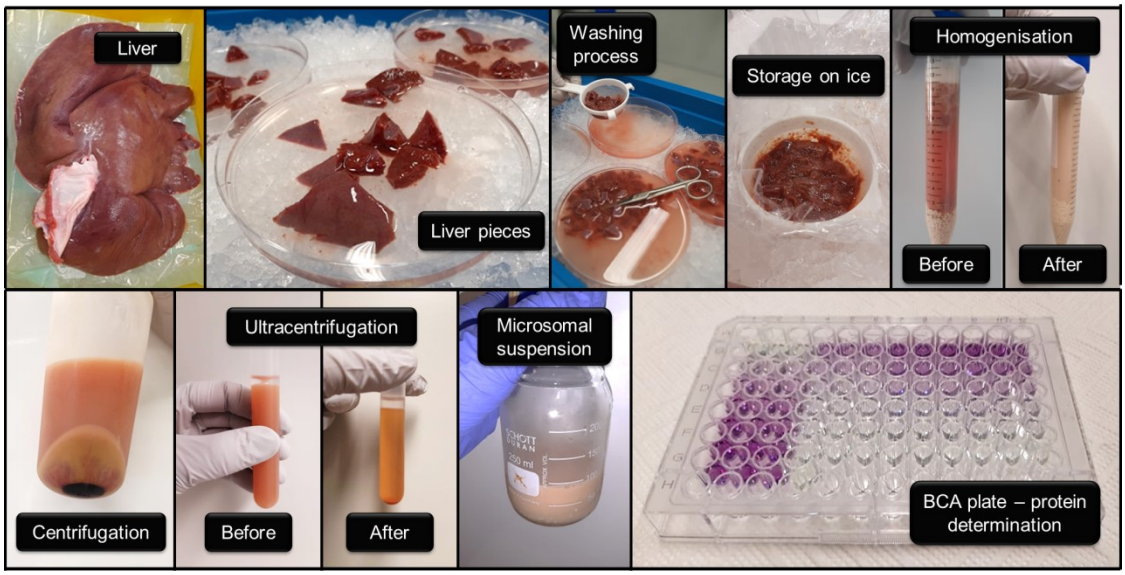

Figure 8: Preparation of porcine liver microsomes

After a sieve was filled with the liver pieces, they were washed with around 100 mL washing solution. We found that the easiest way to shred the pieces is careful squeezing through the sieve after washing, which has been reported to lead to the highest protein activity, as well (Jagow *et al*., 1965).

One part – around 2.5 g – of the liver pieces was filled into a 15 mL homogeniser tube, already provided with lysing matrix. Then three parts, approximately 7.5 mL of the homogenisation buffer was added. Twelve tubes were collected that way, tightly closed with the screw cap, and placed into the homogeniser. The following program was run twice to make the homogenisation as complete as possible:

Adapter:	TeenPrep
Time:	40 sec
Speed:	4.5 m/sec
Lysing matrix:	D
Quantity:	12 mL
Pause time:	193 sec
Cycles:	1

The resulting liver homogenate was filtered through a clean sieve to remove the remaining large liver particles and the lysing matrix (the latter was reused for the next batch of samples deriving from the same liver). The filtrates of every tube were combined and centrifuged at 9,000 *g* for 20 minutes at 4 °C. Most of the supernatant (S9 mix) was further processed, but around 150 mL was aliquoted in 1.5 mL microtubes and stored at -80 °C for future experiments. Each of six ultracentrifugation tubes was filled with approximately 9 mL of the supernatant. Then, the liquid level was overlaid with mineral oil so that the weights of the tubes did not differ more than 5 mg. Thereafter, the ultracentrifugation was carried out at

100,000 *g*, for 1 hour, at 4 °C. The required amount (around 80 mL) of the resulting supernatant – the so-called cytosolic fraction – was aliquoted and stored at -80 °C until further use. After removing all residues of the supernatant, the microsomal pellet was resuspended with 2 mL of the storage buffer. When even after up-and-down pipetting, as well as vortexing insoluble particles remained, the suspension was centrifuged for additional five minutes (1,000 *g*, 4 °C). Then it was filtered through a sieve, and the final microsomal fraction was obtained as the filtrate. The desired amount of the microsomal suspension (ca. 100 mL) could be produced by performing seven subsequent homogenisation, three centrifugation, and seven ultracentrifugation steps. Lastly, it was homogenised, aliquoted into 1.5 mL tubes, and stored at -80 °C.

The protein content of the prepared subcellular fractions was determined with the BCA assay. Several dilutions of each sample were prepared in 500 µL tubes and measured, ensuring that at least one of the triplicates of each suspension is within the calibration range. Table 8 summarises the pipetting scheme of these dilutions, whereas the plate design of this assay is depicted in Appendix II. The experimental workflow and the data evaluation were analogous, as described in subsection 4.5.4.5, but the dilution factors were different.

Table 8: Diluting samples for BCA assay

Dilution factor	Sample (µL)	Storage buffer (µL)
2	50	50
4	50	150
6	50	250
8	50	350

4.5.5.2. Preparation of the reagents

Al-Subeihi *et al.* (2012) published a protocol to investigate the metabolism of methyleugenol. The slight modification of this workflow was used for the liver microsomal incubations of AOH and AME.

The toxin stocks utilised for this assay were more concentrated than in the case of cell culture experiments. On a microbalance, 1186 µg AOH was weighed in a 1.5 mL tube and dissolved in 457 µL DMSO. Similarly, 352 µL solvent was added to 480 µg AME. Both stocks were homogenised not only by vortexing, but also by ultrasonication. These toxin solutions were then further diluted, as summarised in Table 9. Additionally, the stocks were diluted to fit in the calibration range and measured *via* LC-QqQ in triplicates to determine their actual toxin concentration.

Furthermore, Tris-HCl (pH adjusted to 7.4 with 10 M sodium hydroxide) as a buffer, NADPH as co-factor of phase I metabolic reactions, and ascorbic acid as co-factor regenerating substance were included in the incubation solution. Therefore, they were also prepared in advance (Table 9). Tris-HCl was stored at -20 °C, whereas the other solutions at -80 °C while they were not in use.

Table 9: Preparation of stock solutions for liver microsomal incubations

Solution	Preparation					End volume (µL)
	Chemical		Solvent		Concentration (mM)	
Ascorbic acid stock	10.5	solid (mg)	596	Tris-HCl (µL)	100	596
NADPH stock	61.2	solid (mg)	243	Tris-HCl (µL)	300	243
Tris-HCl pH adjusted to 7.4	31.5	solid (g)	1.0	water (L)	200	1,000,000
AOH 0.1 mM	1	10 mM stock (µL)	99	DMSO (µL)	0.1	100
AOH 1 mM	5	10 mM stock (µL)	45	DMSO (µL)	1	50
AOH 2 mM	5	10 mM stock (µL)	20	DMSO (µL)	2	25
AOH 5 mM	10	10 mM stock (µL)	10	DMSO (µL)	5	20
AOH 10 mM	20	10 mM stock (µL)	0	DMSO (µL)	10	20
AME 0.1 mM	2	5 mM stock (µL)	98	DMSO (µL)	0.1	100
AME 1 mM	5	5 mM stock (µL)	20	DMSO (µL)	1	25
AME 2 mM	6	5 mM stock (µL)	9	DMSO (µL)	2	15
AME 5 mM	10	5 mM stock (µL)	0	DMSO (µL)	5	10

4.5.5.3. Porcine liver microsomal incubation

As mentioned in subchapter 4.5.5.1, the porcine hepatic microsomes were produced as a part of this work, distributed into 1 mL aliquots, and stored at -80 °C. Due to the high availability of the porcine liver microsomes, the preliminary experiments were conducted with this biological material.

All preparation steps before the pre-incubation were carried out on ice to prevent the early loss of microsomal activity. The final toxin concentrations were set to 1, 10, 20, and 50 µM for AME, and to 1, 10, 20, 50, and 100 µM in the case of AOH. The investigated incubation times were 0, 5, 10, 20, 30, and 60 minutes in preliminary experiments. However, the last two time points were omitted in some replicates of the main experiments. Since 35 µL sample was taken at each time point, the final volume of each incubation mixture was 300 µL in preliminary studies, whereas 200 µL was proved to be enough for the main experiments. The incubation mix contained a final concentration of 3 mM NADPH and 1 mM ascorbic acid in 200 mM Tris-HCl (pH 7.4). These values were easy to achieve by the 1:100 dilution of the prepared NADPH and ascorbic acid stocks (Table 9).

The protein content in the incubation solution was adjusted to 2 mg/mL, knowing the total protein concentration of the original microsomal suspensions due to BCA measurements:

Porcine liver microsomes, first batch (BCA): 16 mg/mL
Porcine liver microsomes, second batch (BCA): 9 mg/mL

The pre-incubation (37 °C, 250-300 rpm, 1 min) was followed by adding the toxins. To achieve the desired AOH or AME concentration, the corresponding prepared toxin solution (Table 9) was pipetted to the incubation mixture in a 1:100 dilution.

The solvent control was performed by substituting the toxin stock with DMSO. The NADPH-control was carried out by excluding NAPDH from the incubation solution. These controls were treated in the same manner as other samples of the setup, except that the solvent control was only sampled at three time points during the whole incubation process.

In the so-called heat inactivated control, the microsomal enzymes were inactivated through heat treatment at 98 °C for 10 minutes (250-300 rpm). In the first preliminary experiments, the sampling of this control was carried out according to the general protocol. Nevertheless, due to the heating and consequent protein denaturation, taking a representative sample was not possible. As an alternative method, the volume of the incubation solution of the heat control was doubled to allow centrifugation for 1.5 minutes at 10 °C and 21,380 *g* before each sampling. However, placing the incubation mixture into the centrifuge stopped the incubation process leading to the change of test conditions. Eventually, in the main experiments, three incubations of the heat control were set up with 100 µL total incubation mixture, each one corresponding to one desired sampling time point, at the beginning, middle, and end of the whole incubation. The sampling of the heat control was carried out – other than the general sampling protocol described in subsection 4.5.5.5 – by directly adding 200 µL dilution solvent to the corresponding incubation solution in the desired time point. Consequently, a more representative sampling could be guaranteed by terminating possibly occurring enzyme reactions this way rather than taking out samples from the inhomogeneous control solution.

4.5.5.4. Rat and human liver microsomal incubation

In contrast to porcine, human and rat liver microsomes were purchased from commercial sources. Therefore, much lower volumes of these suspensions were available. The delivered amounts were divided into aliquots around 65 µL each and stored at -80 °C.

The lower availability of these microsomal suspensions necessitated changes compared to the workflow of porcine microsomes; however, the main experimental setup remained the same as described in subchapter 4.5.5.3. The protein content in the incubation solution was adjusted to 1 mg/mL, whereas the initial protein concentration of both suspensions claimed by the manufacturer was 20 mg/mL.

The investigated incubation times were reduced to 0, 5, and 10 minutes. Since only 30 µL sample was taken at each time point, 100 µL of incubation mixture was proved to be sufficient per sample.

The reproducibility of these assays was especially desired as the amount of feasible technical replicates was limited. Pipetting volumes below 5 µL for the hundredfold dilution of the prepared toxin solutions might have led to uncertainty of the results. Therefore, they were pre-diluted (1:10) with a modified incubation mixture, which excluded the microsomal suspension. In this case, the reaction was started by adding the diluted toxin solution to the complete incubation mixture in a 1:10 ratio. The heat-inactivation control was carried out according to the final protocol of the porcine hepatic microsomal incubations.

4.5.5.5. Sampling and sample preparation for HPLC-QqQ measurements

When the planned incubation time has passed, one part (35 or 30 µL) of the respective incubation mixture was pipetted into a labelled 1.5 mL tube containing three parts (105 or 90 µL) of ice-cold extraction solution (ACN/MeOH, 1:1, v/v). In that way, the metabolic reactions could be terminated. After vortexing, the samples were placed into the freezer (-20 °C) for 1-16 hours, facilitating protein precipitation, which was followed by preparing the HPLC samples.

After protein precipitation, the samples were centrifuged for 15 minutes, at 17,000-18,040 *g* and 4 °C. They were stored on ice, while the supernatant of each sample was diluted with methanol-water (1:1 or 3:7, v/v) in labelled HPLC vials. The pipetting scheme of the microsomal samples is depicted in Table 10 and Table 11. Some of the dilutions were performed in two subsequent steps to avoid pipetting of small and hence inaccurate volumes. When the total sample volume did not exceed 200 µL, micro-inserts with conical bottom were used to raise the fluid level enabling the sample injection in liquid chromatograph. Similarly, below a sample volume of 300 µL, micro-inserts with flat bottom were placed into the vial. After closing the vials, the samples were homogenised and analysed *via* HPLC-QqQ. The remaining undiluted samples deriving from HepG2 or microsomal incubations were not discarded, but saved for HR-MS measurements and stored at -80 °C.

Table 10: Pipetting scheme of alternariol samples of microsomal incubations

Toxin concentration in the incubation solution (µM)	First dilution		Second dilution	
	Sample volume (µL)	Solvent volume (µL)	Sample volume (µL)	Solvent volume (µL)
1	20	140	-	-
10	20	1480	-	-
20	20	80	30	870
50	20	180	30	870
100	20	380	30	870

Table 11: Pipetting scheme of alternariol monomethyl ether samples of microsomal incubations

Toxin concentration in the incubation solution (µM)	First dilution		Second dilution	
	Sample volume (µL)	Solvent volume (µL)	Sample volume (µL)	Solvent volume (µL)
1	30	670	-	-
10	7	1393	-	-
20	20	380	50	950
50	20	380	20	980

4.5.5.6. Sample preparation for HR-MS measurements

After protein precipitation, a small amount of each sample was diluted to enable the quantification of AOH, AME, and their potential major metabolites *via* HPLC-QqQ, as described for HepG2 and liver microsomal incubation samples in subsections 4.5.4.4 and 4.5.5.5, respectively. However, the HR-MS measurement of the undiluted

samples was necessary to enable detecting metabolites obtained in lower percentages. Therefore, the remaining samples were transferred into HPLC vials containing micro-inserts with conical bottom. The remaining volumes of microsomal samples per technical replicate were not enough for analysis. Consequently, pooled samples were prepared by pipetting defined amounts of each technical replicate, including samples from preliminary experiments. The pipetting scheme is summarised in Table 12. The mixed *Alternaria* toxin standard was co-measured to facilitate qualitative assignment of the analytes.

Table 12: Preparation of the HR-MS samples.
Each HepG2 incubation samples derive from one biological and technical replicate, whereas the microsomal incubation samples are pooled obtained by mixing the samples of several different technical replicates. The abbreviation LM points to liver microsomes as *in vitro* models.

Sample no.	Toxin	*In vitro* model	Toxin concentration (µM)	Incubation time (min)	Number of technical replicates per sample	Volume per replicate (µL)
1174	AOH	HepG2 cells	20	0	1	remaining amount
1181	AOH	HepG2 cells	20	480	1	remaining amount
1193	AOH	HepG2 cells	20	1080	1	remaining amount
1197	AME	HepG2 cells	20	0	1	remaining amount
1205	AME	HepG2 cells	20	480	1	remaining amount
1218	AME	HepG2 cells	20	1080	1	remaining amount
3388	AOH	Porcine LM lot 2	10	0	7	15
3389	AOH	Porcine LM lot 2	10	10		
3390	AOH	Porcine LM lot 2	10	20		
3391	AOH	Porcine LM lot 2	10	60	4	
3392	AME	Porcine LM lot 2	10	0	6	
3393	AME	Porcine LM lot 2	10	10		
3394	AME	Porcine LM lot 2	10	20		
3395	AME	Porcine LM lot 2	10	60	3	
3396	AOH	Rat LM	10	0	4	
3397	AOH	Rat LM	10	10		
3398	AME	Rat LM	10	0	4	
3399	AME	Rat LM	10	10		
3400	AOH	Human LM	10	0	4	
3401	AOH	Human LM	10	10		
3402	AME	Human LM	10	0	5	10
3403	AME	Human LM	10	10		

5. Results and discussion

5.1. Quantification *via* HPLC-QqQ

5.1.1. Method adaptation

The comparison of two analytical procedures published by Puntscher *et al.* (2018, 2019) was the first step of the method adaptation. For this, the same standard solutions and HepG2 incubation samples were measured with both methods. The resulting chromatograms indicate that the shorter method published in 2018 led to satisfying peak shapes for all analytes contrary to the longer one. Figure 9 depicts an example for a fronting peak in detecting alternariol monomethyl ether-3*O*-sulphate with the 20-minute method. Furthermore, this method uses aqueous NH_4F solution as an eluent A, which is considered toxic for aquatic organisms and requires different waste disposal than less harmful chemicals. Overall, due to the listed advantages and the shorter run time, the 15.5-minute method was used for further experiments.

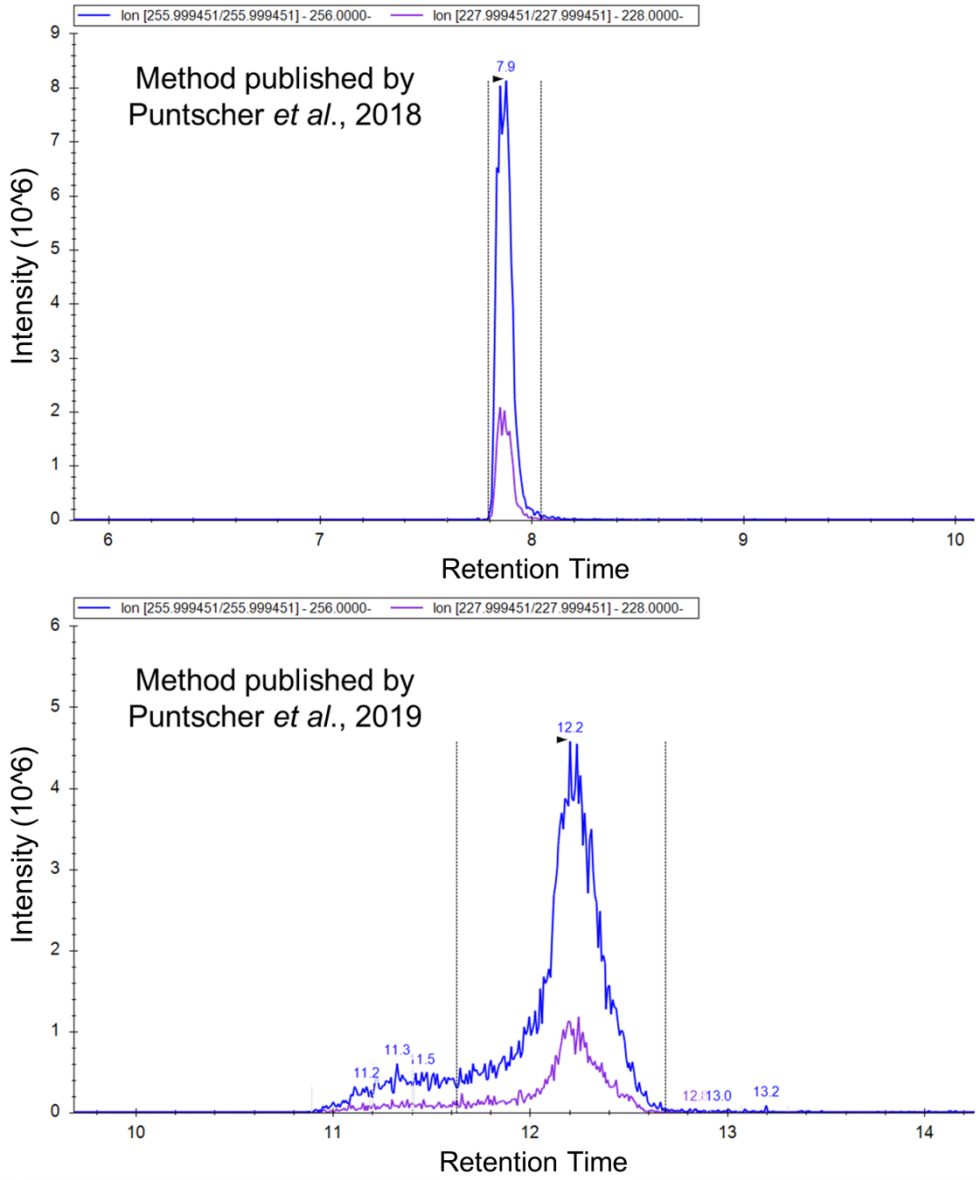

Figure 9: Comparison of two published LC-MS methods regarding the peak shape in the case of the analyte AME-3-S. Please notice the difference of the retention time values between the two depicted chromatograms.

By aiming the selection of the optimal eluent A composition for the chromatographic separation of the four targeted analytes (AOH, AME, and their sulphates), three different eluents were compared in a broad pH range (pH 3.0-8.6). The measurement of the *Alternaria* reference mixture was followed by examining the peak shape and area of the analytes in each transition. For some analytes, such as AOH (Figure 10), the chromatographic separation with LC-MS grade water as eluent A resulted in the highest sensitivity, whereas the alkaline eluent showed overall an acceptable sensitivity. However, the peak shape of the sulphates (such as AOH-3-S, Figure 11) was unsatisfactory in the case of water as eluent, while the alkaline eluent led to more optimal peak shapes for all analytes. Consequently, aqueous NH_4OAc (5 mM, pH adjusted to 8.6 with 25 % ammonia solution) was chosen as eluent A for later analyses.

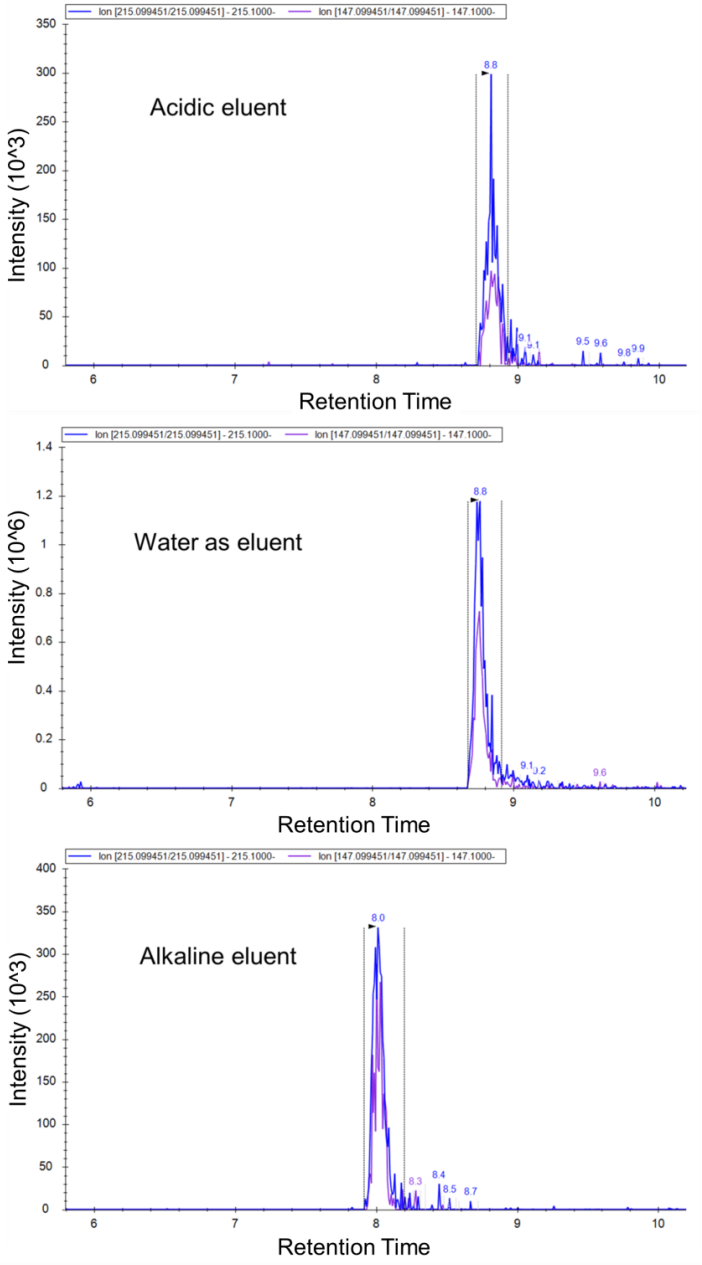

Figure 10: Eluent optimisation – analyte AOH. Please notice the difference in the intensity scale between the depicted chromatograms. STD30 of the multi-component *Alternaria* reference mix (AOH concentration: 30 µg/L) was measured in several replicates, one replicate is depicted.

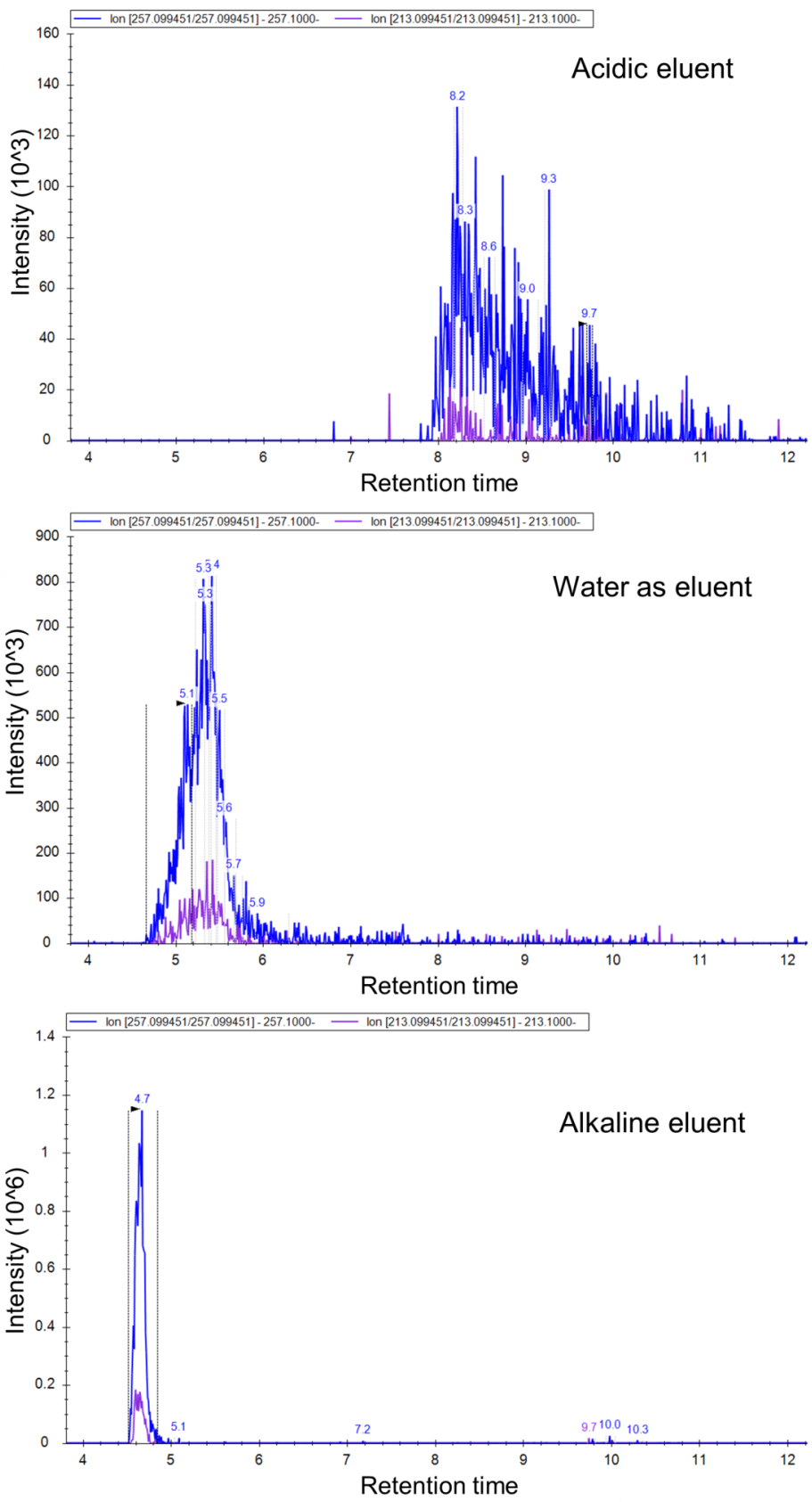

Figure 11: Eluent optimisation – analyte AOH-3-S. Please notice the difference in the intensity scale between the depicted chromatograms. STD30 of the multi-component *Alternaria* reference mix (AOH-3-S concentration: 30 µg/L) was measured in several replicates, one replicate is depicted.

Finally, the comparison of five analytical methods with different run time values (6, 8, 10, 12, 15 minutes) was carried out. As depicted in Figure 12, the chromatogram obtained with the 6-minute method shows the co-elution of AOH and AME-3-S, whereas the 15-minute method provides their baseline separation. As a compromise, the total duration of 10 minutes was chosen for the final method to spare time and still enable the distinction of these two – rarely co-occurring – analytes.

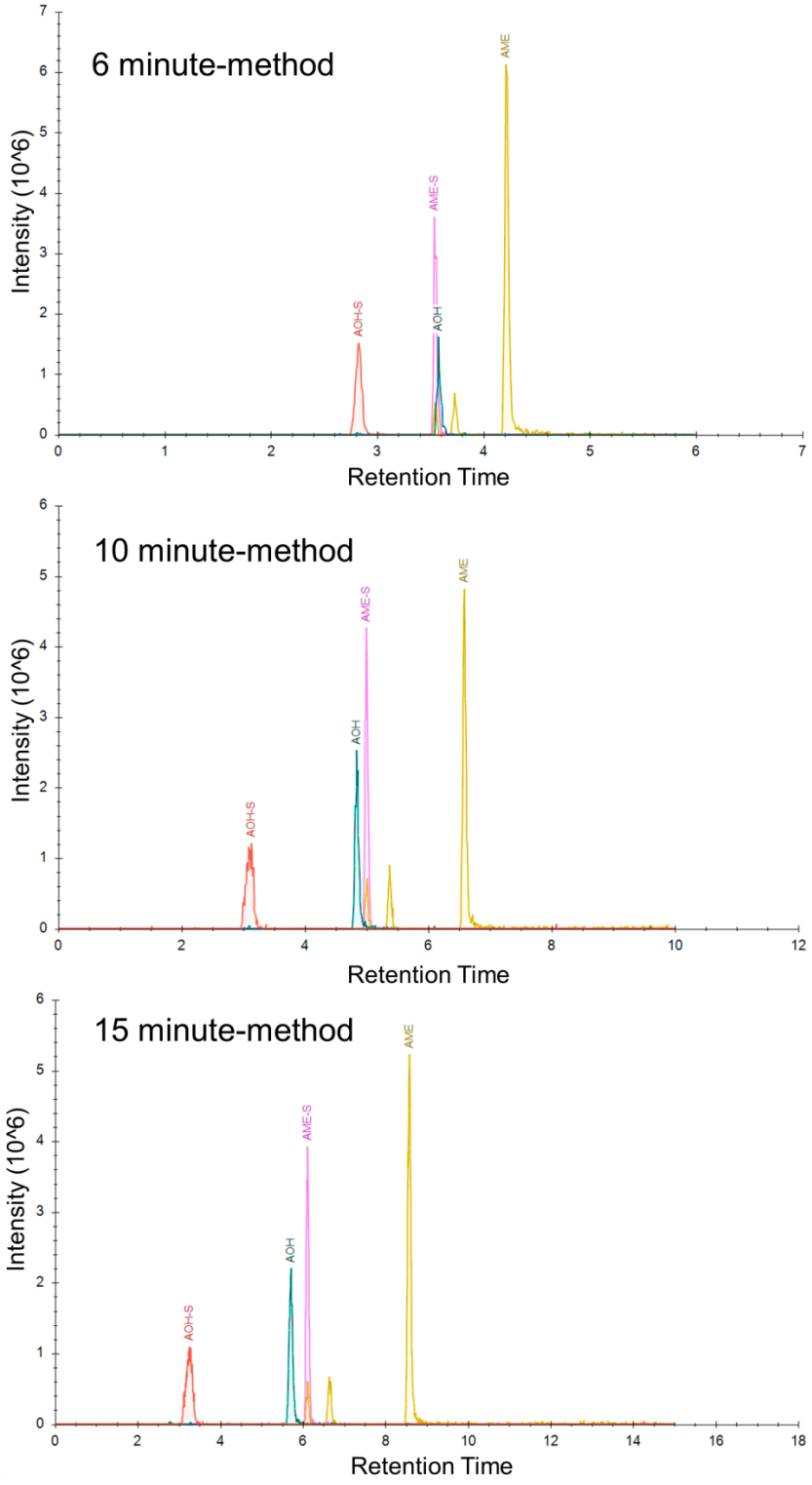

Figure 12: Run time comparison
Please notice the difference of the retention time values between the two depicted chromatograms. Colour code: green – AOH, yellow – AME, red – AOH-3-S, magenta – AME-3-S

5.1.2. Measuring the composition of the reference and stock solutions

As Table 13 indicates, by using the calibration set of the analytical standard mixture for the absolute quantification of AOH and AME in the *Alternaria* multi-component reference solution, a considerably high deviation from the nominal concentration can be observed. The aforementioned confirms the assumption that the *Alternaria* reference mix is only suitable for a magnitude concentration assessment rather than for quantification. Although an operation error is not to exclude by the preparation of both reference mixtures, the reliability of the analytical standard is higher considering that it was freshly prepared.

Table 13: Absolute quantification of AOH and AME in *Alternaria* reference mixture

Name	AOH concentration (µg/L)			AME concentration (µg/L)		
	Nominal	Analytical standard mixture	*Alternaria* reference mixture	Nominal	Analytical standard mixture	*Alternaria* reference mixture
STD 100	100	100.3	86.77	20	20.22	26.97
STD 50	50	50.15	43.39	10	10.11	13.48
STD 30	30	30.09	26.03	8	8.088	10.79
STD 10	10	10.03	8.677	2	2.022	2.697
STD 3	3	3.009	2.603	0.8	0.8088	1.079
STD 1	1	1.003	0.8677	0.2	0.2022	0.2697
STD 0.3	0.3	0.3009	0.2603	0.08	0.08088	0.1079
STD 0.1	0.1	0.1003	0.08677	0.02	0.02022	0.02697

Since the absolute quantification of AOH and AME was based on a calibration set diluted from the analytical standard mix, ensuring the trueness of its nominal toxin content was of particular importance. Therefore, the cross-contamination of the single AOH and AME standards was determined, as they were used for preparing the standard mix. In the 200 µg/L AOH reference solution, 0.038 µg/L AME could be detected, representing an AME contamination of 0.014 %. On the contrary, the observed AOH amount was below the lowest limit of quantification in a 40 µg/L AME standard solution. This extent of cross-contamination should not significantly change the performed analytical results.

Additionally, the toxin concentration of all used stock solutions was determined based on the measurement of three replicates (Table 14). The small weighed quantity of the solid toxins, their incomplete dissolution, as well as operator error might be some causes for a difference between the actual and the nominal toxin concentration.

Table 14: Concentration of AOH and AME in the used toxin stock solutions.

Name	Used for	Nominal AOH concentration (mM)	Measured AOH concentration (mM)		Nominal AME concentration (mM)	Measured AME concentration (mM)	
			Mean	RSD		Mean	RSD
AOH Stock 2 mM	HepG2 incubations	2	2.4	14%	0	< LLOQ	-
AME Stock 2 mM		0	0.042	4%	2	1.8	7%
AOH Stock 10 mM	Microsomal incubations	10	8.0	1%	0	< LLOQ	-
AME Stock 5 mM		0	0.28	0.5%	5	5.0	9%

5.1.3. Analytical performance parameters

Based on the signal-to-noise ratio of the lowest calibration solution, the estimated LOD and LOQ of the final HPLC-QqQ method is in the lower ng/L scale for all four analytes. However, the quantification below the concentration of the lowest calibration solution cannot be representative and was therefore not performed. Hence, in the measurement solution, the lower limit of quantification (LLOQ) of AOH, AOH-3-S, and AME-3-S was 0.1 µg/L, whereas the LLOQ of AME was 0.02 µg/L.

When it comes to sensitivity, the expectable variation of this parameter has to be mentioned. Unfortunately, the change of sensitivity is particularly characteristic for studies like this, where numerous samples are analysed over an extended period. By measuring a reference toxin solution of the same concentration in every sequence, the change in the detected peak area and so in the sensitivity can be monitored. For this purpose, STD30 was analysed, containing 30 µg/L of AOH and 6.67 µg/L of AME. Overall, higher sensitivity, but also higher variation was observable for the analyte AME (Figure 13 and Figure 14). As the measured reference mixture – and even the stock solution it was diluted from – contained both toxins, the difference in the peak area profile of these analytes cannot be caused by pipette error, but by a change in the instrumental sensitivity.

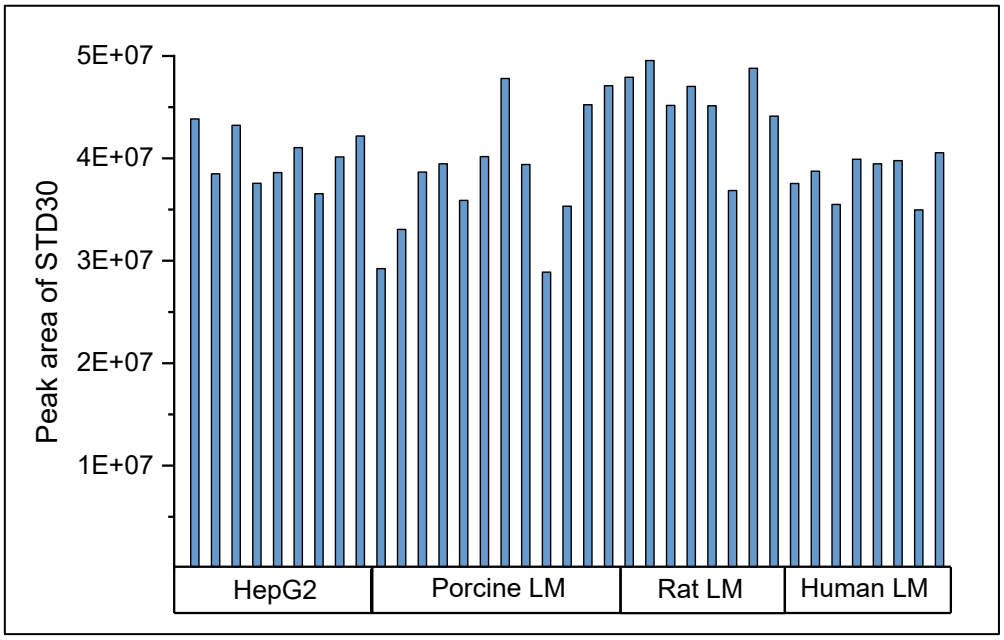

Figure 13: Sensitivity variation of AOH based on the measurement of STD30 in every started analytical sequence. Each data point represents a single analytical result, randomly selected from the several standard measurements of each sequence. The abbreviation LM stands for liver microsome experiments.

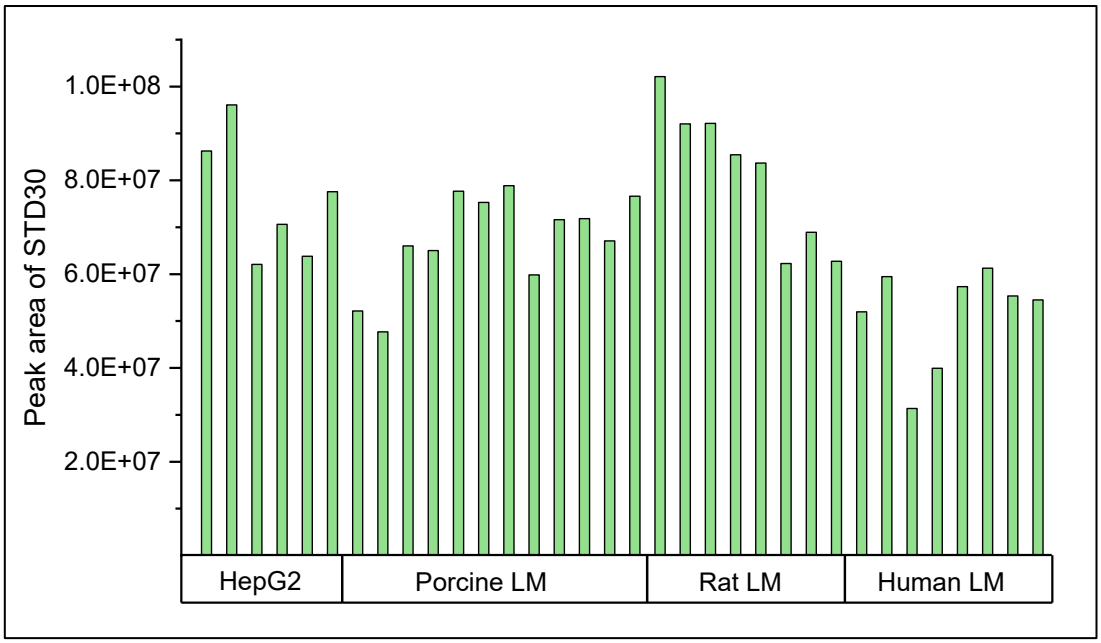

Figure 14: Sensitivity variation of AME based on the measurement of STD30 in every started analytical sequence. Each data point represents a single analytical result, randomly selected from the several standard measurements of each sequence. The abbreviation LM stands for liver microsome experiments.

Besides the changing sensitivity of the LC-MS/MS detection, multiple factors contribute to the uncertainty of the final analytical results, often expressed as standard deviation (SD). Figure 15 groups and summarises potential sources of the variability of the microsomal incubation assay in the form of an Ishikawa cause-and-effect fish-bone diagram. Additionally, the analytical method also carries uncertainty, as illustrated analogously in Figure 16.

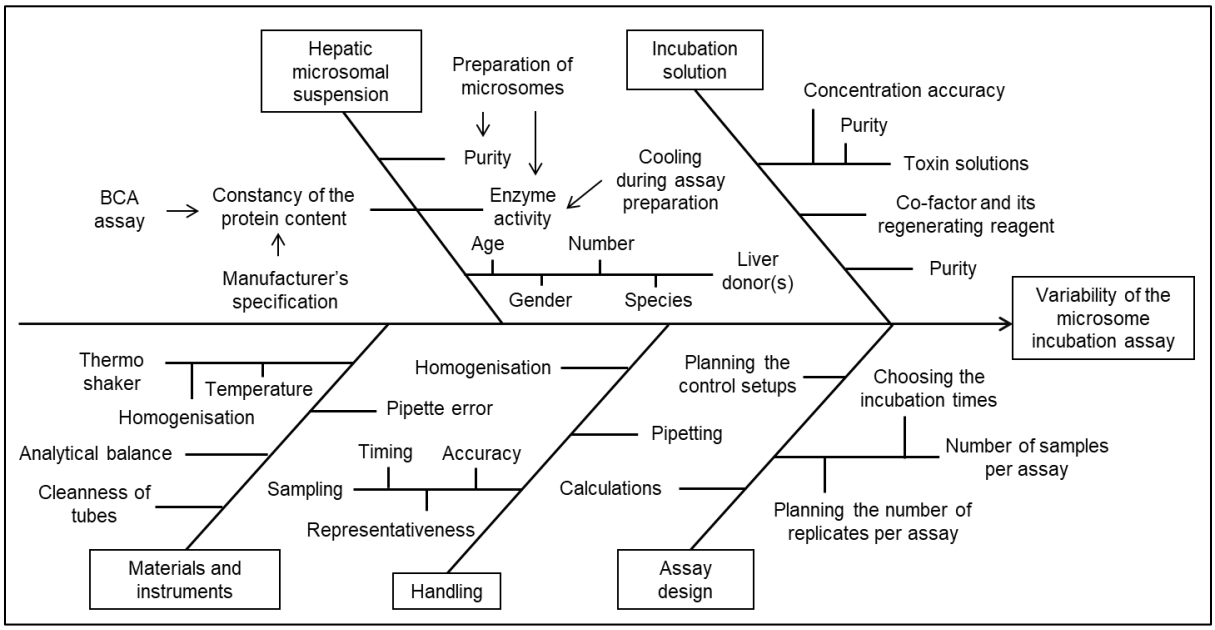

Figure 15: Ishikawa diagram depicting some possible reasons for the variability of the outcome in microsomal incubation assays

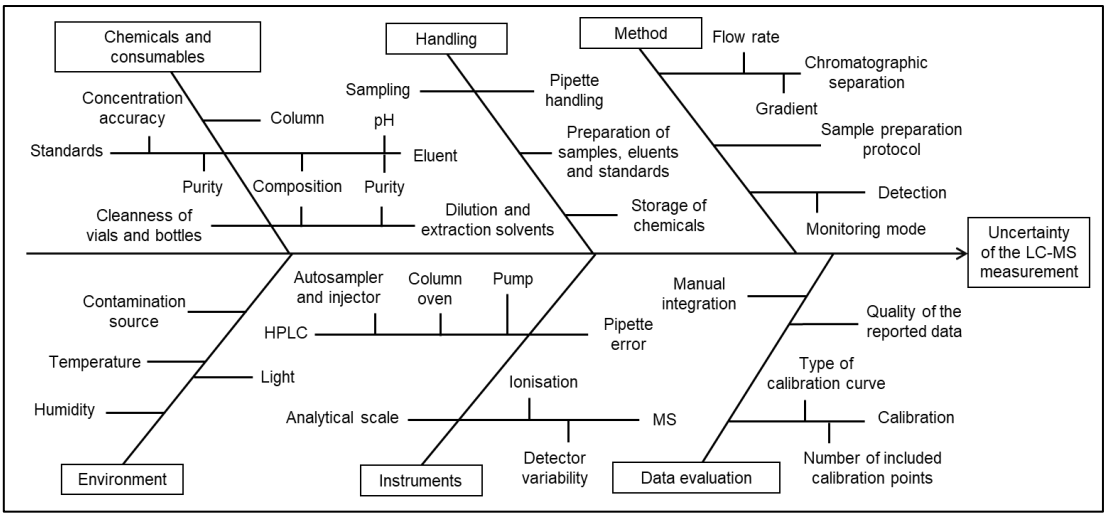

Figure 16: Ishikawa diagram depicting some possible sources for the uncertainty of LC-MS measurements

5.2. Measurements of HepG2 incubation samples

5.2.1. Preliminary results – HepG2 incubations

Although several studies were conducted in HepG2 cells addressing adverse effects of AOH and AME (section 2.3.2), kinetic data regarding the metabolism of these *Alternaria* toxins in the HepG2 cell line is scarce. By monitoring the changing amount of parent toxins due to the cells' biotransformation, choosing the reasonable incubation concentration was of great importance. Since Juan-García *et al.* (2015) reported the IC_{50} value of AOH to be 96 ± 3.1 µM after 24 hours of exposure, in HepG2 cells, a much lower incubation concentration was chosen – 10 µM for both AOH and AME.

The preliminary results contain the data of one biological and two technical replicates. Graph I. in both Figure 17 and Figure 18 shows the concentration profile of the parent toxins. Although the standard deviation values – especially these of AOH – are high, the necessity of further data points between 2 and 24 hours can be assumed, enabling monitoring a concentration decrease due to metabolic activity.

The gene expression of sulphotransferases was reported to be even higher in HepG2 cells than in primary human hepatocytes, in contrast to most of the detoxifying enzymes (Hessel-Pras *et al.*, 2019). Hence, we expected sulphates to be the main metabolites obtained in the HepG2 incubation assays. Indeed, already 30 minutes of incubation with the respective toxins led to sulphate concentrations high enough to be detectable not only during the HR-MS measurement of the non-diluted samples, but even in the HPLC-QqQ analysis of the diluted samples.

Since the *Alternaria* reference mix contained AOH-3-S and AME-3-S, the measurement of the calibration set prepared from this mixture allowed the quantification and qualitative assignment of these particular sulphate metabolites of the parent toxins. As a result, an increasing tendency in the AOH-3-S and AME-3-S concentration could be observed through the incubation with AOH or AME, respectively (Graph II. of Figure 17 and Figure 18). Moreover, the exposure of HepG2 cells towards AOH led to the formation of an additional sulphate metabolite not included in the *Alternaria* standard mix, which was also included by the data evaluation of the main experiments.

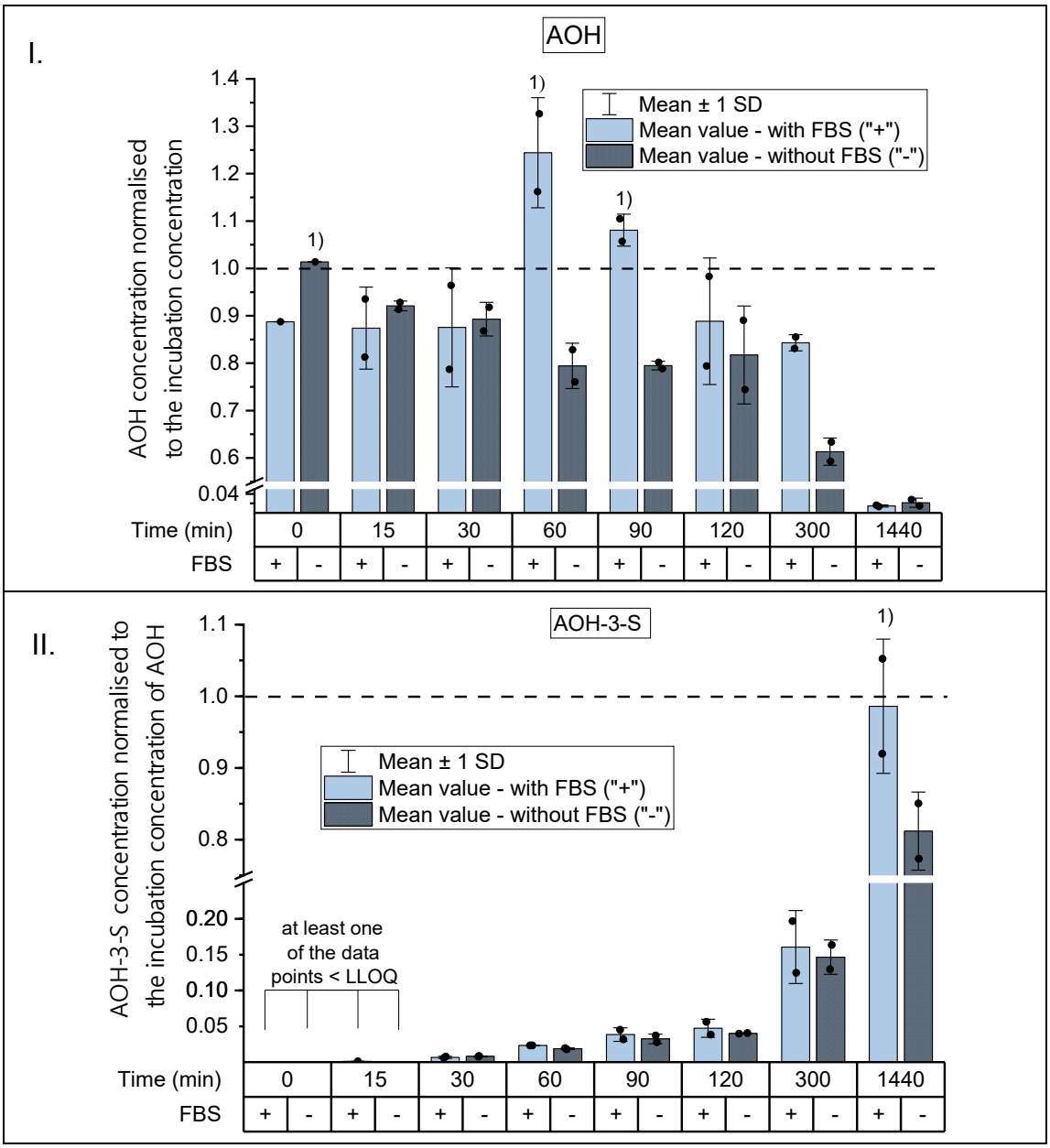

Figure 17: Preliminary results of HepG2 incubations with 10 µM AOH
The data illustrates the decrease in the AOH amount (Graph I.) and the increase in the AOH-3-S amount (Graph II.) in HepG2 cells, normalised to the nominal starting AOH concentration (10 µM) after zero to 1440 minutes of incubation. The average of duplicates within one biological replicate is shown ± standard deviation. Samples at the incubation time of zero minutes were taken directly from the incubation solution, without contact to the cells. Bars marked with 1) represent datasets, where at least one of the depicted data was above the calibration range.

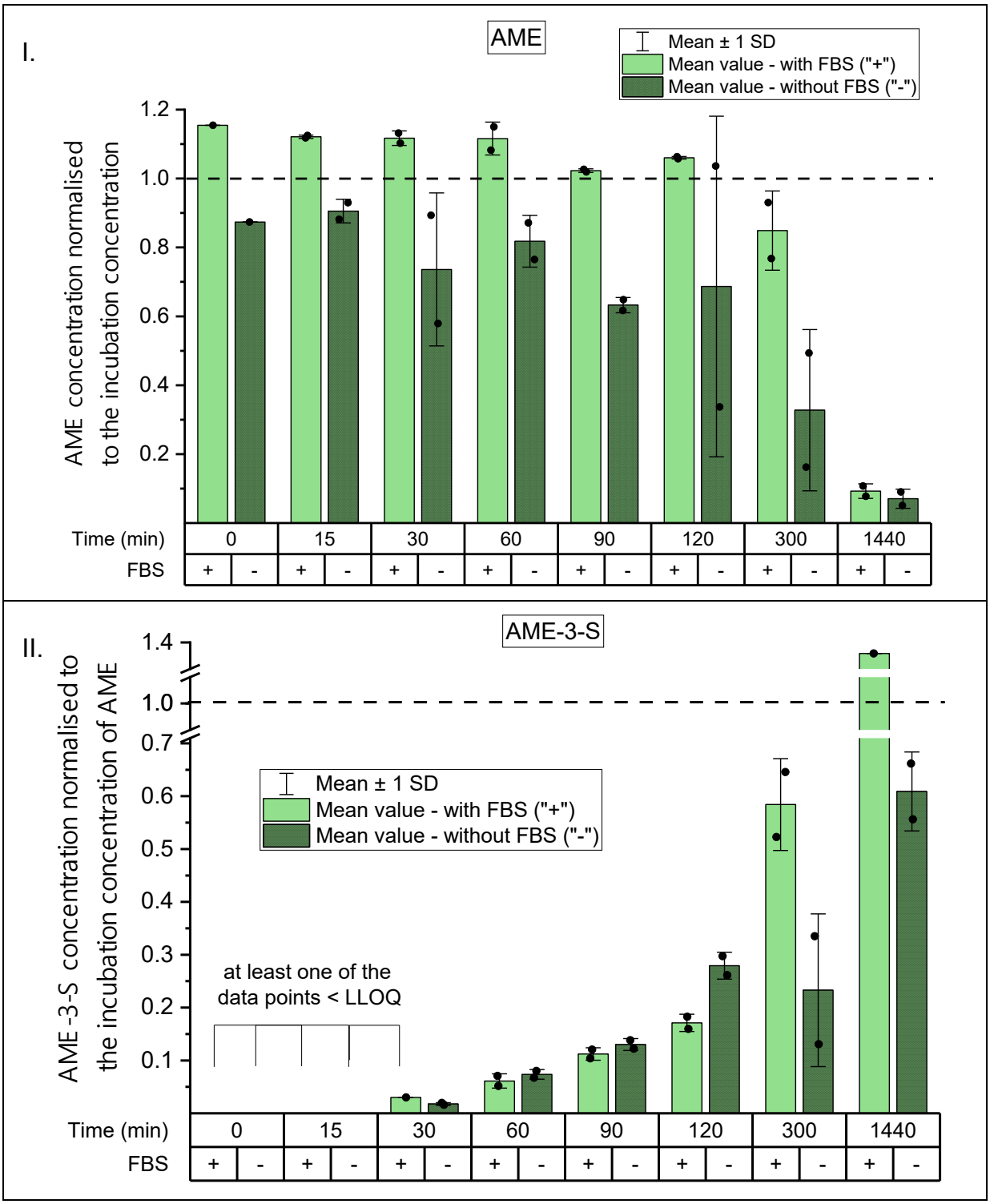

Figure 18: Preliminary results of HepG2 incubations with AME
The data illustrates the decrease in the AME amount (Graph I.) and the increase in the AME-3-S amount (Graph II.) in HepG2 cells, normalised to the nominal starting AME concentration (10 µM) after zero to 1440 minutes of incubation. The average of duplicates within one biological replicate is shown ± standard deviation. Samples at the incubation time of zero minutes were taken directly from the incubation solution, without contact to the cells.

5.2.2. Main experiments – HepG2 incubations

5.2.2.1. Concentration profile of AOH, AME, and their sulphates in HepG2 incubations

In the main experiment, three biological replicates of HepG2 cells were incubated with 10 µM AOH or AME, for 0-18 hours, in three technical replicates each. The analytical results obtained in the quantification of the parent toxins and their sulphate metabolites are depicted in Figure 19 and Figure 20, where each data point represents one biological replicate. Since the incubation of every plate was performed in two steps (see subsection 4.5.4.2), two data points belong to each biological replicate by 0 hours.

This initial concentration of AOH or AME decreased significantly after 4 hours in nearly every case, except when FBS was not present by incubating with AOH (Graph I in Figure 19 and Figure 20). Even there is a decreasing tendency observable already after 4 hours; however, the slightly lower measured data of the first biological replicate resulted in a higher standard deviation, which is why no significant difference could be detected. As this deviation applies to the initial concentration values of AOH and its metabolites, and is not characteristic for AME and AME-3-S, not the difference in the metabolic activity of the three biological replicates, but another causative factor might be responsible for this variation.

Besides the quantification of AOH, AME, and their 3*O*-sulphates, another AOH sulphate not included in the *Alternaria* standard mix was also detected. Since no reference substance was available for this metabolite – labelled as AOH-x-S – its structural alignment was not evident. Both in the HPLC-QqQ and the HR-MS measurements – under RP-LC conditions – this compound eluted later than AOH-3-S (Table 4). Therefore, the potentiality of AOH-x-S carrying the sulphate moiety at position 9-*O* should be considered since, under comparable circumstances, the same elution order of these sulphates was reported (Soukup *et al*., 2016). However, further investigations would be needed to confirm this assumption.

Despite the lack of standard, a relative quantification of the AOH-x-S concentration (c) was possible based on the AOH-3-S reference material and assuming a similar behaviour during the MS measurements:

$$\mathbf{c_{AOH-x-S}} = \frac{\mathbf{peak\ area_{AOH-x-S}}}{\mathbf{peak\ area_{AOH-3-S}}} * \mathbf{c_{AOH-3-S}} \qquad \textbf{Equation 5}$$

While no sulphate metabolites could be detected in the initial incubation solution, the HepG2 metabolism led to a quantifiable amount of all three obtained sulphates, already after 4 hours (Figure 19/II. and III., Figure 20/II.). Moreover, after maximal 18 hours of incubation, the measured AOH-x-S and AME-3-S levels reached and occasionally even exceed the initial concentration of the respective parent toxins. Even assuming the detected sulphates being the only significant metabolites for both parent mycotoxins in this *in vitro* system, the total concentration of the respective sulphate(s) and the remaining parent toxin should stay constant and not exceed the initial incubation concentration. Hence, Figure 21 and Figure 22 were created to study the total concentration profile further. Regardless of the presence of FBS, the sum of AOH and AOH-3-S remains around the expected value or slightly below. In contrast, when the concentration of AOH-x-S is included, much higher concentration levels are reached, and an increasing tendency is observable. When analysing these

results, it has to be kept in mind that the AOH stock solution used for HepG2 samples had an about 20 % higher measured concentration than intended (Table 14). Also, the *Alternaria* reference solution was not freshly prepared, so it carries a more pronounced uncertainty. And most importantly, the relative quantification of AOH-x-S is based on the AOH-3-S standard, assuming the same ionisation efficiency as well as matrix suppression or enhancement effects for both analytes, which seems to be not the case based on the observed data. Therefore, handling the quantitative data of the AOH sulphates with caution is advisable. However, the significance of describing this metabolic pattern of AOH in this cell line for the first time – to the best of our knowledge – should not be underestimated.

Similarly, the total level of the AME and AME-3-S is changing over the expected concentration value (Figure 22). A pronounced increase in the concentration level can be especially seen after 10 and 14 hours of incubation. As the second incubation batch of all plates starts by 14 hours, a variation between the toxin concentration of the first and second incubation solution might explain this discrepancy. Also, these results show relatively high standard deviations, so that this difference to the expected total concentration level is not significant.

Interestingly, independent from the presence or absence of FBS in the incubation solution, similar AOH levels were measured, whereas, in the case of AME, a significant difference was detected by every time point between the data obtained in FBS-containing and serum-free assay conditions (Figure 19 and Figure 20). By measuring the sulphate metabolites, in the vast majority of the monitored time points, no significant difference could be detected between conducting the assay with or without FBS, primarily due to the high standard deviation. However, tendentiously lower levels of all analytes can be observed when performing the assay without FBS in the incubation medium. Further investigations would be necessary to see if this is the consequence of matrix effects in the LC-MS/MS analysis or the result of an influence on the cellular processes. Overall, since a statistically relevant difference only occurred for one analyte and the cell cultivation always took place in a medium containing 10 % FBS, this aspect was not further studied during this work.

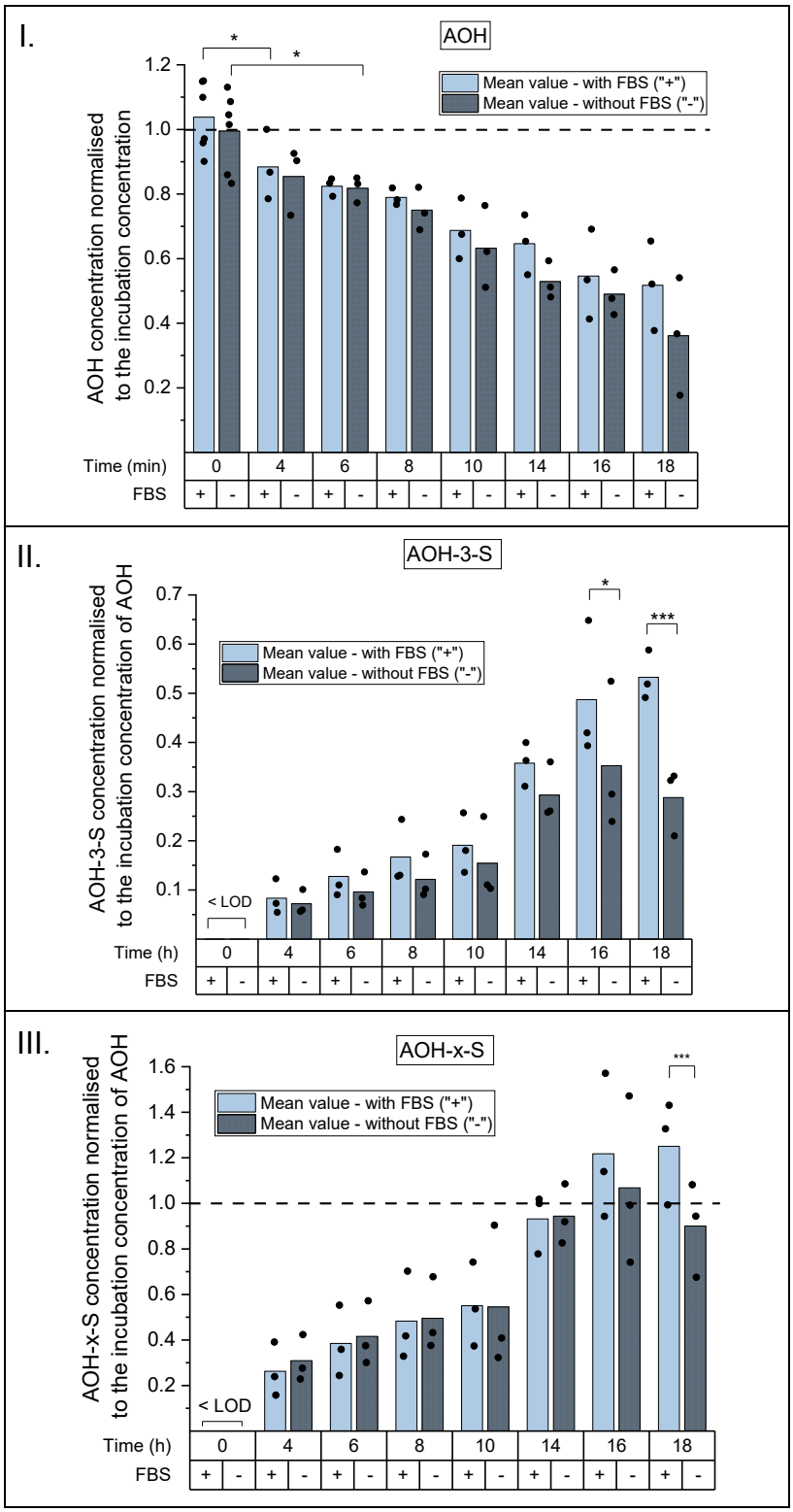

Figure 19: Incubation of HepG2 cells with 10 µM AOH – main experiment
The data illustrates the decrease in the AOH amount (Graph I.) and the increase in the AOH-3-S, as well as AOH-x-S amount (Graph II. and III., respectively) in HepG2 cells, normalised to the nominal starting AOH concentration (10 µM) after zero to 18 hours of incubation. Each data point represents the average of three technical replicates within one biological replicate, each bar shows the average of all biological replicates. Samples at the incubation time of zero hours were taken directly from the incubation solution, without contact to the cells. After testing for normality, one-way ANOVA, followed by Fisher`s LSD post-hoc test was used for testing significant differences. The significance levels were marked in the graphs as follows: * → 0.01 < p < 0.05; ** → 0.001 < p < 0.01; *** → p < 0.001.

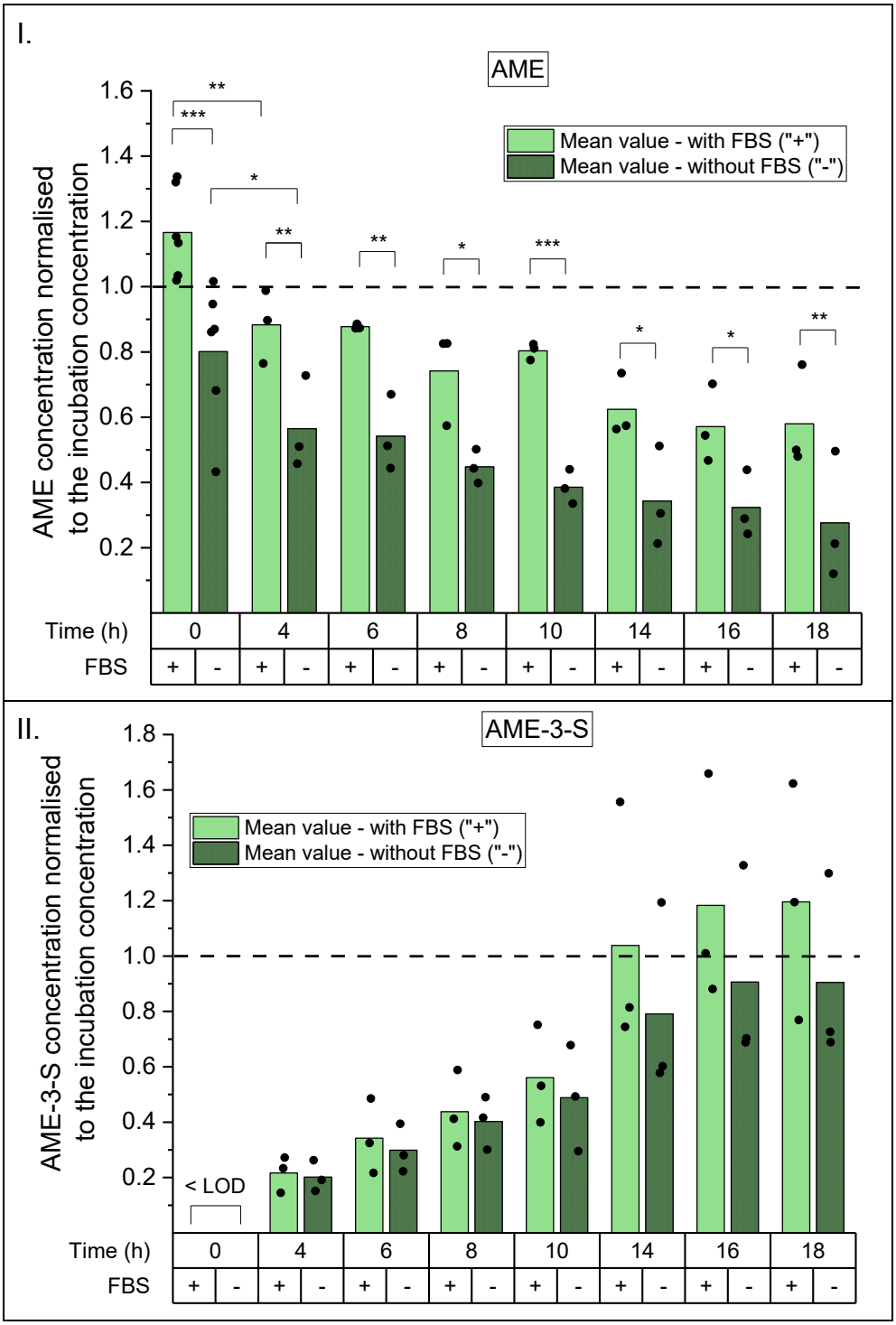

Figure 20: Incubation of HepG2 cells with 10 µM AME – main experiment
The data illustrates the decrease in the AME amount (Graph I.) and the increase in the AME-3-S amount (Graph II.) in HepG2 cells, normalised to the nominal starting AME concentration (10 µM) after zero to 18 hours of incubation. Each data point represents the average of three technical replicates within one biological replicate; each bar shows the average of all biological replicates. Samples at the incubation time of zero hours were taken directly from the incubation solution, without contact to the cells. After testing for normality, one-way ANOVA, followed by Fisher`s LSD post-hoc test was used for testing significant differences. The significance levels were marked in the graphs as follows:
* → $0.01 < p < 0.05$; ** → $0.001 < p < 0.01$; *** → $p < 0.001$.

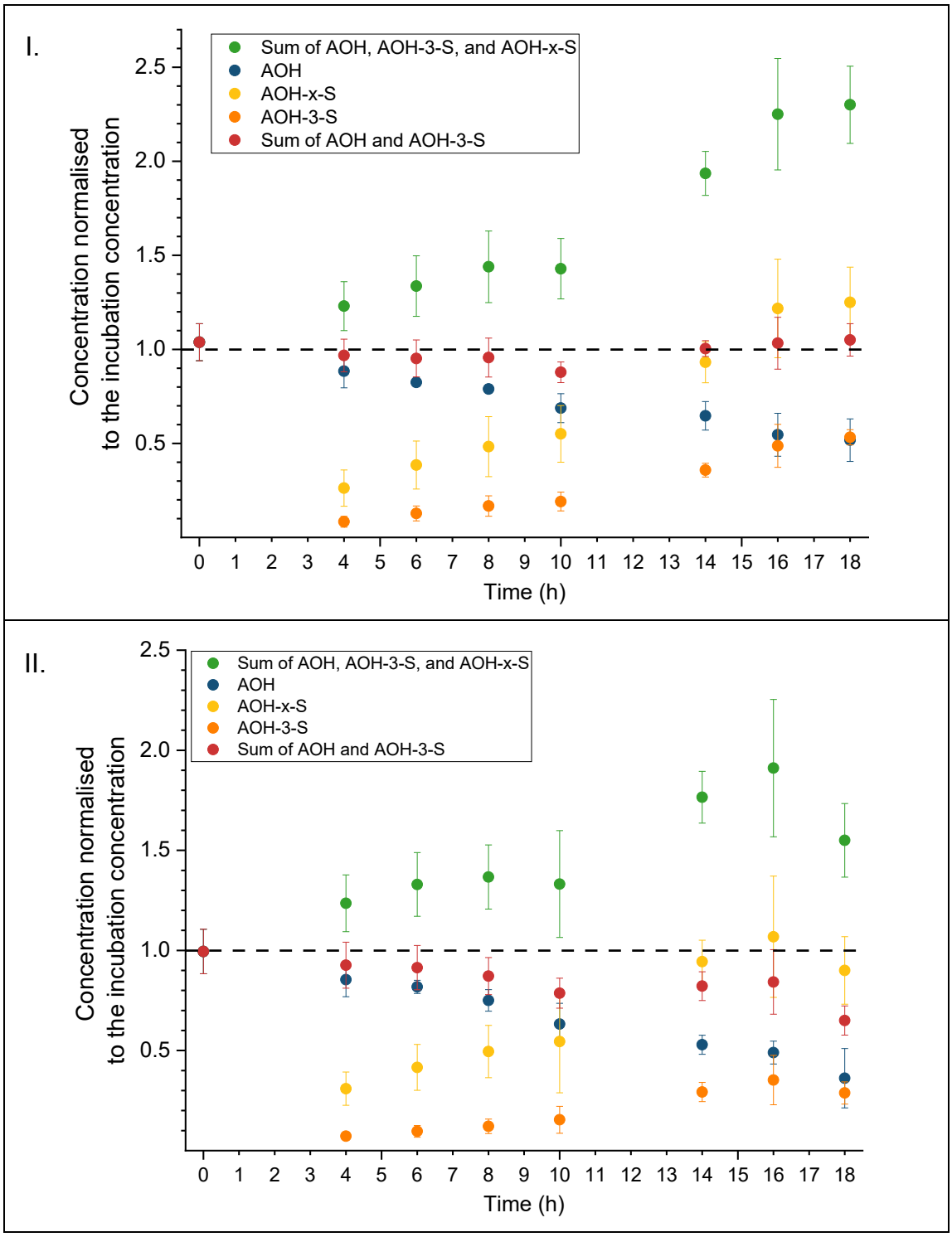

Figure 21: Summary of the HepG2 incubations with AOH
The data illustrates the time-dependency of the concentration of AOH, its sulphate metabolites, and their sum, normalised to the nominal starting AOH concentration (10 µM) in HepG2 cells, after zero to 18 hours of incubation. The assay was conducted in RPMI medium, both in the presence (Graph I.) and in the absence (Graph II.) of FBS. Each data point represents the average of nine technical replicates within three biological replicates ± standard deviation. Samples at the incubation time of zero hours were taken directly from the incubation solution, without contact to the cells.

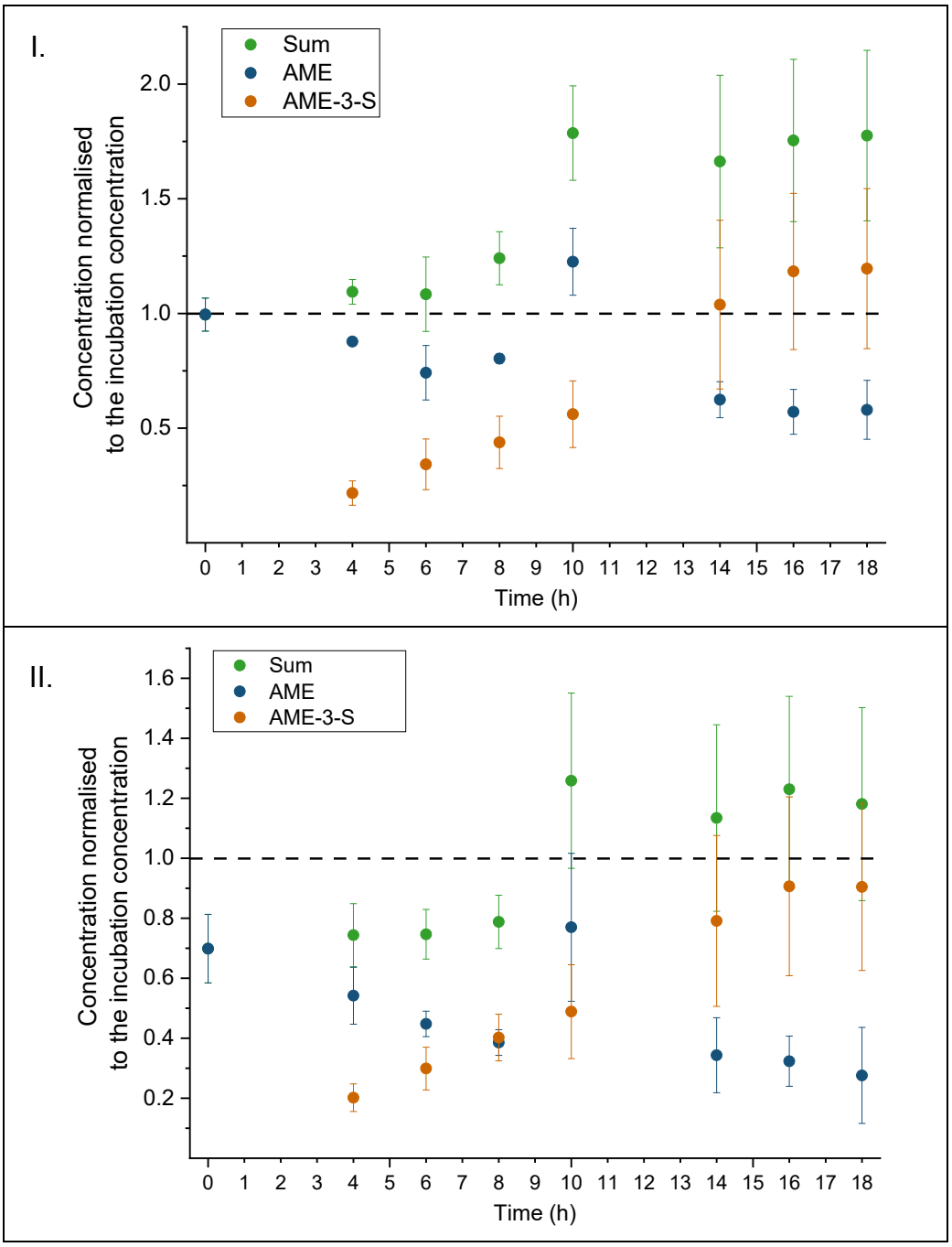

Figure 22: Summary of the HepG2 incubations with AME
The data illustrates the time-dependency of the concentration of AME, AME-3-S, and their sum, normalised to the nominal starting AME concentration (10 µM) in HepG2 cells, after zero to 18 hours of incubation. The assay was conducted in RPMI medium, both in the presence (Graph I.) and in the absence (Graph II.) of FBS. Each data point represents the average of nine technical replicates within three biological replicates ± standard deviation. Samples at the incubation time of zero hours were taken directly from the incubation solution, without contact to the cells.

Comparing the measured toxin concentration in the BPP and APP controls helps to detect a possible negative influence of the protein precipitation on the recovery of the toxin analytes. As Graph I. in Figure 23 shows, there is a significant difference between BPP and APP, as well as between the initial concentration and APP. This result might indicate that the protein precipitation causes a high loss in the original AOH level, which does not occur by the APP control since, in this case, the addition of the toxin followed the protein precipitation. However, the quantified AOH toxin

stock solution used for HepG2 assays (Table 14) had a concentration of 2.4 mM, limiting the maximal AOH concentration of the incubation solution to 12 µM, corresponding to 1.2 in the figure. Therefore, the APP data being clearly above 1.2 indicate probably calculation or pipette error rather than toxin loss during PP since the same modified dilution solvent was used for all three biological replicates (details in subsection 4.5.4.4). This assumption is also supported by the fact that the AME levels of BPP and APP meet the expectations (Figure 24). In future assay designs, a straightforward solution overcoming such interpretation difficulties regarding the APP control might be measuring the toxin content of the modified dilution solvent enabling a direct calculation of the toxin recovery.

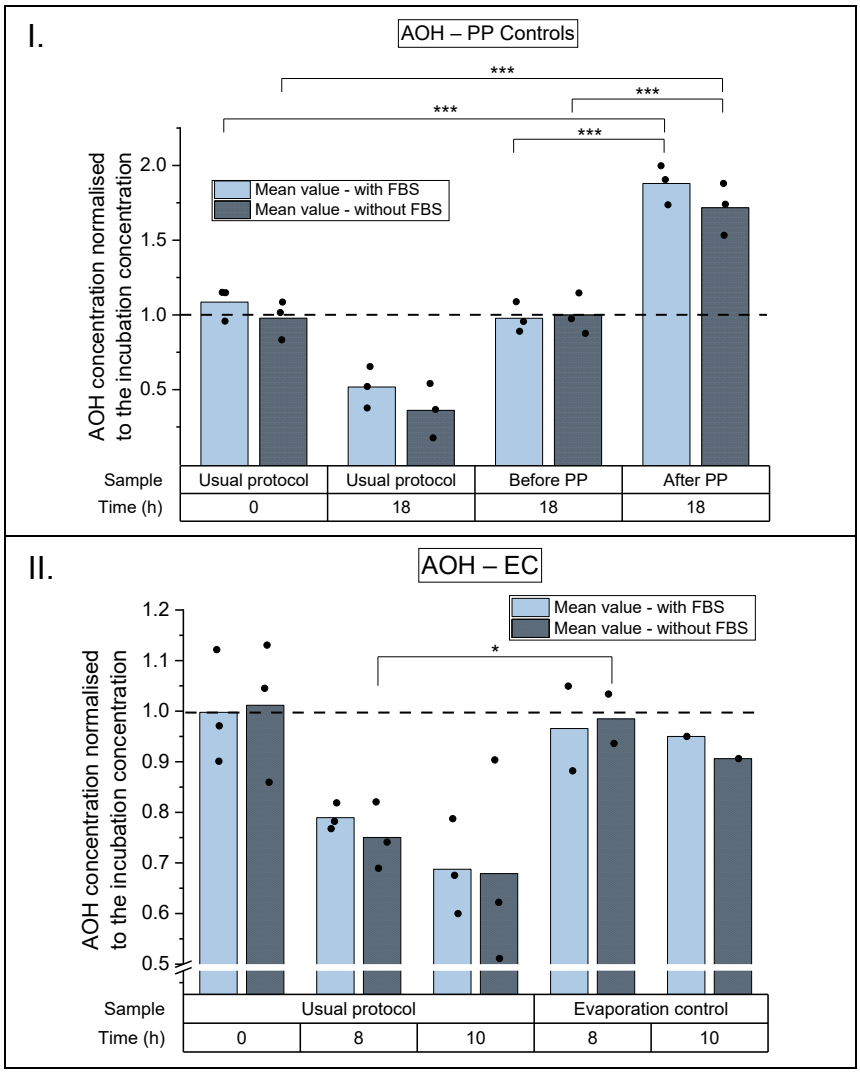

Figure 23: Incubation of HepG2 cells with 10 µM AOH – control experiments
The data illustrates the AOH profile in general samples and control setups, normalised to the nominal starting AOH concentration (10 µM) after zero to 18 hours of incubation, in HepG2 cells. Each data point represents the average of three technical replicates within one biological replicate. Each bar shows the average of all biological replicates. Samples at the incubation time of zero hours were taken directly from the incubation solution, without contact to the cells. Graph I. shows the results of control setups, where the toxin was added before or after the protein precipitation (PP), whereas the evaporation control (Graph II.) was performed without cells. After testing for normality, one-way ANOVA, followed by Fisher`s LSD post-hoc test was used for testing significant differences. The significance levels were marked in the graphs as follows: * → $0.01 < p < 0.05$; ** → $0.001 < p < 0.01$; *** → $p < 0.001$.

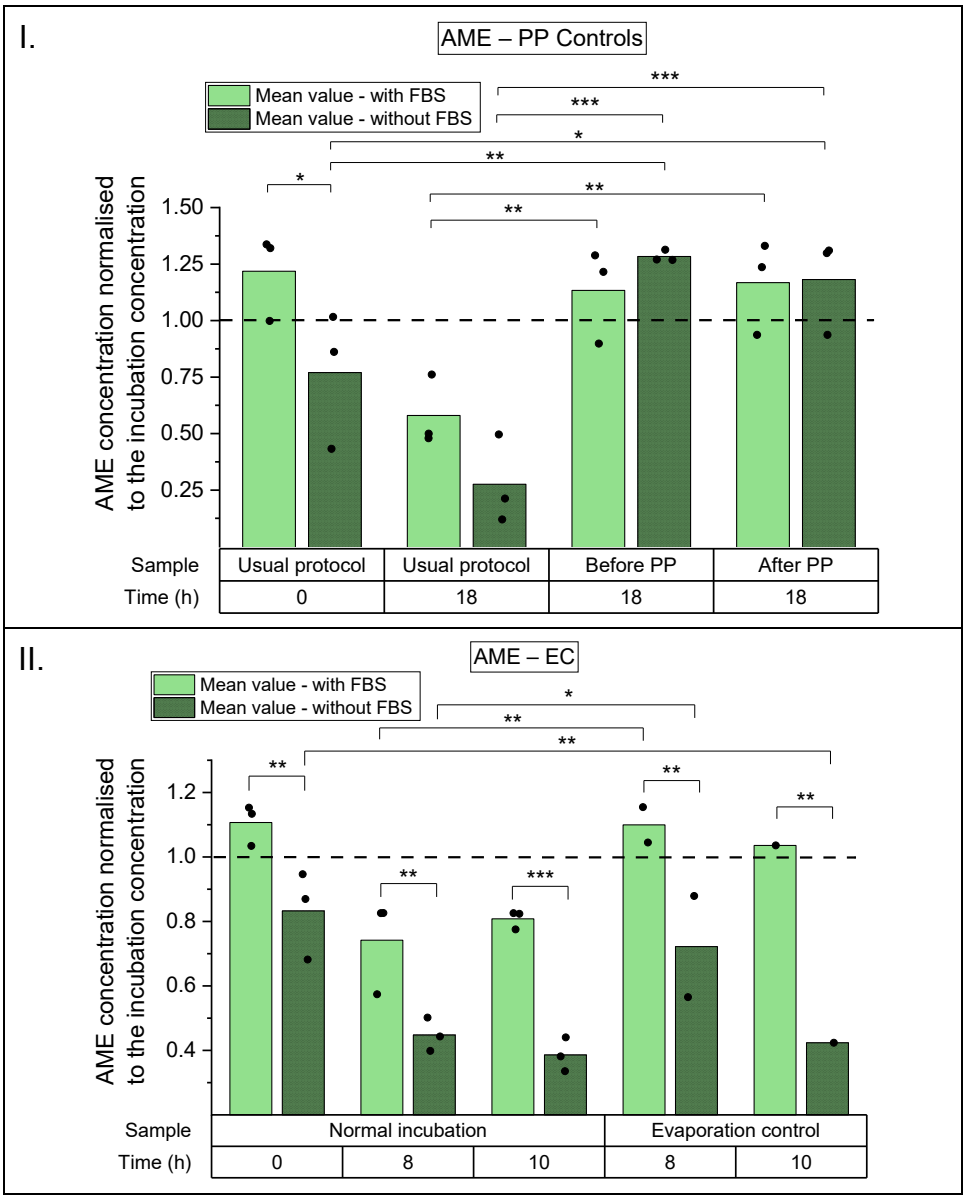

Figure 24: Incubation of HepG2 cells with 10 µM AME – control experiments
The data illustrates the AME profile in general samples and control setups, normalised to the nominal starting AME concentration (10 µM) after zero to 18 hours of incubation, in HepG2 cells. Each data point represents the average of three technical replicates within one biological replicate. Each bar shows the average of all biological replicates. Samples at the incubation time of zero hours were taken directly from the incubation solution, without contact to the cells. Graph I. shows the results of control setups, where the toxin was added before or after the protein precipitation (PP), whereas the evaporation control (Graph II.) was performed without cells. After testing for normality, one-way ANOVA, followed by Fisher`s LSD post-hoc test was used for testing significant differences. The significance levels were marked in the graphs as follows: * → $0.01 < p < 0.05$; ** → $0.001 < p < 0.01$; *** → $p < 0.001$.

For one of three biological replicates, the evaporation controls were not incubated for 8 but 10 hours because of practical reasons. Unfortunately, statistically relevant reasoning based on these data is less reliable due to fewer replicates per time point. Nevertheless, no significant difference could be found between the initial toxin concentration and the EP measurements when exposing HepG2 cells to AOH (Graph II of Figure 23). Consequently, the evaporation of the AOH incubation solution seems not to change the research outcome significantly despite the higher incubation times.

This finding is in line with the observation appearing by incubations with AME in the presence of FBS. In contrast, when FBS is absent, tendentiously lower AME recovery can be observed, and significantly lower AME concentration could be measured than the initial toxin amount in the case of the 10-hour incubation. Since this result only appeared by one analyte, in one of the two monitored conditions, by one time point, no further investigations were addressed to study this issue. However, as no cells were included in the evaporation controls, this difference between incubations with and without FBS cannot be related to cellular processes but play a role in the matrix effects caused by the medium. Overall, in future approaches regarding the AOH and especially AME metabolism in HepG2 cells, including FBS in the incubation solution is recommended.

5.2.2.2. Transformation rate of AOH and AME in HepG2 incubations

As described in the previous subsection, the AOH and AME concentration was monitored at several time points of the HepG2 incubation. Furthermore, the total protein content in every individual well was determined with the BCA assay, correlating with the number of adherent cells (Tuszynski and Murphy, 1990). Based on these quantitative data, the transformation rate of each technical replicate could be calculated individually at every investigated time point. The resulting statistical summary of all biological replicates is depicted in Figure 25 and Figure 26. The uncertainty of cell seeding and cell proliferation, the toxin incubation assay, LC-MS/MS measurements, and the BCA assay contribute to the high standard deviation, making it difficult to recognise any pattern in this dataset. Although tendentiously higher transformation rates seem to be reached without FBS than with FBS in the incubations with AME, a significant difference cannot be observed due to the high SD. Nevertheless, knowing the transformation rates in HepG2 cells being in the 10^{-8}-10^{-7} µmol/(mg*min) magnitude allows the direct comparison between two different *in vitro* models: HepG2 cells and liver microsomes.

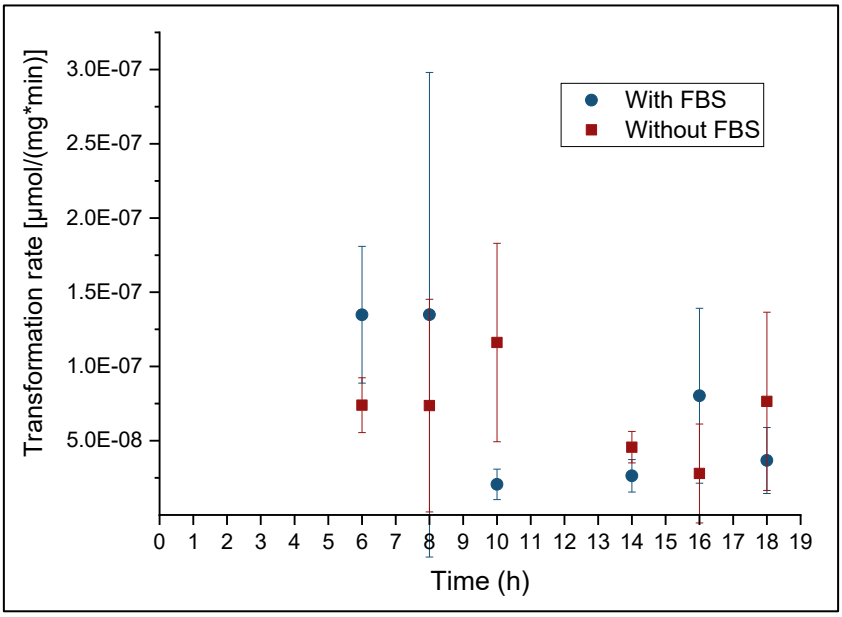

Figure 25: Biotransformation rate of AOH in HepG2 cells
The data illustrates the transformation rate values of AOH after zero to 18 hours of incubation, in HepG2 cells. The values are normalised to the protein content of the metabolising HepG2 cells, based on the results of the BCA assay. Each data point represents the average of nine technical replicates within three biological replicates.

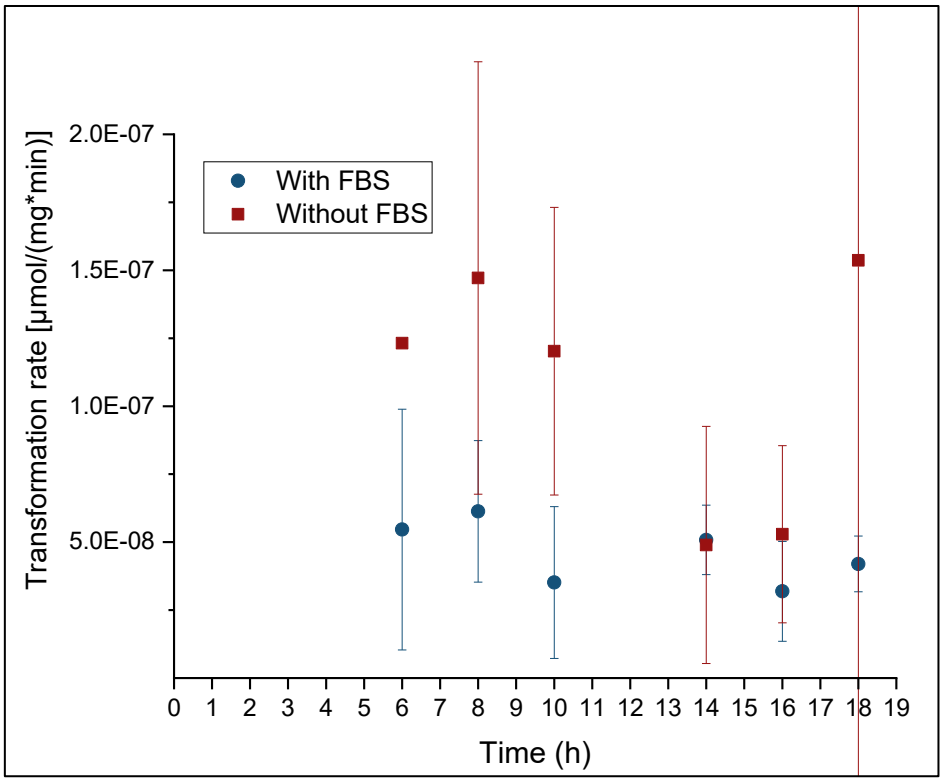

Figure 26: Biotransformation rate of AME in HepG2 cells
The data illustrates the calculated transformation rate values of AOH after zero to 18 hours of incubation, in HepG2 cells. The values are normalised to the protein content of the metabolising HepG2 cells, based on the results of the BCA assay. Each data point represents the average of nine technical replicates within three biological replicates.

5.3. Measurements of porcine liver microsomal incubation samples

5.3.1. Preliminary results – porcine hepatic microsomal incubations

The preliminary studies of the microsomal incubations were conducted with the first batch of the porcine liver microsomal suspension because it was available in relatively large quantities compared to other biological materials (section 4.5.5.1). Since it originates from a single liver donor, the entire preliminary dataset can be characterised as one biological replicate.

The first experiment aimed to choose the time frame of the assay with a final incubation time long enough to see a significant decrease of the monitored toxins, but not unnecessarily long. For this screening, the microsomes were incubated with 1, 10, and 20 µM AOH or AME, each in one replicate only, for 0-180 minutes. One of the resulting diagrams is depicted in Figure 27. Considering that the initial AOH concentration decreased to less than one-third in an hour, 60 minutes was chosen as the longest incubation time of the further experiments.

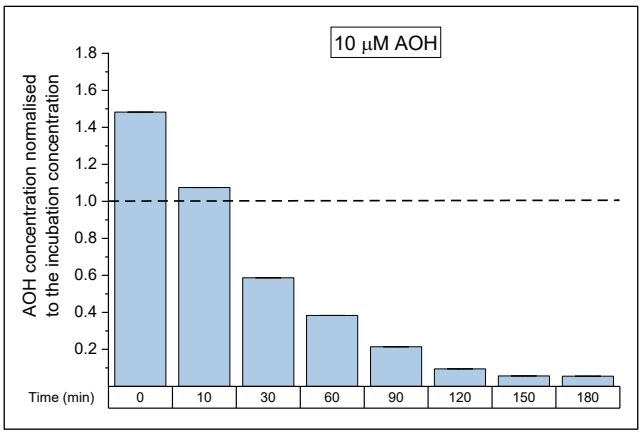

Figure 27: Incubation of porcine hepatic microsomes with AOH – first screening
The data illustrates decrease of the AOH amount normalised to the nominal starting AOH concentration (10 µM) after zero to 180 minutes of incubation, in porcine liver microsomes. Each data point represents the one technical replicate.

The preliminary results – summarised in Figure 28 and Figure 29 – consists of the data of eleven technical replicates, although not every time point was included in some of the experiments, and outliers – identified with the Nalimov test – are not depicted. Generally, the incubation with AOH resulted in a higher measured initial toxin concentration than expected. As this effect occurred at every incubation concentration, and the quantification of the AOH toxin solution did not explain this issue (Table 14), matrix effects might be a possible reason. However, several results of the 1 µM AOH incubation showed such high deviations that an operational error is presumable. A significant decrease of the initial AOH level can be observed after 10 minutes when incubating with 20 or 50 µM toxin. In contrast, a significant difference is only reached after 20 minutes by exposing the microsomes to 1, 10, or 100 µM AOH (Figure 28). Similar to AOH, the measured AME levels also exceed the nominal initial concentration values, for which matrix enhancement might be responsible. When incubating with 1 µM AME, a significant decrease in this toxin level could be detected after 5 minutes. Higher initial AME concentrations could only be significantly reduced after longer incubation times (10-20 minutes, Figure 29).

In contrast to the expectations, omitting the addition of the co-factor NADPH (NADPH-control solution) did not hinder the toxin decrease entirely, only reduced its extent (Figure 28 and Figure 29). Possibly, NADPH residues were present in the microsomal suspension due to inadequate phase separation during its preparation. In contrast, in the heat inactivated control, no permanent and significant toxin decrease could be observed. The particularly high standard deviations of the AME heat control results might be caused by not-optimised heat inactivation protocols, as further described in section 4.5.5.3. In addition to the presumed presence of the NADPH residues, an enzyme activity variation of the microsome aliquots was assumed due to the high standard deviations in the preliminary results. These imperfections of the microsomal preparation – if indeed present – can be attributed to the lacking experience of the operators in this process, as well as suboptimal environmental conditions (high lab temperature, hence time pressure). Consequently, the second batch of porcine liver microsomes was prepared to overcome this issue and hopefully providing more reliable data. Besides, obtaining quantitative information in an additional biological replicate aimed to confirm and validate the already available data, elevating it from the level of an individual liver donor.

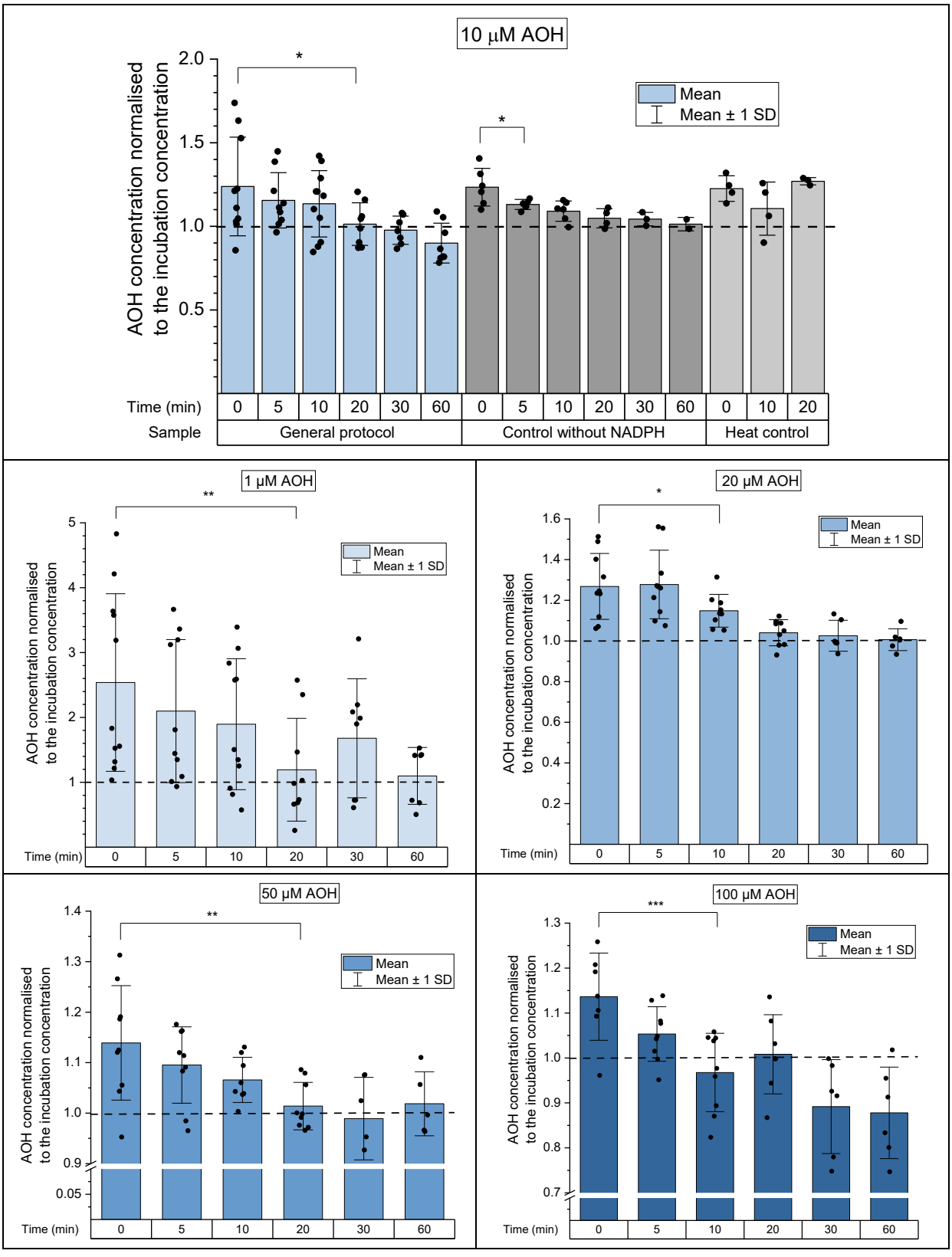

Figure 28: Incubation of porcine hepatic microsomes with AOH – preliminary experiment
The data illustrates the decrease in the AOH amount in porcine liver microsomes, normalised to the nominal starting AOH concentration (1-100 µM) after zero to 60 minutes of incubation. The average of 6-11 technical replicates within one biological replicate is shown ± standard deviation. After testing for normality, one-way ANOVA, followed by Fisher`s LSD post-hoc test was used for testing significant differences. The significance levels were marked in the graphs as follows:
* → 0.01 < p < 0.05; ** → 0.001 < p < 0.01; *** → p < 0.001.

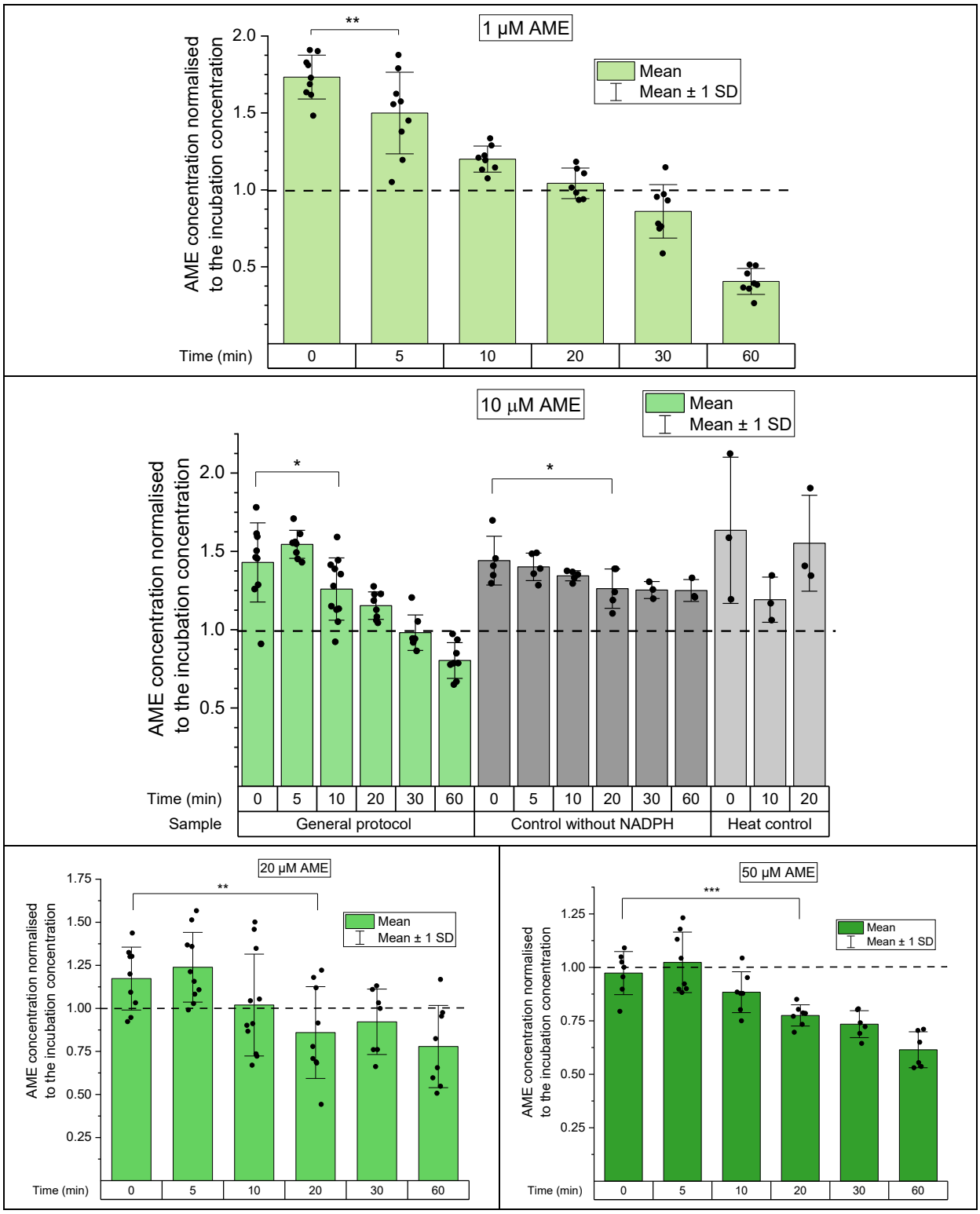

Figure 29: Incubation of porcine hepatic microsomes with AME – preliminary experiment
The data illustrates the decrease in the AME amount in porcine liver microsomes, normalised to the nominal starting AME concentration (1-50 µM) after zero to 60 minutes of incubation. The average of 6-11 technical replicates within one biological replicate is shown ± standard deviation. After testing for normality, one-way ANOVA, followed by Fisher`s LSD post-hoc test was used for testing significant differences. The significance levels were marked in the graphs as follows:
* → 0.01 < p < 0.05; ** → 0.001 < p < 0.01; *** → p < 0.001.

5.3.2. Main experiments – porcine hepatic microsomal incubations

The second batch of the porcine liver microsomes was incubated with AOH or AME in six technical replicates. Herein, the incubation times varied between 0 and 60 minutes. However, as shown in the preliminary studies, a significant difference in the toxin level could be expected no later than after 20 minutes. Therefore, three of the experiments were already terminated after 20 minutes to spare time, chemicals, consumables, and storage space.

As opposed to the first biological replicate, a statistically significant reduction of the toxin concentration – regardless of the initial mycotoxin level – can be already seen after 5 or 10 minutes (Figure 30 and Figure 31). Furthermore, the remaining non-metabolised AOH or AME amount after 60 minutes is much lower in the second than in the first biological replicate, implying higher enzyme activity. Besides the possible individual differences of the liver donors, another plausible reason might be more experienced handling during the microsome preparation, in particular continuous cooling and quicker operation. The comparison of the metabolic activity of different microsomal fractions is further detailed in section 5.6.

As expected, the incubation of the second batch of microsomes with AME resulted in much lower standard deviations than the preliminary experiments, suggesting that the detoxifying enzymes were uniformly distributed in these microsomal aliquots. In contrast, the main experiments with AOH still show comparably high standard deviations. Possible causative factors of this variation might be one of the listed ones in Figure 15 and Figure 16. In general, AME seems to be metabolised in a faster fashion than AOH in porcine liver microsomes. Namely, a significant toxin decrease appears earlier by incubations with AME, and a lower percentage of this toxin could be determined after 60 minutes compared to AOH (Figure 30 and Figure 31).

The heat inactivated control worked as anticipated in the sense of not showing a significant AOH or AME decrease in the monitored period. This result ensures that the microsomal enzyme activity caused the toxin decrease detected in general incubations rather than other factors. Conclusively, the heat control protocol utilised for the second batch of porcine microsomal assays proved its good applicability in a reproducible manner and was used for further experiments. Showing the necessity of two instead of one control incubations, the results of the NADPH control were less satisfying. Although the decreasing tendency of the parent toxins was more moderate than that of the general samples, a significant decrease of AOH and AME could be detected in the NAPDH control after 60 and 10 minutes, respectively (Figure 30 and Figure 31).

Since Pfeiffer *et al.* (2007b) already published a study regarding the oxidative metabolism of AOH and AME in liver microsomes of the mammalian species investigated in this work, comparing the obtained data with the literature would be reasonable. However, as their work predominantly focused on the interspecies differences in the metabolic pattern of AOH and AME, quantitative information of the remaining parent toxins after 40 minutes of incubation with 50 µM substrate is not available. Consequently, this study provides a valuable tool for discussing the HR-MS results rather than the kinetic information.

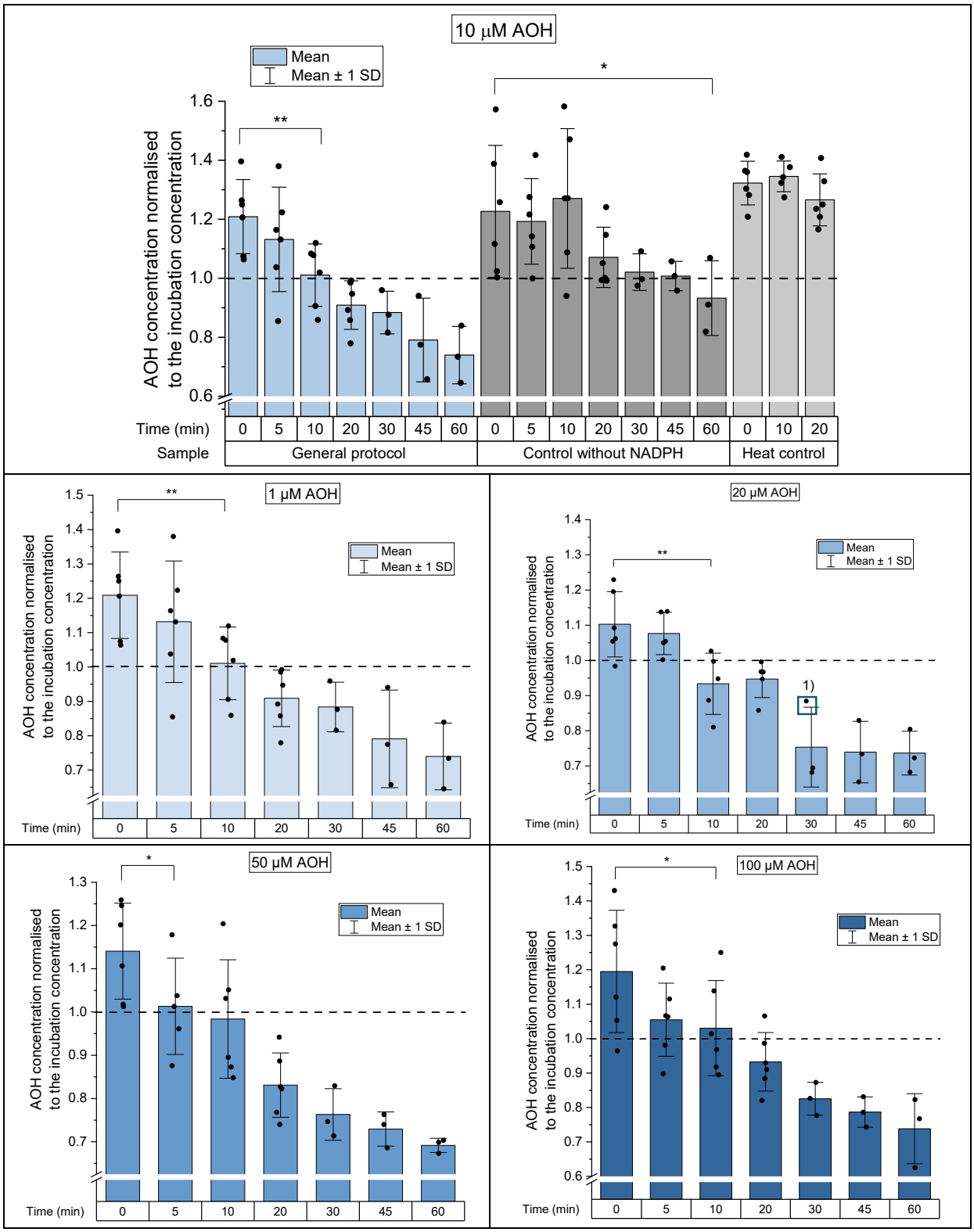

Figure 30: Incubation of porcine hepatic microsomes with AOH – main experiment
The data illustrates the decrease in the AOH amount in porcine liver microsomes, normalised to the nominal starting AOH concentration (1-100 µM) after zero to 60 minutes of incubation. The average of 3-6 technical replicates within one biological replicate is shown ± standard deviation. The data point marked with 1) was identified as an outlier with the Nalimov test, but it was still included in the dataset to show a complete image about the measured AOH tendency. After testing for normality, one-way ANOVA, followed by Fisher`s LSD post-hoc test was used for testing significant differences. The significance levels were marked in the graphs as follows: * → 0.01 < p < 0.05; ** → 0.001 < p < 0.01; *** → p < 0.001.

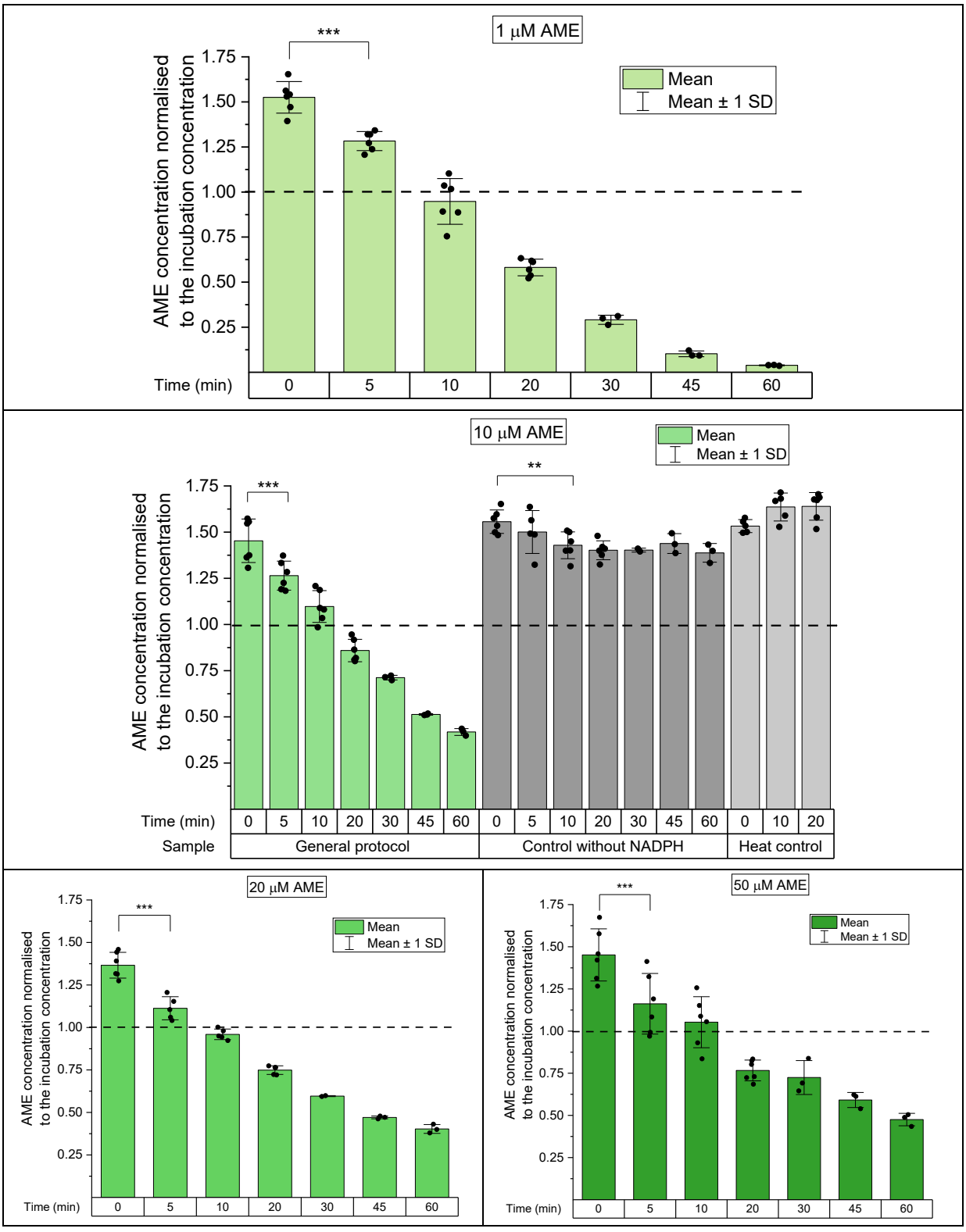

Figure 31: Incubation of porcine hepatic microsomes with AME – main experiment
The data illustrates the decrease in the AME amount in porcine liver microsomes, normalised to the nominal starting AME concentration (1-50 µM) after zero to 60 minutes of incubation. The average of 3-6 technical replicates within one biological replicate is shown ± standard deviation. After testing for normality, one-way ANOVA, followed by Fisher`s LSD post-hoc test was used for testing significant differences. The significance levels were marked in the graphs as follows:
* → 0.01 < p < 0.05; ** → 0.001 < p < 0.01; *** → p < 0.001.

In addition to the respective incubating mycotoxin, the other toxin counterpart was also quantified in the samples. When treating microsomes with AOH, the AME level remained below the LLOQ.

In contrast, the metabolism of AME led to the formation of AOH in amounts exceeding the LLOQ. Figure 32 shows the AOH profile (red data points) in samples resulting from exposing porcine liver microsomes to AME (green bars). The depicted toxin levels are average values calculated from all technical replicates of the second porcine hepatic microsome batch. It is important to note that all the graphs consist of two y-axes with a ten-fold difference. Also, for some data points the AOH concentration are below the LLOQ and have therefore doubtful reliability. Since the LLOQ of AOH is known to be 0.1 µg/L in the measurement solutions, the LLOQ of each incubation solution – marked with a red dashed line – was calculated based on the dilution factors of the corresponding samples (Table 11).

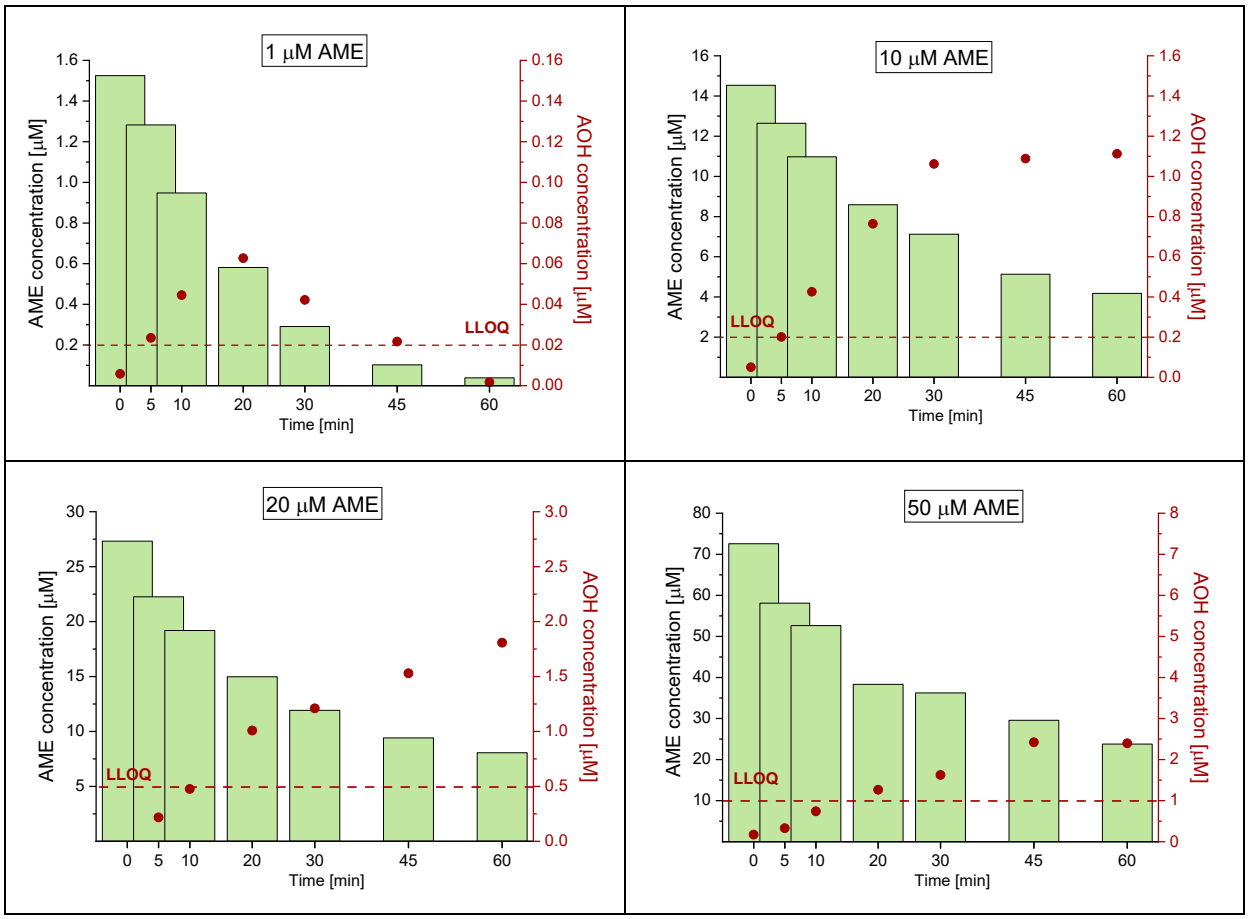

Figure 32: Demethylation of AME in porcine liver microsomes
The data illustrates the decrease in the AME amount (green bars, left y-axis) and the increase in the AOH amount (red data points, right y-axis), after zero to 60 minutes of incubation, in porcine liver microsomes. The average of 3-6 technical replicates within one biological replicate is shown. The red dashed line represents the LLOQ of AOH in the original incubation solutions, knowing that the LLOQ in the measurement solution is 0.1 µg/L and samples with different initial AME concentrations changed in their dilution factors, but samples with different incubation times did not (Table 11). Results below the LOD are not shown.

The data acquired during the incubation with 1 µM AME showed an increasing AOH tendency, followed by its decrease. This trend suggests the demethylation of AME, leading to AOH formation and its subsequent metabolism. In respect of higher

incubation concentrations, the monitored time frame is only sufficient for AOH formation but not for its reduction. Alternariol as one of the phase I metabolites of AME was already reported (discussed in section 2.2.4; published by Pollock *et al*., 1982, Olsen and Visconti, 1988). A more comprehensive overview of additional oxidative metabolites of AOH and AME follows in section 5.6.3. However, the concentration profile depicted in Figure 32 represents novel toxicological information, providing a better understanding of the kinetic behaviour of these *Alternaria* toxins in mammalian liver models.

5.4. Measurements of rat liver microsomal incubation samples

The incubation of pooled rat liver microsomes with AOH or AME was carried out in four technical replicates. As described in the previous section, a significant decrease of the detected toxins could be observed already after 5-10 minutes in porcine liver microsomes. Since hepatic microsomes of rats showed even higher total cytochrome P450 enzyme content than that of pigs, experiencing a significant toxin reduction was expected at least within 10 minutes (Nebbia *et al*., 2002). Hence, 0-10 minutes was chosen as the monitored time frame for rat liver microsomes to spare chemicals, consumables, and – most importantly – biological material. Indeed, the anticipated statistically significant decrease of AOH and AME was observable within the mentioned time frame with one exception – exposing rat liver microsomes to 50 µM AOH for 10 minutes did not lead to a significant toxin decrease (Figure 33 and Figure 34).

As opposed to porcine liver microsomes, the AOH and AME levels recovered in rat hepatic microsomes were – in most cases – below the nominal initial toxin concentration. Given that the same toxin stocks were used for the assay of both biological materials, besides variations of the operation, differences of the matrix composition and consequently in the obtained matrix effects are considerable.

In addition to the causative factors of variation playing a role in all analogous tests (Figure 15 and Figure 16), the comparatively low number of technical replicates performed with rat liver microsomes makes it hard to detect and exclude outliers. Consequently, some of the datasets show a relatively high standard deviation. Nevertheless, in the vast majority of rat microsomal incubations, the significantly decreasing trend is still detectable and validated through comparison with the control incubations not showing a significant decrease.

The incubation with AME resulted in the formation of AOH in rat liver microsomes, similar to the porcine liver microsomes. Whereas the 0-minute sampling did not contain an AOH amount above the LOD, after 5 and especially 10 minutes, a detectable AOH amount was present. However, most of these data were between the LOD and the LLOQ, pointing out that the monitored incubation time was too short to observe a tendentious AOH profile with analytically reliable data. Pollock *et al.* (1982) provided kinetic information about the metabolism of AME in rat liver post-mitochondrial supernatant already in the 1980s. Although the preparation of this *in vitro* model – centrifugation at 10,000 *g* – reminds more of the whole S9 mix rather than of the microsomes, they refer to the used fraction as "active liver microsomes˝. Therefore, the comparison of the gained data with their findings could be of interest. However, since their incubation lasted longer (60 minutes), expecting the correspondence of the numerical toxin concentrations would not be reasonable.

Nevertheless, their observation AOH being one of the AME metabolites is in line with the results of this work.

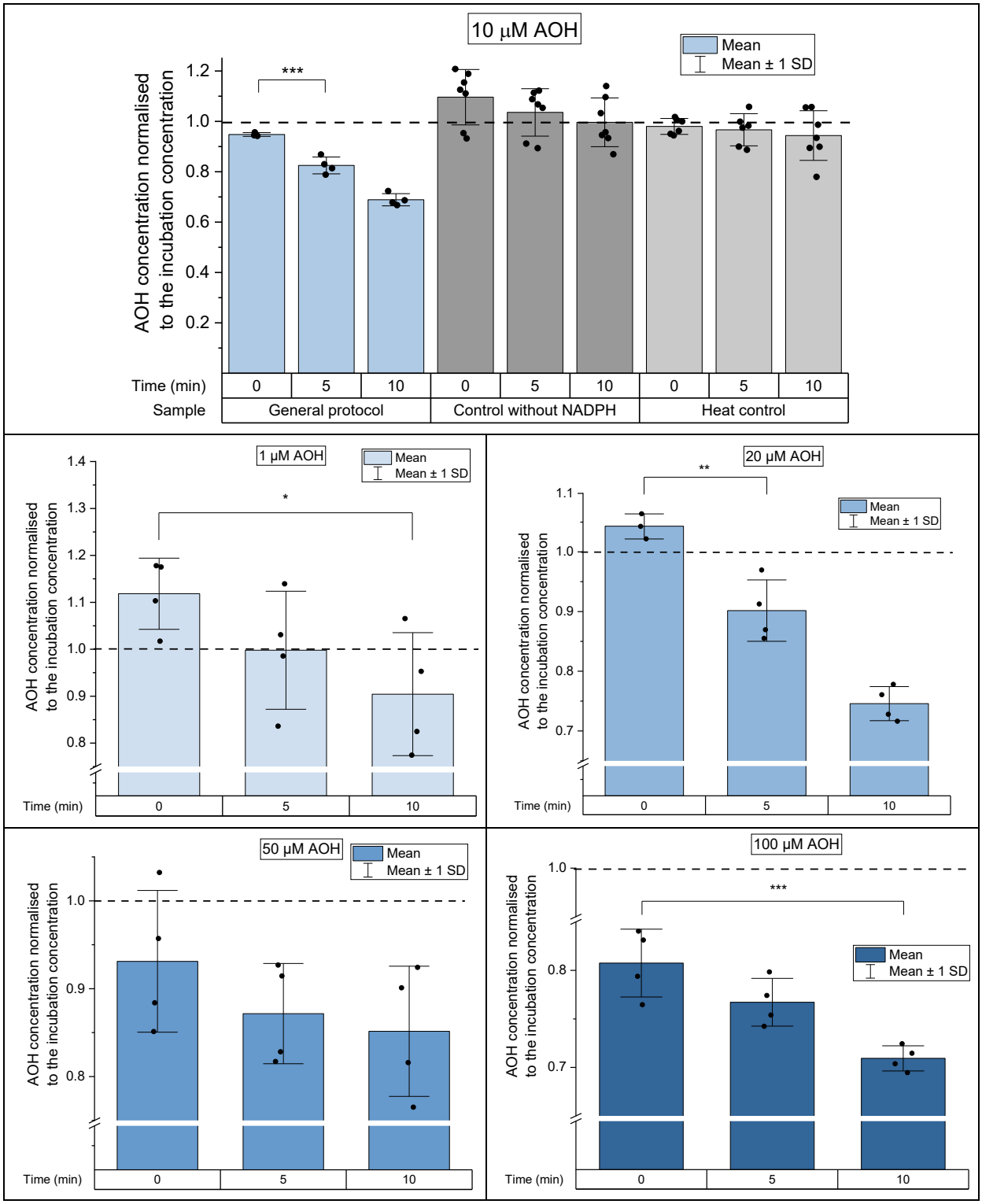

Figure 33: Incubation of rat hepatic microsomes with AOH
The data illustrates the decrease in the AOH amount in pooled rat liver microsomes, normalised to the nominal starting AOH concentration (1-100 µM) after zero to 10 minutes of incubation. The average of 4-7 technical replicates is shown ± standard deviation. After testing for normality, one-way ANOVA, followed by Fisher`s LSD post-hoc test was used for testing significant differences. The significance levels were marked in the graphs as follows: * → $0.01 < p < 0.05$; ** → $0.001 < p < 0.01$; *** → $p < 0.001$.

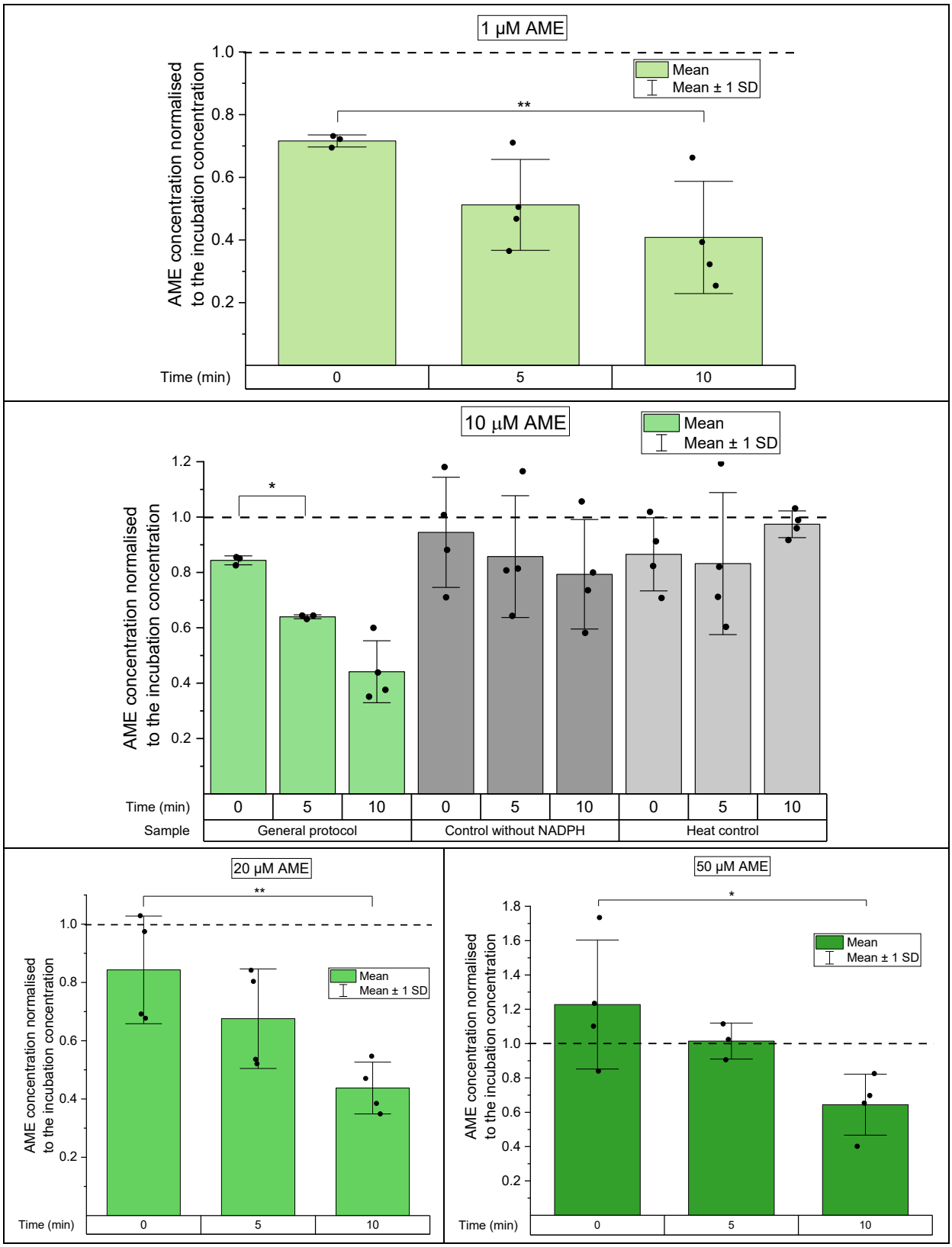

Figure 34: Incubation of rat hepatic microsomes with AME
The data illustrates the decrease in the AME amount in pooled rat liver microsomes, normalised to the nominal starting AME concentration (1-50 µM) after zero to 10 minutes of incubation. The average of four technical replicates is shown ± standard deviation. After testing for normality, one-way ANOVA, followed by Fisher`s LSD post-hoc test was used for testing significant differences. The significance levels were marked in the graphs as follows: * → 0.01 < p < 0.05; ** → 0.001 < p < 0.01; *** → p < 0.001.

Some of the considerations listed above may indicate that the monitored time frame of the rat-microsomal incubations was too short for providing valuable data from some aspects. It is important to emphasise that this work predominantly aimed to detect possible interspecies differences in the metabolic kinetics of AOH and AME, with a particular focus on the transformation rate to toxin concentration correlation. Thus, the utilised assay setup was adequate for the primary research interest.

5.5. Measurements of human liver microsomal incubation samples

The incubation of pooled human liver microsomes with AOH and AME was performed in four and five technical replicates, respectively. Similar to rat liver microsomal incubations, 0-10 minutes was chosen for HLM as the monitored time frame providing a straightforward comparison of these biological materials. Alike in rat liver microsomes, the expected statistically significant decrease of AOH is observable with one exception – exposing HLM to 50 µM AOH for 10 minutes did not lead to a significant toxin decrease (Figure 35). In contrast, the AME level – apart from testing 1 µM AME – was not significantly reduced in HLM (Figure 36). This finding might suggest that the tested substances will be metabolised slower in HLM than in porcine or rat liver microsomes.

Alternariol could be recovered with moderate variations from the nominal concentration. On the contrary, the measured AME levels were – for the most part – significantly below the anticipated values, probably due to a systematic error occurring when pipetting small volumes in the preparation of the diluted toxin stocks (Table 9). This and the generally higher standard deviations indicate the necessity to approach these data with caution.

In four out of five replicates, exposing human hepatic microsomes to AME did not lead to the formation of AOH above the LOD. Even in the only exception, the detected AOH level was below the LLOQ.

In the case of AOH, a significant decrease in the toxin level of the NADPH control was also detectable. However, this change occurred after a longer incubation time (10 minutes) than in the samples prepared with the general protocol (5 minutes, Figure 35). Considering the outcome of all performed microsomal incubations, the heat-inactivation control based on the final protocol was more reliable than the NADPH control.

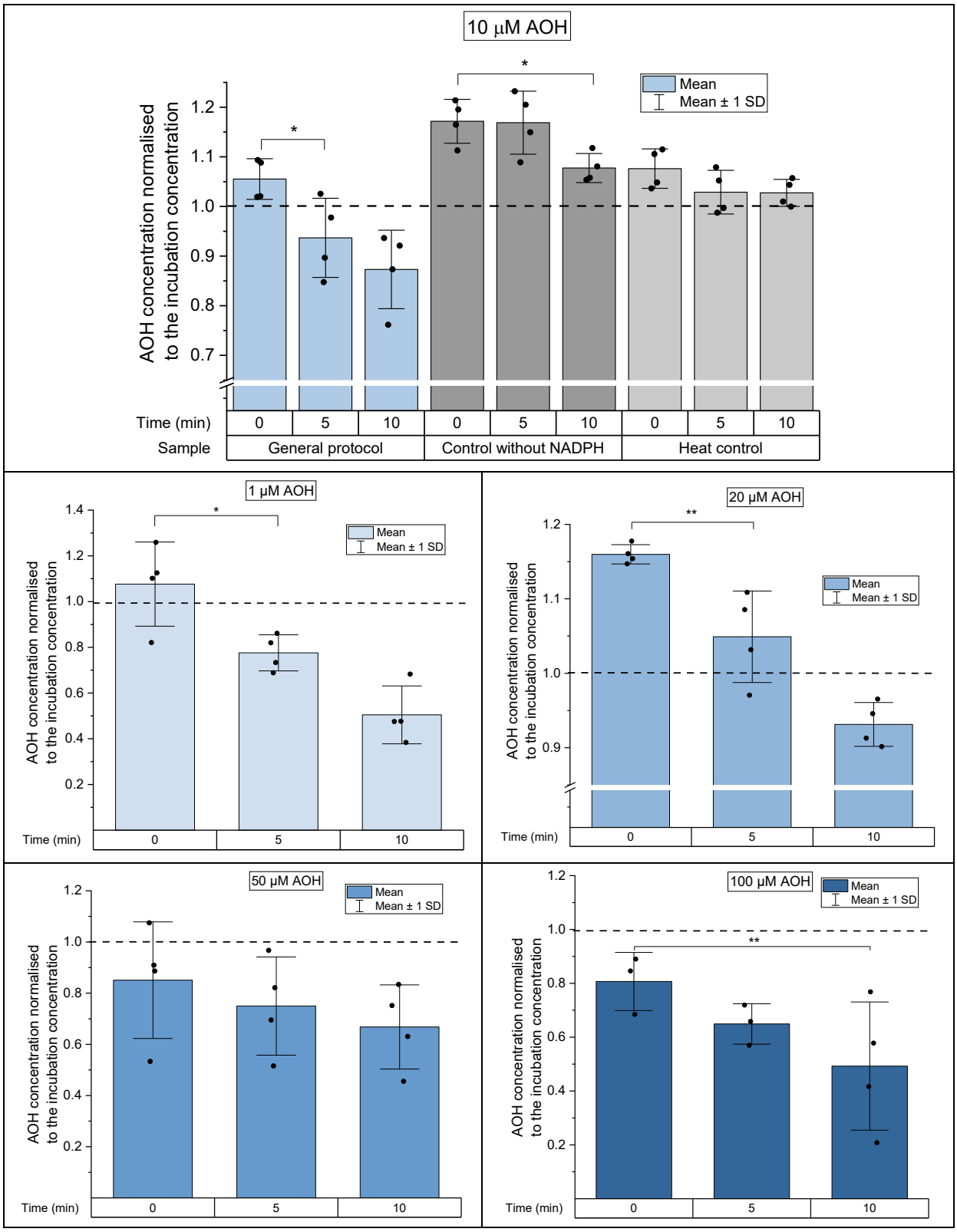

Figure 35: Incubation of human hepatic microsomes with AOH
The data illustrates the decrease in the AOH amount in pooled human liver microsomes, normalised to the nominal starting AOH concentration (1-100 µM) after zero to 10 minutes of incubation. The average of four technical replicates is shown ± standard deviation. After testing for normality, one-way ANOVA, followed by Fisher`s LSD post-hoc test was used for testing significant differences. The significance levels were marked in the graphs as follows: * → 0.01 < p < 0.05; ** → 0.001 < p < 0.01; *** → p < 0.001.

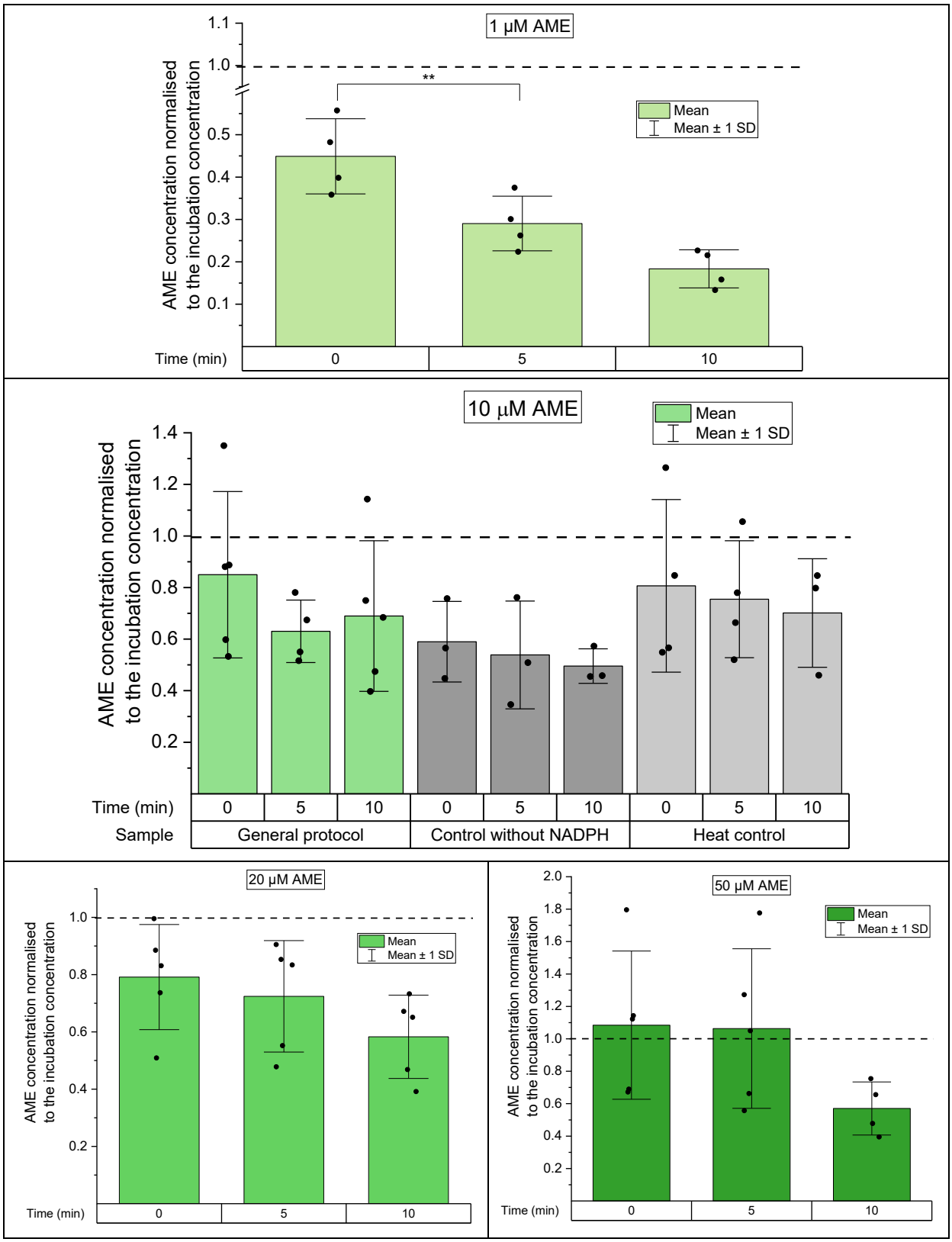

Figure 36: Incubation of human hepatic microsomes with AME
The data illustrates the decrease in the AME amount in pooled human liver microsomes, normalised to the nominal starting AME concentration (1-50 µM) after zero to 10 minutes of incubation. The average of 4-5 technical replicates is shown ± standard deviation. After testing for normality, one-way ANOVA, followed by Fisher`s LSD post-hoc test was used for testing significant differences. The significance levels were marked in the graphs as follows: * → 0.01 < p < 0.05; ** → 0.001 < p < 0.01; *** → p < 0.001. It is important to note the break in the y-axis of AME 1 µM.

5.6. Interspecies differences

5.6.1. Interspecies differences in the toxin concentration decrease

It has been known for a long time that interspecies variations occur in the metabolism of xenobiotics (Williams, 1974). Capturing these differences helps to get a more realistic and reliable image of the effect of these substances on the organism of interest. As *Alternaria* toxins infect various plants in the field or during storage, the exposure of farm livestock to these mycotoxins through the feed is also considerable besides the direct human intake (EFSA, 2011). Consequently, investigating the metabolism of AOH and AME in different mammalian species and observing the species-specific differences is of interest.

One of the relevant aspects of comparison is the time point when a significant decrease of the incubating toxin concentration is reached. Table 15 summarises this information for all incubation studies. It is immediately apparent that HepG2 cells reduce the toxin concentration after several hours, whereas liver microsomes exert this effect already after a few minutes. As suggested in section 5.3.2, the second batch of prepared porcine liver microsomes showed overall a faster metabolism of both monitored toxins than the first batch. Beyond interindividual variability, a deviation in the microsomal preparation process might have contributed to this difference. In general, AOH seems to be metabolised faster in rat and human liver microsomes than AME, while the opposite applies to porcine liver microsomes. Notably, the 10-minute incubation of AME with HLM did not lead in most cases to a significant reduction of the toxin level, suggesting a slower metabolism of AME in HLM than in other tested species.

Table 15: Interspecies variability in the elapsed incubation time until a detected significant toxin decrease. The darker the colour, the shorter incubation time was sufficient. It is important to mention that rat and human liver microsomes were only incubated for 10 minutes with AOH or AME.

Toxin	Incubation concentration (µM)	Incubation time (min)				
		HepG2 cells	First porcine LM	Second porcine LM	Rat LM	Human LM
AOH	1	-	20	10	10	5
	10	240-360	20	10	5	5
	20	-	10	10	5	5
	50	-	20	5	not detected	not detected
	100	-	10	10	10	10
AME	1	-	5	5	10	5
	10	240	10	5	5	not detected
	20	-	20	5	10	not detected
	50	-	20	5	10	not detected

Although extracted from the same dataset, the extent of the toxin decrease provides information about the interspecies variability from a slightly different perspective than the previously described aspect. The heatmaps in Figure 37 and Figure 38 visualise the percentual concentration decrease in porcine liver microsomal incubations. The immediately discernible observation is in line with previous findings – the second batch of porcine liver microsomes provided the metabolism of AOH and AME more

readily than the first one. Besides, the assay performed with 1 µM incubation concentration stands out for both toxins, so that in the main porcine liver microsomal experiment, less than 10 % of the initial toxin concentration remained. In contrast, the further incubations seem to show comparable results, and no correlation appears between the metabolised toxin amount and the initial incubation concentration.

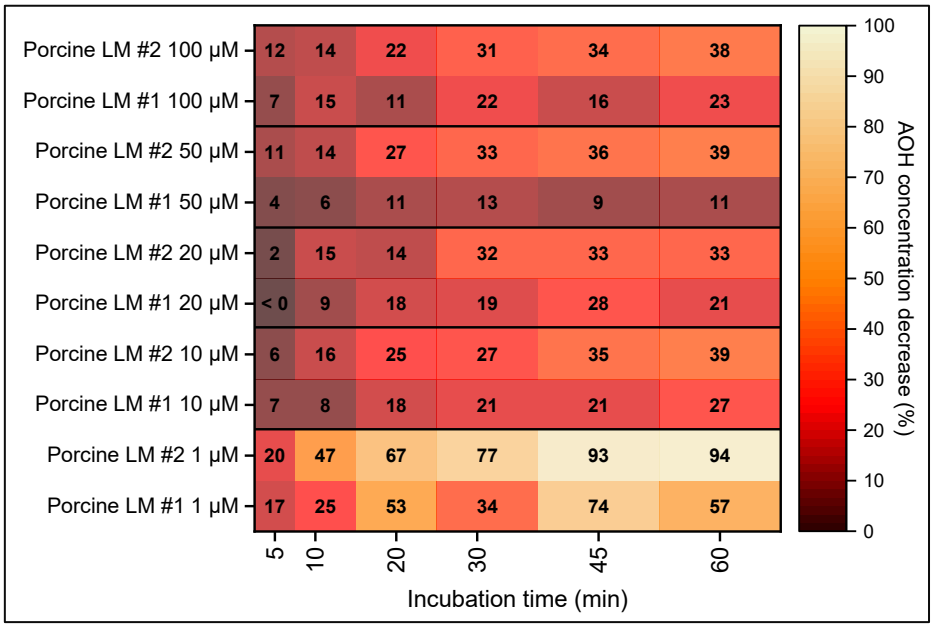

Figure 37: Percentage decrease of AOH in porcine liver microsomes
Each data point was calculated based on the respective mean AOH concentration of 3-11 independent experiments. The results of two biological replicates are displayed, distinguished through the label #1 and #2. The abbreviation LM stands for liver microsomes.

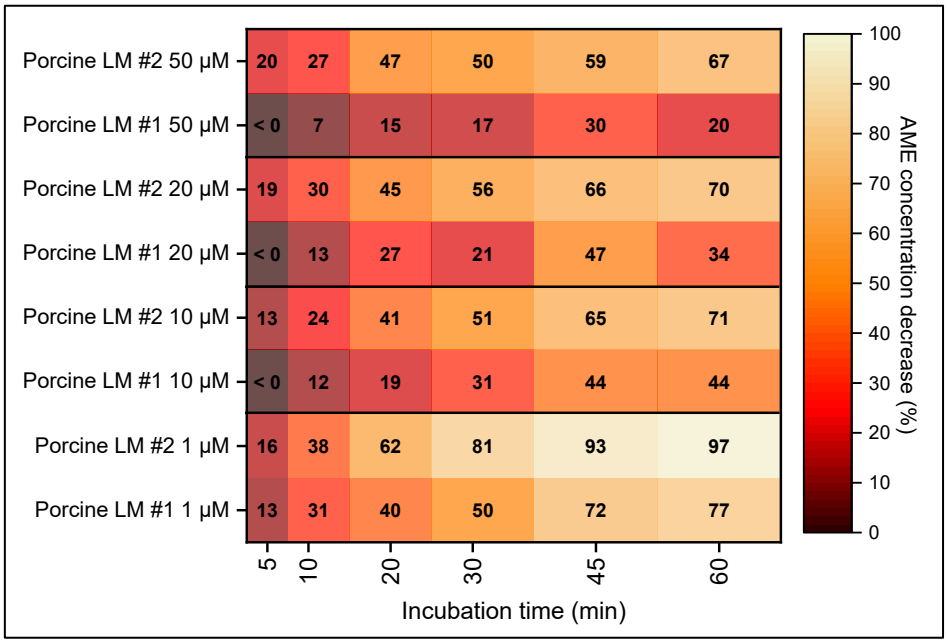

Figure 38: Percentage decrease of AME in porcine liver microsomes
Each data point was calculated based on the respective mean AME concentration of 3-11 independent experiments. The results of two biological replicates are displayed, distinguished through the label #1 and #2. The abbreviation LM stands for liver microsomes.

Figure 39 and Figure 40 summarise the concentration decrease results of all conducted microsomal assays, from 0-10 minutes. Generally, in the measured time frame, AME was metabolised to a greater extent than AOH. Tendentiously, the more the initial AOH concentration, the less percentage of it seems to be metabolised by porcine and rat liver microsomes. In contrast, especially rat liver microsomes metabolise even higher amounts of AME with nearly the same percentage as only 1 µM AME, suggesting that no enzyme saturation is reached within this concentration range. Interestingly, HLM shows an unexpected pattern by metabolising the lowest and the highest measured toxin amount to the greatest extent. However, due to the peculiarly high standard deviations of the HLM data, this observation might be misleading.

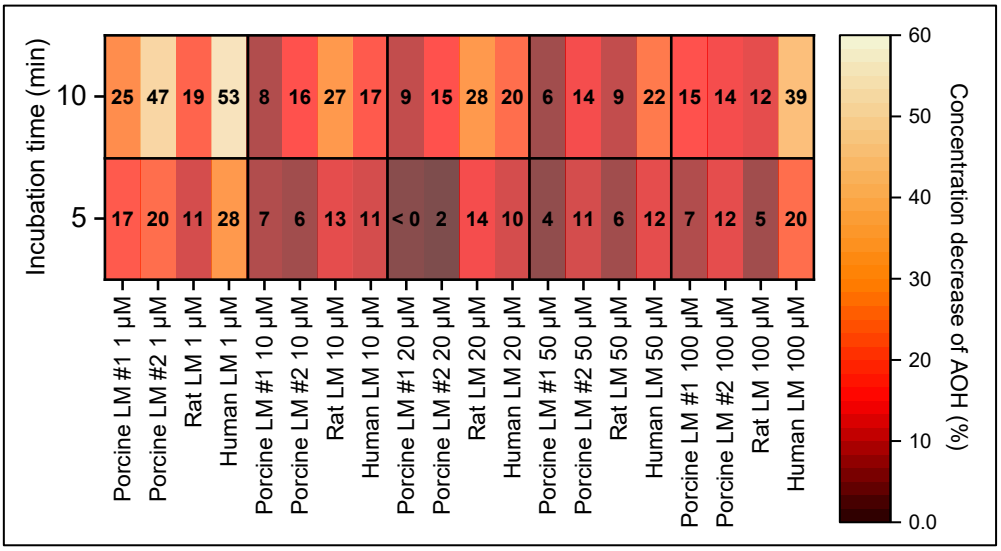

Figure 39: Percentage decrease of AOH in liver microsomes (LM), within 10 minutes
Each data was calculated based on the mean AOH concentration of 3-6 independent experiments. The results of two biological replicates of porcine liver microsomes are displayed, distinguished through the label #1 and #2. The examined rat and human liver microsomes were pooled.

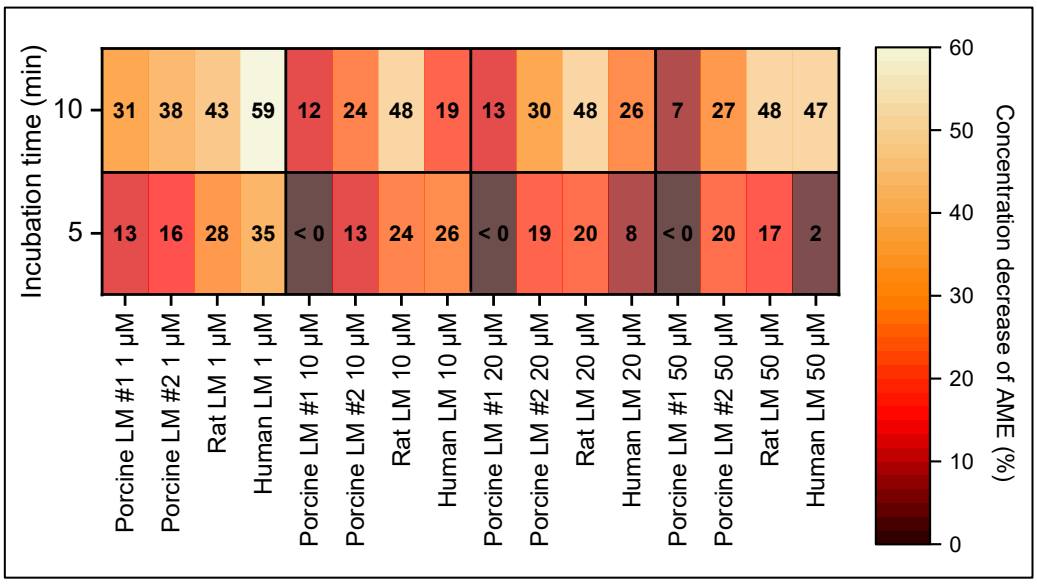

Figure 40: Percentage decrease of AME in liver microsomes (LM), within 10 minutes
Each data was calculated based on the mean AME concentration of 3-6 independent experiments. The results of two biological replicates of porcine liver microsomes are displayed, distinguished through the label #1 and #2. The examined rat and human liver microsomes were pooled.

When interpreting these data, it has to be kept in mind that the variations between the different incubation tests can be caused by numerous factors and not necessarily point to interspecies differences. First of all, both porcine liver microsomal fractions were derived from one single female liver donor and delivered quite variant results. Furthermore, the utilised human liver microsomes only contained microsomes of males. Therefore, in addition to operational errors and measurement uncertainty, interindividual and intergender differences cannot be excluded.

5.6.2. Interspecies differences in the transformation rate

For comparing the metabolic kinetics of AOH and AME in different liver microsomes, the transformation rates were calculated for each performed assay. Subsequently, the optimal incubation time for capturing interspecies differences in the transformation rate – toxin concentration profile was chosen. Given that data were only gathered after 5 and 10 minute incubations in rat and human liver microsomal incubations, these were the considered time points. Although both were within the linear range of the transformation rate – incubation time relation (an example shown in Figure 41), 10 minutes were decided for calculations of quantitative parameters since it resulted in a significant difference in more incubations (Table 15). Nevertheless, a visual comparison of the toxin metabolism observable in the examined species is possible for both time points, based on Figure 42 and Figure 43.

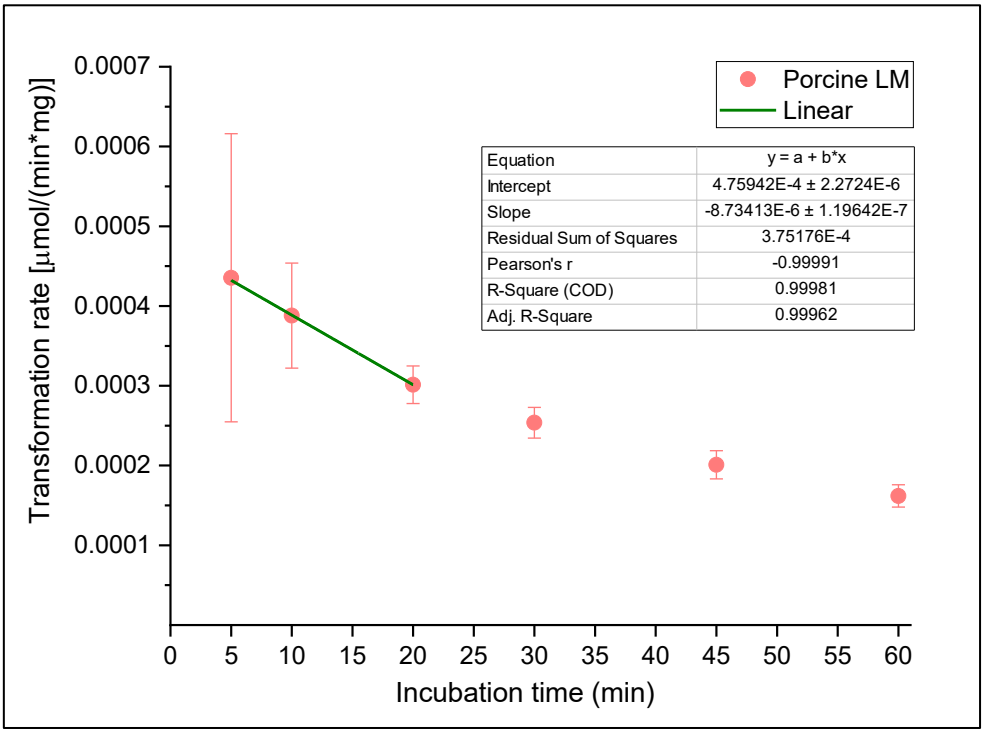

Figure 41: Determining the linear range in the transformation rate – incubation time relation in the data of porcine liver microsomes. Each data point represents mean values of 3-6 independent experiments of one biological replicate ± standard deviation. The first three points were used for linear regression.

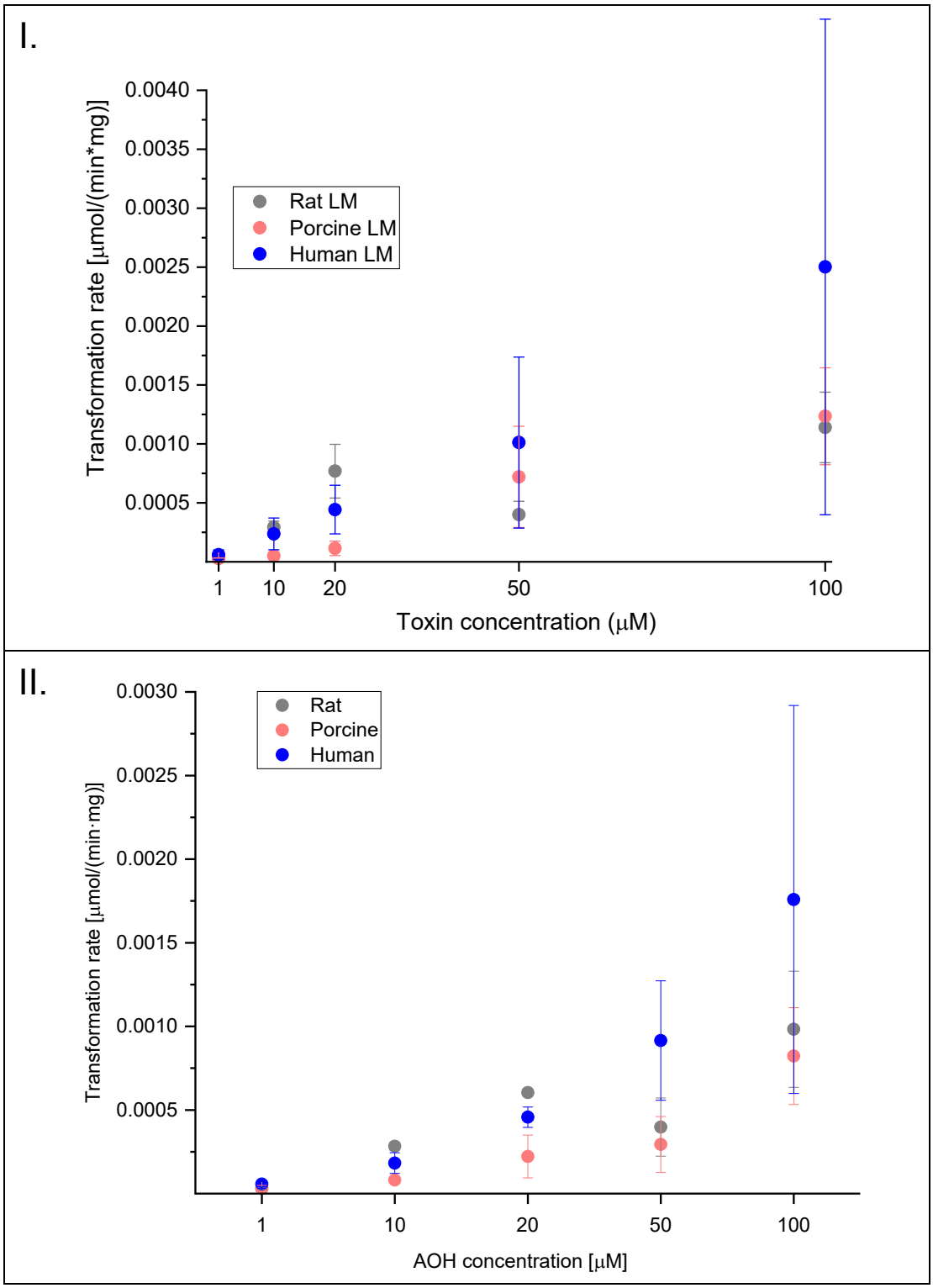

Figure 42: Interspecies differences in the incubation of AOH with liver microsomes (LM) derived from different mammalian species. The data illustrates the transformation rate values of AOH after 5 (Graph I.) or 10 minutes (Graph II.) of incubation, as a function of the nominal initial toxin concentration. The values are normalised to the protein content of the metabolising microsomes, based on the results of the BCA assay (porcine liver microsomes) or on information provided by the manufacturer (rat and human liver microsomes). Each data point represents the average of 3-6 technical replicates ± standard deviation. The results of one biological replicate of porcine liver microsomes are shown, whereas the human and rat liver microsomes were pooled.

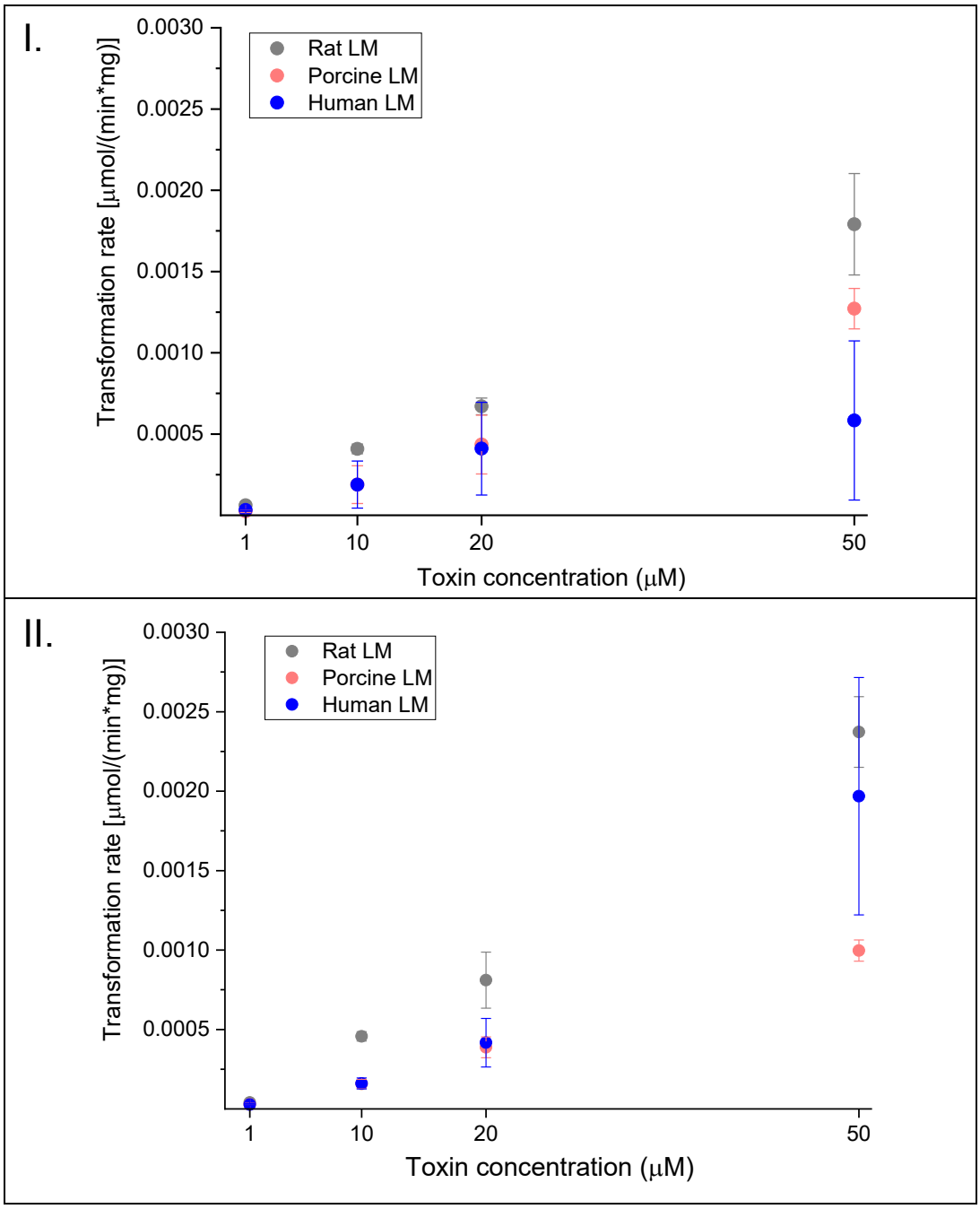

Figure 43: Interspecies differences in the incubation of AME with liver microsomes (LM) derived from different mammalian species. The data illustrates the transformation rate values of AME after 5 (Graph I.) or 10 minutes (Graph II.) of incubation, as a function of the nominal initial toxin concentration. The values are normalised to the protein content of the metabolising microsomes, based on the results of the BCA assay (porcine liver microsomes) or on information provided by the manufacturer (rat and human liver microsomes). Each data point represents the average of 3-6 technical replicates ± standard deviation. The results of one biological replicate of porcine liver microsomes are shown, whereas the human and rat liver microsomes were pooled.

The first observation by looking at Figure 42 and Figure 43 is that – as expected – higher transformation rates were reached in the microsomal incubation studies than in the cell culture assays (Figure 25 and Figure 26). Whereas biotransformation rates are in the order of magnitude of 10^{-2}-10^{-1} pmol/(mg*min) for HepG2 cells, hepatic microsomal incubations resulted in conversion rates in the 100-1,000 pmol/(mg*min) range.

A noteworthy aspect when looking for interspecies variations is that the main porcine liver microsomal study was conducted with only one biological replicate, but 2 mg/mL microsomal protein, whereas 1 mg/mL protein was used for pooled rat and human liver microsomes. Besides, the results obtained with human liver microsomal incubations showed the highest standard deviations, indicating lower reliability than the data of the other two species. Still, AOH seems to be metabolised more effectively in human than in porcine liver microsomes. Interestingly, rat liver microsomes show the highest biotransformation rates up to 20 µM AOH. However, the conversion rates obtained for 100 and particularly 50 µM were unexpectedly low in both monitored time points (Figure 42). For AME, rat liver microsomes tendentiously showed the highest transformation rates. Herein, both in porcine and human hepatic microsomes similar, lower results were detected (Figure 43). This finding based on a visual data comparison is in line with the statistical data. Table 16 summarises the significance levels of the transformation rates determined in three different species. For this, the transformation rates obtained in single technical replicates were used, and not only the depicted mean values.

Table 16: Significance of interspecies differences in the transformation ratio calculated for liver microsomal incubations of AOH and AME. One-way ANOVA, followed by Fisher`s LSD post-hoc test was used for testing significant differences. The significance levels were marked in the graphs as follows: * → 0.01 < p < 0.05; ** → 0.001 < p < 0.01; *** → p < 0.001; n. s. → no significant difference.

Toxin	Compared species	Incubation concentration (µM)				
		1	10	20	50	100
AOH	rat vs. porcine	n. s.	***	***	n. s.	n. s.
	rat vs. human	n. s.	**	n. s.	*	n. s.
	porcine vs. human	n. s.	**	**	**	n. s.
AME	rat vs. porcine	*	**	***	**	-
	rat vs. human	*	*	**	n. s.	-
	porcine vs. human	n. s.	n. s.	n. s.	*	-

The Michaelis-Menten equation represents an enzyme kinetic model enabling the quantitative description of the AOH and AME metabolism in liver microsomes. Before presenting the results obtained by fitting the available data in this model, some limitations of its applicability have to be discussed. Among others, steady-state conditions are assumed in this model but not ensured or investigated during the assays performed in this work. Besides, some UGT and – more relevantly – CYP enzymes were reported to show atypical kinetic profiles so that the hyperbolic kinetics characterised by the Michaelis-Menten equation may not fit the obtained data points (Kramer and Tracy, 2012). Also, the Michaelis-Menten model is often used to describe the interaction between a substrate with a single enzyme. Nevertheless, there are publications in the literature using this concept for the kinetic analysis of the detoxification of xenobiotics obtained by microsomes (Hou *et al.*, 2018; Yan *et al.*, 2021). Therefore, this model was chosen for the present study, as well.

The Michaelis-Menten equation describes the relationship between the rate of an enzyme reaction (v) and the substrate concentration ([S]) with the following formula:

$$\mathbf{v} = \frac{\mathbf{V_{max}} * [\mathbf{S}]}{\mathbf{K_m} + [\mathbf{S}]}$$ **Equation 6**

V_{max}: maximal velocity of the reaction

K_m: Michaelis constant

In reactions with a high Michaelis constant, or in the lower substrate concentration range, K_m is much higher than [S] and thus it becomes negligible from the denominator, resulting in the following linear relation:

$$\mathbf{v} \approx \frac{\mathbf{V_{max}} * [\mathbf{S}]}{\mathbf{K_m}} = \frac{\mathbf{V_{max}}}{\mathbf{K_m}} * [\mathbf{S}]$$ **Equation 7**

Beyond the hyperbolic curve based on the Michaelis-Menten equation, also a linear curve was fitted to the transformation rate – toxin concentration data points where it seemed reasonable, as a simplified Michaelis-Menten model based on Equation 7. Applying the linear regression as an additional kinetic model – at least in the lower concentration range – might imply enzyme reactions following non-Michaelis-Menten kinetics, as several of these curves have a linear range, too. The fitted curves are depicted in Appendix II, whereas the calculated kinetic parameters are summarised in Table 17.

Table 17: Kinetic parameters estimated by the Michaelis-Menten model or linear regression for describing the detoxification of AOH and AME in hepatic microsomes, within 10 minutes. The standard deviations of these parameters are depicted in Appendix II. Rows marked with blue represent models with lower coefficient of determination (R^2) than 0.95 pointing to inaccurate kinetic modelling.

Toxin	Species	Michaelis-Menten model					Linear regression		
		K_m (µM)	V_{max} [µmol/(mg*min)]	V_{max}/K_m	R^2	Data points	V_{max}/K_m	R^2	Data points
AOH	Porcine	6.72E+02	5.73E-03	**8.526E-06**	0.806	5	**7.398E-06**	0.999	5
	Rat	7.86E+01	2.82E-03	**3.586E-05**	0.988	4	**2.989E-05**	0.999	3
	Human	1.30E+02	3.37E-03	**2.584E-05**	0.919	5	**1.990E-05**	0.979	3
AME	Porcine	8.26E+06	1.61E+02	**1.950E-05**	0.984	4	**1.898E-05**	0.991	4
	Rat	1.01E+07	4.56E+02	**4.519E-05**	0.997	4	**4.618E-05**	0.999	4
	Human	2.94E+01	7.71E-04	**2.627E-05**	0.790	4	**1.579E-05**	0.978	3

The ratio between the obtained V_{max} and K_m values – often referred to as the *in vitro* hepatic clearance – provides the relative analysis of the detoxification efficiencies (Kramer and Tracy, 2012). Although the Michaelis-Menten model was proved to be – both visually and mathematically – inadequate for some of the enzyme reactions, the kinetic constants obtained were in the same magnitude as with the linear regression. Moreover, when sorting the V_{max}/K_m ratios in ascending order, the resulting metabolic activity order is in accordance with the above-detailed findings. As an exception, based on Table 17, rat liver microsomes appear to detoxify AOH more effectively than human liver microsomes, which is not evident according to the non-fitted scatter plot (Figure 42). This discrepancy can be resolved by recognising that the first three data points – pointing to higher metabolic efficiency towards AOH in rat than in

human liver microsomes – are more emphatically or even exclusively represented in the kinetic models (Figure A9).

Overall, the captured interspecies differences highlight the importance of utilising species-specific *in vitro* models for each research question. Otherwise, the adverse effects of exogenous compounds exerted on human or animal health might be underestimated. Moreover, the gathered data may provide valuable information for a PBTK model developed for AOH and AME (please see also section 2.4).

5.6.3. Interspecies differences in the pattern of oxidative metabolites formed during the incubation of AOH and AME with liver microsomes – HR-MS results

The HR-MS measurement of pooled microsomal incubation samples opened the opportunity to examine the correlation between the obtained data and the already published interspecies variations in the pattern of oxidative metabolites formed during the incubation of AOH and AME with liver microsomes (Pfeiffer *et al*., 2007b). Although a wide variety of possibly occurring substances was investigated (Appendix III), only the major AOH and AME metabolites are further discussed, as speculations about compounds detected in traces would go beyond the scope of this work.

The total peak area of the detected oxidative metabolites may provide additional information about the toxin metabolising efficacy shown by different mammalian microsomal fractions. The species order seen in the total amount of formed AOH metabolites listed below is in line with that observed in the parent toxin decrease (Figure 39). In contrast, a higher total peak area of the AME metabolites was found in porcine than in rat liver microsomes, which contradicts the results shown in Figure 40. Nevertheless, there is no reason to assume the same ionisation efficacy for all the detected analytes, so the peak area of a substance does not unquestionably correspond to its concentration. Therefore, the absolute quantitation of AME based on a reference material should be considered more significantly when concluding the relative metabolising efficacy of the tested liver microsomes.

AOH:	Species order:	Porcine LM < Rat LM < Human LM
	Total peak area (counts^2):	9.9×10^5 1.1×10^6 1.7×10^6
AME:	Species order:	Human LM << Rat LM < Porcine LM
	Total peak area (counts^2):	1.7×10^6 3.8×10^6 4.3×10^6

When exposing hepatic microsomes to AOH, two major peaks were detected in all three species at the retention times of 6.9 and 7.3 minutes. The earlier eluting one was identified as 4-hydroxy-alternariol based on the measurement of the *Alternaria* reference mixture (Figure 44). Further peak assignments relied on the elution order obtained under RP-LC conditions by Pfeiffer and co-workers, recognising that minor variations in this order cannot be ruled out and should therefore be considered as tentative assignments:

Retention time (r. t.): 8-OH-AOH < 4-OH-AOH < 10-OH-AOH < 2-OH-AOH

Since 2-OH-AOH was reported to elute lastly from all hydroxy metabolites, it was assumed to be the other major detoxification product (r. t. = 7.3 minutes). Analogously, since the compound by 4.8 minutes showed the least retention of all detected analytes and comparably low relative concentration as 8-OH-AOH in the publication of Pfeiffer *et al*., this peak was assigned as 8-OH-AOH. Nevertheless, the

fourth metabolite – 10-OH-AOH – could not be associated with any peak, although the already published study would indicate its level to be significantly above the LOD. A plausible explanation for this contradiction might be the co-elution of 2- and 10-OH-AOH. With this assumption, the herein obtained results regarding the interspecies variations are in good agreement with the previously reported data. Nevertheless, applying reference materials for each hydroxylated metabolite would be necessitated to verify the qualitative assignments. Furthermore, even if the ionisation behaviour of these isomers differs, a more accurate determination of their relative amounts could have been ensured when their reference materials would have been available for this study.

In contrast to AOH, the qualitative assignment of the AME-incubation results was more straightforward considering the published elution order of the oxidative metabolites of AME (Pfeiffer *et al.*, 2007b):

Retention time (r. t.): 8-OH-AME < AOH < 10-OH-AME < 4-OH-AME < 2-OH-AME

Apart from minor differences, the oxidative AME metabolites in the liver microsomes of all three species showed a comparable pattern as reported (Figure 45).

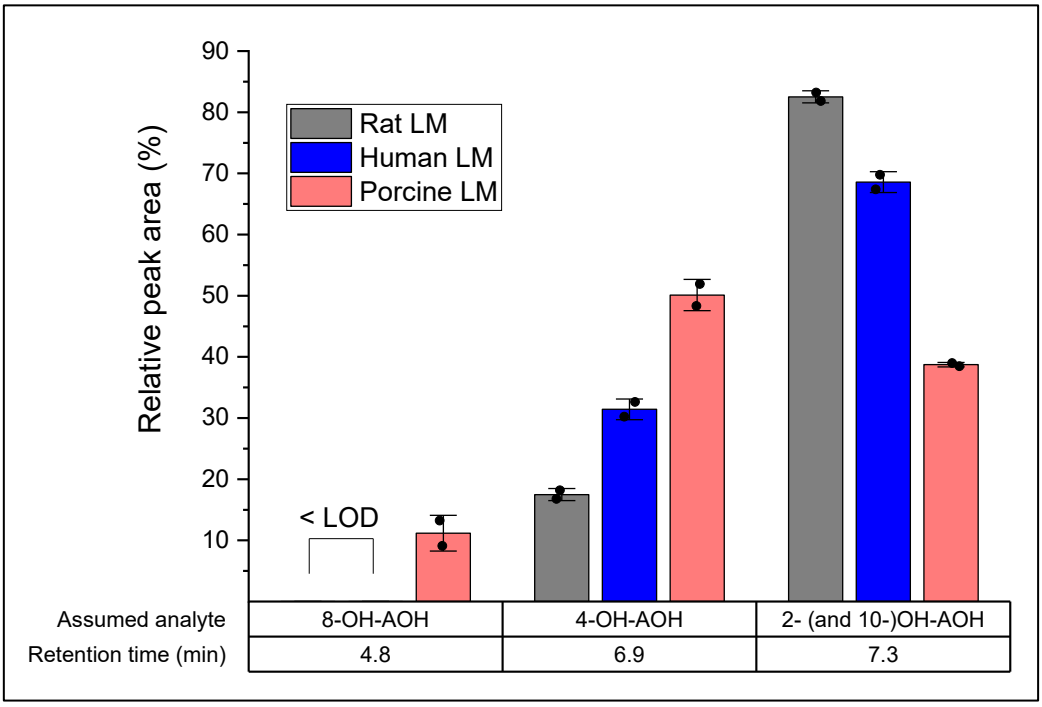

Figure 44: Interspecies differences in the pattern of oxidative metabolites occurred in liver microsomes (LM) subsequent to a 10-minute incubation with 10 µM AOH. The depicted values are normalised to the sum of the measured peak areas per species. Each bar shows the average of two measurements of one pooled sample ± standard deviation.

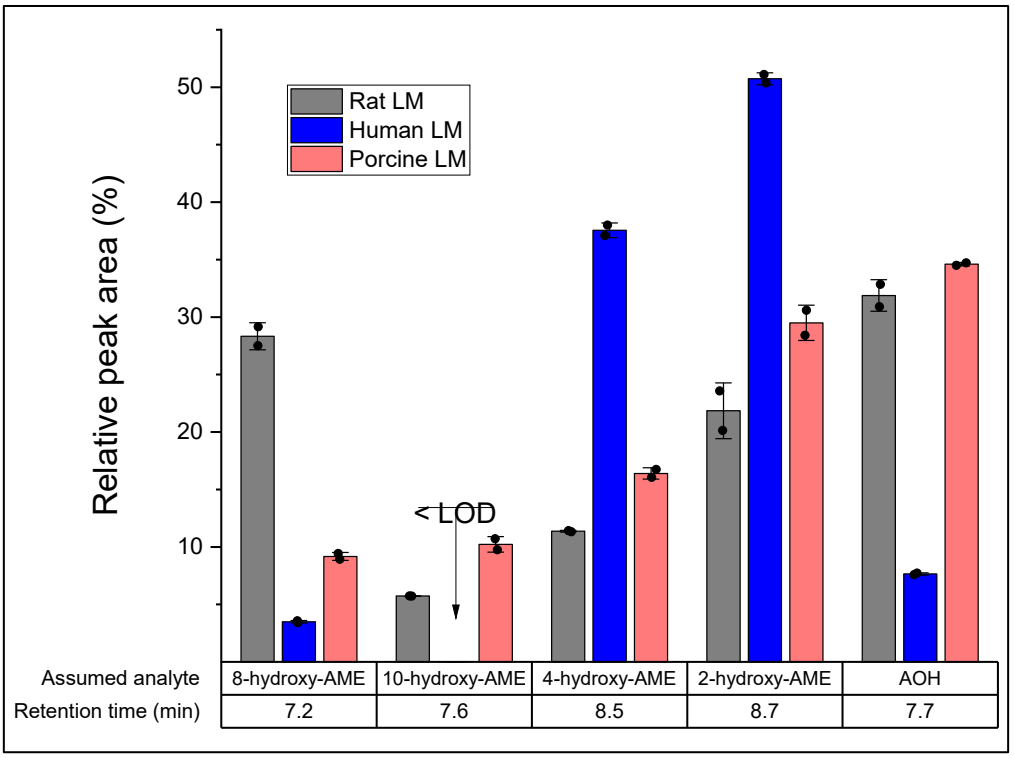

Figure 45: Interspecies differences in the pattern of oxidative metabolites occurred in liver microsomes (LM) subsequent to a 10-minute incubation with 10 µM AME. The depicted values are normalised to the sum of the measured peak areas per species. Each bar shows the average of two measurements of one pooled sample ± standard deviation.

Accepting the above-detailed peak assignments, the pattern of the oxidative AOH and AME metabolites depicted in Figure 44 and Figure 45 can easily be compared with Figures 12 and 7 in the publication of Pfeiffer *et al.* (2007b). First of all, when considering one specific metabolite, the species producing less and most of this compound are the same in this work and the literature.

However, there are deviations in the calculated relative values. For example, the relative amount of 8-OH-AME exceeded 50 % in rat liver microsomes in the reported study, whereas the relative peak area was found to be only about 30 % of the total metabolites in this thesis. A possible reason might be the difference in the incubation conditions (e. g. toxin concentration) between this work and the publication of Pfeiffer *et al*. (2007b). Most importantly, the reported dataset applies for a 40-minute incubation of liver microsomes with 50 µM substrate, while Figure 44 and Figure 45 present the results of exposing the hepatic microsomes to only 10 µM of the respective toxin for 10 minutes. As without individual reference materials for each analyte, the differences in the ionisation efficiency of the formed oxidative metabolites cannot be incorporated in the data evaluation, these may also contribute to any deviations in the quantitative results. Despite the small variations, both the published and herein performed datasets indicate remarkable differences between the qualitative composition of the metabolic products of AOH and especially AME in the three examined species emphasizing the significance of using species-specific models for toxicological tests.

In addition to the species comparison in one time point already known in the literature, the time-dependency of these relative concentration values was investigated in porcine liver microsomes. The initially not or only in traces detectable hydroxylated metabolites showed a more or less constant relative amount in porcine liver microsomes (Figure 46), whereas their absolute amount increased in the 10-60-minute time frame. This observation may suggest that equilibrium is reached where none of the CYP450 enzyme isoforms are saturated. Thus, the ratio of the transformation rates remains unchanged.

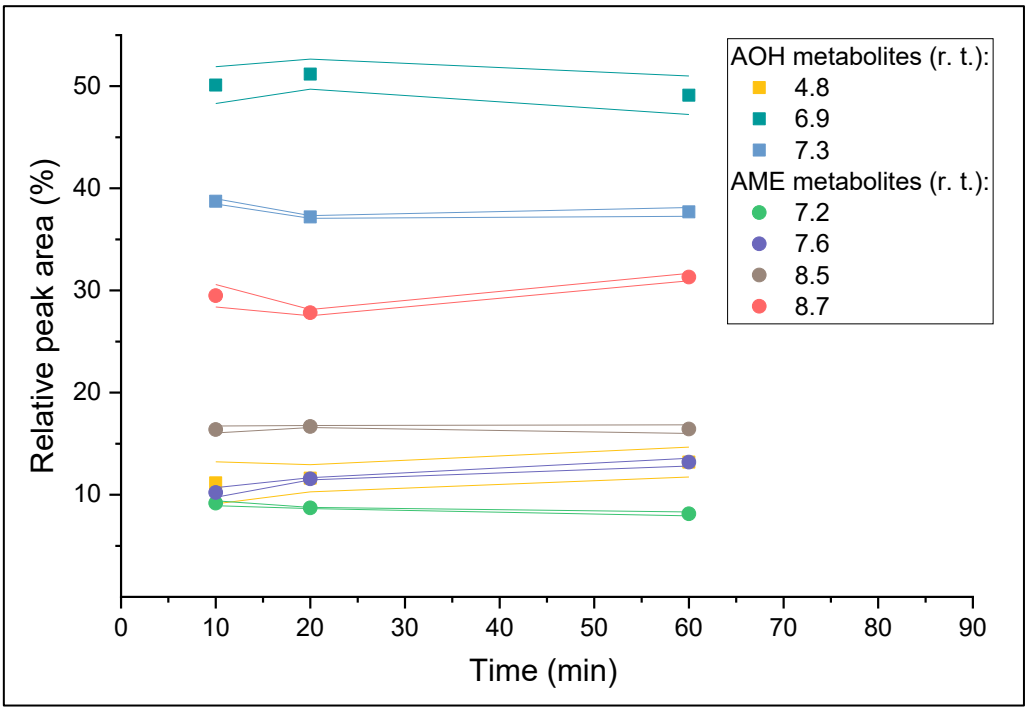

Figure 46: Time-dependency of the relative amounts of the hydroxylated AOH and AME metabolites when incubating porcine liver microsomes with 10 µM toxin. The depicted values are normalised to the sum of the measured peak areas of all detected metabolites, formed during the incubation with either AOH or AME, respectively. Please note that the sum of the relative peak area values of the hydroxy-AME metabolites is not 100 %, considering that further metabolites were detected during the incubation of porcine liver microsomes with AME. Each data point represents the mean of two independent measurements of the same pooled sample, while the lines indicate the SD.

The relative peak area of all measured hydroxy-AME isomers stayed nearly constant over time when incubating porcine liver microsomes with AME (Figure 46). In contrast, in the same incubation, the relative amount of AOH changed over time (Figure 47). Besides the decreasing tendency in the relative AOH level, detectable concentrations of hydroxylated AOH derivatives appeared already after 10 minutes of incubation. Thus, a part of the formed alternariol is readily metabolised within the monitored time frame. This finding supports and completes the conclusion drawn from Figure 32. There is a noteworthy difference between the two graphs, though, as one shows the relative, the other the absolute AOH level.

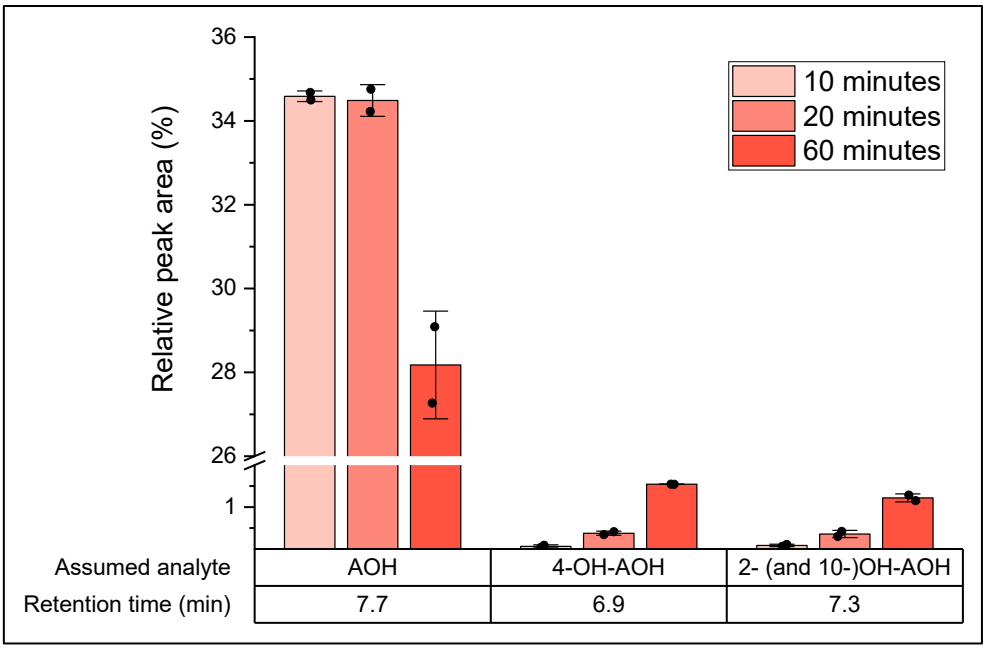

Figure 47: Changing AOH and hydroxyl-AOH level in AME-treated porcine liver microsomes The depicted values are normalised to the sum of the measured peak areas of all detected AME metabolites (see also Figure 45). Each bar shows the average of two measurements of one pooled sample ± standard deviation.

It is a common knowledge that the metabolism of xenobiotics is not necessarily detoxification and might even lead to the formation of more toxic substances than the initial compound. This issue was already addressed in the case of the 4-hydroxylated products of AOH and AME finding them to be less harmful as their parent compounds (Tiessen *et al*., 2017). AOH or the combination of AOH and AME elucidating even higher cytotoxic effects than pure AME reveals the value of the gathered information about AOH profile in an AME-treated biological system (Bensassi *et al*., 2015).

Conclusions

This thesis focused on the metabolic kinetics of AOH and AME in a few *in vitro* liver models. Firstly, metabolically active porcine hepatic microsomes could be prepared from liver tissue for later incubation studies. Subsequently, when treating NADPH-fortified liver microsomal fractions of three different mammalian species with AOH or AME, the vast majority of assays led to a significant decrease of the initial toxin concentration within the monitored incubation time (0-60 minutes for porcine, 0-10 minutes for rat and human liver microsomes). Calculating the conversion rate values and kinetic parameters based on the Michaelis-Menten model enabled to analyse possibly occurring interspecies differences. Although variations were present, the transformation rates of AOH were comparable in all three species, as the fastest metabolising species varied with the incubation concentration (1-100 µM). In contrast, more prominent species-specific variations were present in the phase I metabolism of AME – regardless of the initial toxin level (1-50 µM), rat liver microsomes stand out from the other two species, showing a more effective conversion of AME. Even though some publications investigated the microsomal metabolism of AOH and AME in different mammalian species, they only addressed the identification of the formed metabolites and the quantitative composition of the resulting metabolic mixture (Pfeiffer *et al*., 2007a and 2009). Hence, this work – predominantly focusing on the toxicokinetics of AOH and AME in hepatic microsomes of different species – delivers valuable quantitative information.

Besides, the already reported pattern in the oxidative metabolites of AOH and AME (Pfeiffer *et al*., 2007b) was successfully confirmed relying on the HR-MS measurements. Consistent with the literature, high interspecies variations were found in the relative amounts of the produced phase I metabolites. Additionally, the absolute and relative concentration of AOH was evaluated when incubating porcine liver microsomes with AME. After the initial AOH formation through AME demethylation, a consequent hydroxylation was observed. However, it remains a pending question whether this metabolic process generates less harmful substances than the initial incubating toxin, AME. Although there are examples in the literature investigating or predicting the adverse effects of the hydroxylated AOH and AME metabolites and their further fate in the body, more data would be required to answer this question (Dellafiora *et al.,* 2018; Tiessen *et al*., 2017).

The incubation studies of HepG2 cells with AOH or AME were performed in previous research to evaluate the cytotoxic and DNA strand-breaking activity of these substances (Juan-García *et al*., 2015; Juan-García *et al*., 2016; Pfeiffer *et al*., 2007a). Thus, these studies did not focus on the kinetic information regarding the AOH and AME metabolism in HepG2 cells and dealt with only a few and longer incubation time points (e.g. 24 hours). In contrast, this work reports about a significant decrease in the toxin concentration already after 4-6 hours when incubating HepG2 cells with AOH or AME. Furthermore, the major metabolites of the examined *Alternaria* toxins were identified for the first time. AME was predominantly converted to AME-3-S, whereas the HepG2 metabolism of AOH resulted in the formation of two sulphates – AOH-3-S and probably AOH-9-S. Based on this qualitative information, the HepG2 metabolism of these toxins can legitimately be considered detoxification. As opposed to the AOH concentration, the AME level showed a significant difference between the presence and absence of FBS in the incubation solution, probably due to matrix effects.

Overall, this work started to fill a data gap regarding the metabolic kinetics of the *Alternaria* toxins AOH and AME. The provided time-dependent toxin concentration data obtained in hepatic microsomal incubations, the transformation rate values, and the kinetic parameters calculated thereof might contribute to developing a PBTK model for AOH and AME. This approach would enable the estimation of local toxin concentrations in different organs, and consequently, provide a better understanding of the toxicological behaviour and health risk of these toxins.

Besides, the major metabolites of AOH and AME in HepG2 cells were identified, and the time-dependency of their metabolism was estimated. As discussed in section 2.3.2, the HepG2 cell line was versatilely utilised in published *in vitro* studies, both as a metabolically less active cell line and as an *in vitro* model for the xenobiotic metabolism of the human liver. The findings of this work may help to reconsider the applicability of this cell line for studying toxicodynamics.

Summary

The mycotoxins alternariol (AOH) and its monomethyl ether (AME) are food contaminants of natural biotic origin reported to exert various adverse effects *in vitro*. Yet, limited information is available about the toxicokinetics – absorption, distribution, metabolism, and excretion – of these compounds, specifically quantitative data regarding the concentration profile and kinetic parameters of the toxins are scarce.

Thus, this work aimed to unravel the phase I metabolism of AOH and AME in NADPH-fortified liver microsomes, both qualitatively and quantitatively. To pursue this goal, porcine, rat, and human hepatic microsomes were incubated with AOH or AME in a concentration range of 1-100 and 1-50 µM, respectively. The concentration-incubation time profile of the parent toxins and their metabolites was monitored with HPLC-MS/MS and HR-MS measurements. Deriving from these gathered data, this is the first study to report the total transformation rates of oxidative AOH and AME metabolism. Moreover, the kinetic parameters of the metabolic conversion were estimated based on the Michaelis-Menten model and the linear regression approach, providing valuable information for developing a physiologically-based toxicokinetic model for AOH and AME.

These incubation tests with liver microsomes originating from three different mammalian species allowed analysing interspecies variations. Indeed, the metabolic activity towards AME was significantly higher in pooled microsomal fractions of rats than of humans or particularly of porcine microsomes. Furthermore, the previously reported pattern of oxidative metabolites showing species-specific variations could be confirmed and completed. Both the qualitative and quantitative data dealing with interspecies differences highlight the significance of using *in vitro* models deriving from the respective species of interest. Otherwise, false assumptions might be drawn regarding the efficiency or mode of metabolism of xenobiotics.

Moreover, the human hepatocarcinoma cell line HepG2 was exposed to 10 µM AOH or AME aiming to determine the main metabolites and quantify them besides the parent toxins. As a result, sulphates were identified and quantified as the major detoxification products of both AOH and AME in this cell line. Although the high sulphotransferase activity in HepG2 cells is well-known in literature – to the best of my knowledge – no publications addressed the sulphation of AOH and AME in HepG2 cells.

The long-term objective of this research would be to estimate local concentrations of xenobiotics in specific organs *via* PBTK modelling, facilitating an understanding of the mode of action of their adverse health effects. Producing more quantitative data is indispensable to pursue this goal. This work as one of the few studies dealing with the toxicokinetics in AOH and AME contributed to reaching this overall aim.

Zusammenfassung

Das Mykotoxin Alternariol (AOH) und sein Monomethylether (AME) sind Lebensmittelkontaminanten natürlichen biotischen Ursprungs. Zahlreiche Studien berichteten, dass sie in der Lage sind unter *in vitro* Bedingungen toxische Wirkungen auszuüben. Über die Toxikokinetik – Resorption, Verteilung, Metabolisierung und Ausscheidung – dieser Verbindungen liegen jedoch nur begrenzte Informationen vor, insbesondere sind quantitative Daten zum Konzentrationsprofil der Toxine und zu kinetischen Parametern selten.

Daher zielte diese Arbeit darauf ab, den Phase-I-Metabolismus von AOH und AME in NADPH-angereicherten Lebermikrosomen sowohl qualitativ als auch quantitativ aufzuklären. Um dieses Ziel zu realisieren, wurden Schweine-, Ratten- und humane Lebermikrosomen mit AOH oder AME in einem Konzentrationsbereich von 1-100, bzw. 1-50 µM inkubiert. Das Konzentration-Inkubationszeit-Profil der herkömmlichen Toxine und ihrer Metaboliten wurde mit HPLC-MS/MS- und HR-MS-Messungen bestimmt. Dies ist die erste Studie, die – ausgehend von den erzeugten quantitativen Daten – über die Gesamtumwandlungsraten des oxidativen AOH- und AME-Metabolismus berichtet. Darüber hinaus wurden die kinetischen Parameter der metabolischen Umwandlung auf Basis der Michaelis-Menten-Kinetik, sowie des linearen Regressionsmodells abgeschätzt und liefert wertvolle Informationen für die Erstellung eines Models über die Toxikokinetik von AOH und AME.

Diese Inkubationstests mit Mikrosomen von drei verschiedenen Säugetierarten ermöglichten sogar die Detektion von etwaigen artspezifischen Variationen. Tatsächlich war die metabolische Aktivität gegenüber AME in der mikrosomalen Fraktion von Ratten signifikant höher als in menschlichen Mikrosomen oder Schweinelebermikrosomen. Außerdem konnte das zuvor publizierte speziesabhängige Muster von oxidativen Metaboliten bestätigt und vervollständigt werden. Sowohl die qualitativen als auch die quantitativen Daten zu diesen speziesspezifischen Unterschieden veranschaulichen die Bedeutung von *in-vitro*-Modellen. Diese sollten von den jeweiligen relevanten Spezies abgeleitet sein und in wissenschaftlichen Studien verwendet werden um aussagekräftige Daten produzieren zu können. Andernfalls könnte man zu falschen Annahmen über die Effizienz oder das Muster des Metabolismus von Xenobiotika kommen.

Darüber hinaus wurde die humane Hepatokarzinom-Zelllinie HepG2 mit 10 µM AOH oder AME behandelt, um die entstandenen Hauptmetaboliten zu bestimmen und sie neben den Ausgangstoxinen zu quantifizieren. Als Ergebnis wurden Sulfate als die Hauptentgiftungsprodukte von sowohl AOH als auch AME identifiziert und quantifiziert. Obwohl die hohe Sulfotransferase-Aktivität in HepG2-Zellen in der Literatur bekannt ist, gibt es meines Wissens nach keinen Publikationen, die die Sulfatierung von AOH und AME in HepG2 Zellen nachgewiesen hätten.

Das langfristige Ziel dieses Forschungsgebiets wäre es, die lokalen Konzentrationen von Xenobiotika in den betroffenen Organen abzuschätzen, um die Wirkungsweise ihrer gesundheitsgefährdenden Effekte zu verstehen. Um dieses Ziel zu verfolgen, ist es von großer Notwendigkeit, weitere quantitative Daten in unterschiedlichen Zellmodellen zu produzieren. Diese Arbeit trug als eine der wenigen Studien, die sich mit der Toxikokinetik von AOH und AME beschäftigen, zum Erreichen des Gesamtziels bei.

Directories

References

Aden, D.P., Fogel, A., Plotkin, S., Damjanov, I., Knowles, B.B., 1979. Controlled synthesis of HBsAg in a differentiated human liver carcinoma-derived cell line. Nature 282, 615–616. https://doi.org/10.1038/282615a0

Aichinger, G., Beisl, J., Marko, D., 2017. Genistein and delphinidin antagonize the genotoxic effects of the mycotoxin alternariol in human colon carcinoma cells. Molecular Nutrition & Food Research 61, 1600462. https://doi.org/10.1002/mnfr.201600462

Aichinger, G., Del Favero, G., Warth, B., Marko, D., 2021. *Alternaria* toxins - Still emerging? Comprehensive Reviews in Food Science and Food Safety 1541-4337.12803. https://doi.org/10.1111/1541-4337.12803

Al-Jaal, B.A., Jaganjac, M., Barcaru, A., Horvatovich, P., Latiff, A., 2019. Aflatoxin, fumonisin, ochratoxin, zearalenone and deoxynivalenol biomarkers in human biological fluids: A systematic literature review, 2001–2018. Food and Chemical Toxicology 129, 211–228. https://doi.org/10.1016/j.fct.2019.04.047

Al-Subeihi, A.A.A., Spenkelink, B., Punt, A., Boersma, M.G., van Bladeren, P.J., Rietjens, I.M.C.M., 2012. Physiologically based kinetic modeling of bioactivation and detoxification of the alkenylbenzene methyleugenol in human as compared with rat. Toxicology and Applied Pharmacology 260, 271–284. https://doi.org/10.1016/j.taap.2012.03.005

Anuj, M., Rajib, R., Jagatpati, T., 2013. *Alternaria* pathogenicity and its strategic controls. Research Journal of Biology 1, 01–09.

Asha, S., Vidyavathi, M., 2010. Role of Human Liver Microsomes in *In Vitro* Metabolism of Drugs—A Review. Applied Biochemistry and Biotechnology 160, 1699–1722. https://doi.org/10.1007/s12010-009-8689-6

Bensassi, F., Gallerne, C., Sharaf el dein, O., Rabeh Hajlaoui, M., Bacha, H., Lemaire, C., 2015. Combined effects of alternariols mixture on human colon carcinoma cells. Toxicology Mechanisms and Methods 25, 56–62. https://doi.org/10.3109/15376516.2014.985354

Berthiller, F., Dall'Asta, C., Schuhmacher, R., Lemmens, M., Adam, G., Krska, R., 2005. Masked Mycotoxins: Determination of a Deoxynivalenol Glucoside in Artificially and Naturally Contaminated Wheat by Liquid Chromatography−Tandem Mass Spectrometry. Journal of Agricultural and Food Chemistry 53, 3421–3425. https://doi.org/10.1021/jf047798g

Borchers, A.T., Chang, C., Eric Gershwin, M., 2017. Mold and Human Health: a Reality Check. Clinical Reviews in Allergy and Immunology 52, 305–322. https://doi.org/10.1007/s12016-017-8601-z

Braun, D., Ezekiel, C.N., Marko, D., Warth, B., 2020a. Exposure to Mycotoxin-Mixtures via Breast Milk: An Ultra-Sensitive LC-MS/MS Biomonitoring Approach. Frontiers in Chemistry 8, 423. https://doi.org/10.3389/fchem.2020.00423

Braun, D., Schernhammer, E., Marko, D., Warth, B., 2020b. Longitudinal assessment of mycotoxin co-exposures in exclusively breastfed infants. Environment International 142, 105845. https://doi.org/10.1016/j.envint.2020.105845

Brugger, E.-M., Wagner, J., Schumacher, D.M., Koch, K., Podlech, J., Metzler, M., Lehmann, L., 2006. Mutagenicity of the mycotoxin alternariol in cultured mammalian cells. Toxicology Letters 164, 221–230. https://doi.org/10.1016/j.toxlet.2006.01.001

Burkhardt, B., Pfeiffer, E., Metzler, M., 2009. Absorption and metabolism of the mycotoxins alternariol and alternariol-9-methyl ether in Caco-2 cells *in vitro*. Mycotoxin Research 25, 149–157. https://doi.org/10.1007/s12550-009-0022-2

Chiesi, C., Fernandez-Blanco, C., Cossignani, L., Font, G., Ruiz, M.J., 2015. Alternariol-induced cytotoxicity in Caco-2 cells. Protective effect of the phenolic fraction from virgin olive oil. Toxicon 93, 103–111. https://doi.org/10.1016/j.toxicon.2014.11.230

Claude, A., 1946. Fractionation of mammalian liver cells by differential centrifugation: II. Experimental procedures and results. Journal of Experimental Medicine 84, 61–89.

Dellafiora, L., Warth, B., Schmidt, V., Del Favero, G., Mikula, H., Fröhlich, J., Marko, D., 2018. An integrated *in silico*/*in vitro* approach to assess the xenoestrogenic potential of *Alternaria* mycotoxins and metabolites. Food Chemistry 248, 253–261. https://doi.org/10.1016/j.foodchem.2017.12.013

DeWoskin, R.S., 2007. PBPK models in risk assessment—A focus on chloroprene. Chemico-Biological Interactions 166, 352–359. https://doi.org/10.1016/j.cbi.2007.01.016

Dong, M.W., 2019. HPLC and UHPLC for practicing scientists, Second edition. Wiley, Hoboken, New Jersey.

European Food Safety Authority, 2011. Scientific Opinion on the risks for animal and public health related to the presence of *Alternaria* toxins in feed and food, EFSA Journal. https://doi.org/10.2903/j.efsa.2011.2407

European Food Safety Authority, Arcella, D., Eskola, M., Gómez Ruiz, J.A., 2016. Dietary exposure assessment to *Alternaria* toxins in the European population. EFSA Journal. https://doi.org/10.2903/j.efsa.2016.4654

Fehr, M., Pahlke, G., Fritz, J., Christensen, M.O., Boege, F., Altemöller, M., Podlech, J., Marko, D., 2009. Alternariol acts as a topoisomerase poison, preferentially affecting the IIα isoform. Molecular Nutrition & Food Research 53, 441–451. https://doi.org/10.1002/mnfr.200700379

Fernández-Blanco, C., Font, G., Ruiz, M.-J., 2015. Oxidative DNA damage and disturbance of antioxidant capacity by alternariol in Caco-2 cells. Toxicology Letters 235, 61–66. https://doi.org/10.1016/j.toxlet.2015.03.013

Freire, M. das G.M., Mussi-Dias, V., Mattoso, T.C., Henk, D.A., Mendes, A., Macedo, M.L.R., Turatti, C., Machado, S.W., Samuels, R.I., 2017. Survey of endophytic *Alternaria* species isolated from plants in the Brazilian restinga biome. IOSR Journal of Pharmacy and Biological Sciences 12, 84–94. https://doi.org/10.9790/3008-1202038494

Gómez-Lechón, M.J., Tolosa, L., Donato, M.T., 2014. Cell-based models to predict human hepatotoxicity of drugs. Revista de Toxicología. 31, 149-156. https://www.redalyc.org/articulo.oa?id=91932969007, accessed online 25/5/2021

Grimm, D., 2019. U.S. EPA to eliminate all mammal testing by 2035. Science. https://doi.org/10.1126/science.aaz4593

Gruber-Dorninger, C., Novak, B., Nagl, V., Berthiller, F., 2017. Emerging Mycotoxins: Beyond Traditionally Determined Food Contaminants. Journal of Agricultural and Food Chemistry 65, 7052–7070. https://doi.org/10.1021/acs.jafc.6b03413

Gstraunthaler, G., Lindl, T., 2013. Zell- und Gewebekultur: allgemeine Grundlagen und spezielle Anwendungen, Seventh edition. Springer Spektrum, Berlin Heidelberg.

Habschied, K., Kanižai Šarić, G., Krstanović, V., Mastanjević, K., 2021. Mycotoxins—Biomonitoring and Human Exposure. Toxins 13, 113. https://doi.org/10.3390/toxins13020113

Hessel-Pras, S., Kieshauer, J., Roenn, G., Luckert, C., Braeuning, A., Lampen, A., 2019. *In vitro* characterization of hepatic toxicity of *Alternaria* toxins. Mycotoxin Research 35, 157–168. https://doi.org/10.1007/s12550-018-0339-9

Hou, R., Huang, C., Rao, K., Xu, Y., Wang, Z., 2018. Characterized *in Vitro* Metabolism Kinetics of Alkyl Organophosphate Esters in Fish Liver and Intestinal Microsomes. Environmental Science and Technology 52, 3202–3210. https://doi.org/10.1021/acs.est.7b05825

Hussein, H.S., Brasel, J.M., 2001. Toxicity, metabolism, and impact of mycotoxins on humans and animals. Toxicology 167, 101–134. https://doi.org/10.1016/S0300-483X(01)00471-1

Jagow, R., Kampffmeyer, H., Kinese, M., 1965. The preparation of microsomes. Naunyn-Schmiedeberg's Archives of Pharmacology 251, 73–87. https://doi.org/10.1007/BF00245731

Juan-García, A., Juan, C., König, S., Ruiz, M.-J., 2015. Cytotoxic effects and degradation products of three mycotoxins: Alternariol, 3-acetyl-deoxynivalenol and 15-acetyl-deoxynivalenol in liver hepatocellular carcinoma cells. Toxicology Letters 235, 8–16. https://doi.org/10.1016/j.toxlet.2015.03.003

Juan-García, A., Juan, C., Manyes, L., Ruiz, M.-J., 2016. Binary and tertiary combination of alternariol, 3-acetyl-deoxynivalenol and 15-acetyl-deoxynivalenol on HepG2 cells: Toxic effects and evaluation of degradation products. Toxicology *in Vitro* 34, 264–273. https://doi.org/10.1016/j.tiv.2016.04.016

Khodaei, S., Arzanlou, M., 2013. Morphology, phylogeny and pathogenicity of *Alternaria* species, involved in leaf spot disease of sunflower in northern Iran. Archives Of Phytopathology And Plant Protection 46, 2224–2234. https://doi.org/10.1080/03235408.2013.790259

Kollarova, J., Cenk, E., Schmutz, C., Marko, D., 2018. The mycotoxin alternariol suppresses lipopolysaccharide-induced inflammation in THP-1 derived macrophages targeting the NF-κB signalling pathway. Archives of Toxicology 92, 3347–3358. https://doi.org/10.1007/s00204-018-2299-4

Kramer, M.A., Tracy, T.S., 2012. Enzyme Kinetics of Drug-Metabolizing Reactions and Drug-Drug Interactions, in: Encyclopedia of Drug Metabolism and Interactions. John Wiley & Sons, Inc., Hoboken, New Jersey, p. edm003. https://doi.org/10.1002/9780470921920.edm003

Krishnan, K., Peyret, T., 2009. Physiologically Based Toxicokinetic (PBTK) Modeling in Ecotoxicology, in: Devillers, J. (Ed.), Ecotoxicology Modeling, Emerging Topics in Ecotoxicology. Springer US, Boston, MA, pp. 145–175. https://doi.org/10.1007/978-1-4419-0197-2_6

Kromidas, S., 2016. The HPLC expert: possibilities and limitations of modern high performance liquid chromatography. Wiley-VCH, Weinheim

Kustrzeba-Wójcicka, I., Siwak, E., Terlecki, G., Wolańczyk-Mędrala, A., Mędrala, W., 2014. *Alternaria alternata* and Its Allergens: a Comprehensive Review. Clinical Reviews in Allergy and Immunology 47, 354–365. https://doi.org/10.1007/s12016-014-8447-6

Lehmann, L., Wagner, J., Metzler, M., 2006. Estrogenic and clastogenic potential of the mycotoxin alternariol in cultured mammalian cells. Food and Chemical Toxicology 44, 398–408. https://doi.org/10.1016/j.fct.2005.08.013

López-Terrada, D., Cheung, S.W., Finegold, M.J., Knowles, B.B., 2009. HepG2 is a hepatoblastoma-derived cell line. Human Pathology 40, 1512–1515. https://doi.org/10.1016/j.humpath.2009.07.003

Marin, S., Ramos, A.J., Cano-Sancho, G., Sanchis, V., 2013. Mycotoxins: Occurrence, toxicology, and exposure assessment. Food and Chemical Toxicology 60, 218–237. https://doi.org/10.1016/j.fct.2013.07.047

Martins, C., Vidal, A., De Boevre, M., De Saeger, S., Nunes, C., Torres, D., Goios, A., Lopes, C., Assunção, R., Alvito, P., 2019. Exposure assessment of Portuguese population to multiple mycotoxins: The human biomonitoring approach. International Journal of Hygiene and Environmental Health 222, 913–925. https://doi.org/10.1016/j.ijheh.2019.06.010

Moore, G. E., Gerner, R. E., Franklin, H. A., 1967. Culture of Normal Human Leukocytes. The Journal of the American Medical Association, 199, 519-524. doi:10.1001/jama.1967.03120080053007

Mukherjee, D., Royce, S.G., Alexander, J.A., Buckley, B., Isukapalli, S.S., Bandera, E.V., Zarbl, H., Georgopoulos, P.G., 2014. Physiologically-Based Toxicokinetic Modeling of Zearalenone and Its Metabolites: Application to the Jersey Girl Study. PLOS One 9, e113632. https://doi.org/10.1371/journal.pone.0113632

Nebbia, C., Ceppa, L., Dacasto, M., Nachtmann, C., Carletti, M., 2002. Oxidative monensin metabolism and cytochrome P450 3A content and functions in liver microsomes from horses, pigs, broiler chicks, cattle and rats: Monensin metabolism in food producing species. Journal of Veterinary Pharmacology and Therapeutics 24, 399–403. https://doi.org/10.1046/j.1365-2885.2001.00362.x

Nič, M., Jirát, J., Košata, B., Jenkins, A., McNaught, A. (Eds.), 2009. chromatography, in: IUPAC Compendium of Chemical Terminology. IUPAC, Research Triagle Park, North Carolina. https://doi.org/10.1351/goldbook.C01075

Olsen, M., Visconti, A., 1988. Metabolism of alternariol monomethyl ether by porcine liver and intestinal mucosa *in vitro*. Toxicology *in Vitro* 2, 27–29. https://doi.org/10.1016/0887-2333(88)90033-1

Ostry, V., 2008. *Alternaria* mycotoxins: an overview of chemical characterization, producers, toxicity, analysis and occurrence in foodstuffs. World Mycotoxin Journal 1, 175–188. https://doi.org/10.3920/WMJ2008.x013

Otieno, B.A., Krause, C.E., Rusling, J.F., 2016. Bioconjugation of Antibodies and Enzyme Labels onto Magnetic Beads, in: Methods in Enzymology. Elsevier, pp. 135–150. https://doi.org/10.1016/bs.mie.2015.10.005

Pastor, F.J., Guarro, J., 2008. *Alternaria* infections: laboratory diagnosis and relevant clinical features. Clinical Microbiology and Infection 14, 734–746. https://doi.org/10.1111/j.1469-0691.2008.02024.x

Pfeiffer, E., Burkhardt, B., Altemöller, M., Podlech, J., Metzler, M., 2008. Activities of human recombinant cytochrome P450 isoforms and human hepatic microsomes for the hydroxylation of *Alternaria* toxins. Mycotoxin Research 24, 117–123. https://doi.org/10.1007/BF03032337

Pfeiffer, E., Eschbach, S., Metzler, M., 2007a. *Alternaria* toxins: DNA strand-breaking activity in mammalian cells *in vitro*. Mycotoxin Research s 23, 152–157. https://doi.org/10.1007/BF02951512

Pfeiffer, E., Schebb, N.H., Podlech, J., Metzler, M., 2007b. Novel oxidative *in vitro* metabolites of the mycotoxins alternariol and alternariol methyl ether. Molecular Nutrition & Food Research 51, 307–316. https://doi.org/10.1002/mnfr.200600237

Pfeiffer, E., Schmit, C., Burkhardt, B., Altemöller, M., Podlech, J., Metzler, M., 2009. Glucuronidation of the mycotoxins alternariol and alternariol-9-methyl ether *in vitro*: chemical structures of glucuronides and activities of human UDP-glucuronosyltransferase isoforms. Mycotoxin Research 25, 3–10. https://doi.org/10.1007/s12550-008-0001-z

Pinto, V.E.F., Patriarca, A., 2017. *Alternaria* Species and Their Associated Mycotoxins, in: Moretti, A., Susca, A. (Eds.), Mycotoxigenic Fungi, Methods in Molecular Biology. Springer New York, New York, pp. 13–32. https://doi.org/10.1007/978-1-4939-6707-0_2

Pollock, G.A., DiSabatino, C.E., Heimsch, R.C., Coulombe, R.A., 1982. The distribution, elimination, and metabolism of ^{14}C-alternariol monomethyl ether. Journal of Environmental Science and Health, Part B 17, 109–124. https://doi.org/10.1080/03601238209372306

Puntscher, H., Aichinger, G., Grabher, S., Attakpah, E., Krüger, F., Tillmann, K., Motschnig, T., Hohenbichler, J., Braun, D., Plasenzotti, R., Pahlke, G., Höger, H., Marko, D., Warth, B., 2019. Bioavailability, metabolism, and excretion of a complex *Alternaria* culture extract versus altertoxin II: a comparative study in rats. Archives of Toxicology 93, 3153–3167. https://doi.org/10.1007/s00204-019-02575-7

Puntscher, H., Kütt, M.-L., Skrinjar, P., Mikula, H., Podlech, J., Fröhlich, J., Marko, D., Warth, B., 2018. Tracking emerging mycotoxins in food: development of an LC-MS/MS method for free and modified *Alternaria* toxins. Analytical and Bioanalytical Chemistry 410, 4481–4494. https://doi.org/10.1007/s00216-018-1105-8

Puntscher, H., Marko, D., Warth, B., 2020. First determination of the highly genotoxic fungal contaminant altertoxin II in a naturally infested apple sample. Emerging Contaminants 6, 82–86. https://doi.org/10.1016/j.emcon.2020.01.002

Qiao, X., Zhang, J., Yang, Y., Yin, J., Li, H., Xing, Y., Shao, B., 2020. Development of a simple and rapid LC-MS/MS method for the simultaneous quantification of five *Alternaria* mycotoxins in human urine. Journal of Chromatography B 1144, 122096. https://doi.org/10.1016/j.jchromb.2020.122096

Richard, J.L., 2007. Some major mycotoxins and their mycotoxicoses — An overview. International Journal of Food Microbiology 119, 3–10. https://doi.org/10.1016/j.ijfoodmicro.2007.07.019

Rico-Yuste, A., Walravens, J., Urraca, J.L., Abou-Hany, R.A.G., Descalzo, A.B., Orellana, G., Rychlik, M., De Saeger, S., Moreno-Bondi, M.C., 2018. Analysis of alternariol and alternariol monomethyl ether in foodstuffs by molecularly imprinted solid-phase extraction and ultra-high-performance liquid chromatography tandem mass spectrometry. Food Chemistry 243, 357–364. https://doi.org/10.1016/j.foodchem.2017.09.125

Rodríguez-Carrasco, Y., Mañes, J., Berrada, H., Juan, C., 2016. Development and Validation of a LC-ESI-MS/MS Method for the Determination of *Alternaria* Toxins Alternariol, Alternariol Methyl-Ether and Tentoxin in Tomato and Tomato-Based Products. Toxins 8, 328. https://doi.org/10.3390/toxins8110328

Rotem, J., 1994. The genus *Alternaria*: biology, epidemiology, and pathogenicity. APS Press, St. Paul, Minnesota.

Russell, R., Paterson, R.R.M., Lima, N., 2016. Molecular biology of food and water borne mycotoxigenic and mycotic fungi. CRC Press, Boca Raton, Florida.

Rychlik, M., Humpf, H.-U., Marko, D., Dänicke, S., Mally, A., Berthiller, F., Lorenz, N., 2014. Proposal of a comprehensive definition of modified and other forms of mycotoxins including “masked” mycotoxins. Mycotoxin Research 30(4), 197-205. https://doi.org/10.1007/s12550-014-0203-5

Schmutz, C., Cenk, E., Marko, D., 2019. The *Alternaria* Mycotoxin Alternariol Triggers the Immune Response of IL-1β-stimulated, Differentiated Caco-2 Cells. Molecular Nutrition & Food Research 63, 1900341. https://doi.org/10.1002/mnfr.201900341

Schneckener, S., Preuss, T.G., Kuepfer, L., Witt, J., 2020. A workflow to build PBTK models for novel species. Archives of Toxicology 94, 3847–3860. https://doi.org/10.1007/s00204-020-02922-z

Schuchardt, S., Ziemann, C., Hansen, T., 2014. Combined toxicokinetic and *in vivo* genotoxicity study on *Alternaria* toxins. EFSA Journal. https://doi.org/10.2903/sp.efsa.2014.EN-679

Schwarz, C., Kreutzer, M., Marko, D., 2012. Minor contribution of alternariol, alternariol monomethyl ether and tenuazonic acid to the genotoxic properties of extracts from *Alternaria alternata* infested rice. Toxicology Letters 214, 46–52. https://doi.org/10.1016/j.toxlet.2012.08.002

Shin, B.S., Hong, S.H., Bulitta, J.B., Lee, J.B., Hwang, S.W., Kim, H.J., Yang, S.D., Yoon, H.-S., Kim, D.J., Lee, B.M., Yoo, S.D., 2009. Physiologically Based Pharmacokinetics of Zearalenone. Journal of Toxicology and Environmental Health, Part A 72, 1395–1405. https://doi.org/10.1080/15287390903212741

Shivani Grover, Christopher Lawrence, 2017. The *Alternaria alternata* Mycotoxin Alternariol Suppresses Lipopolysaccharide-Induced Inflammation. International Journal of Molecular Sciences 18, 1577. https://doi.org/10.3390/ijms18071577

Shwed, J.A., Walle, U.K., Walle, T., 1992. HepG2 cell line as a human model for sulphate conjugation of drugs. Xenobiotica 22, 973–982. https://doi.org/10.3109/00498259209049903

Siegel, D., Feist, M., Proske, M., Koch, M., Nehls, I., 2010. Degradation of the *Alternaria* Mycotoxins Alternariol, Alternariol Monomethyl Ether, and Altenuene upon Bread Baking. Journal of Agricultural and Food Chemistry 58, 9622–9630. https://doi.org/10.1021/jf102156w

Simon, H., Hoffmann, G., Hübner, F., Humpf, H.-U., Karst, U., 2016. Electrochemical simulation of metabolic reactions of the secondary fungal metabolites alternariol and alternariol methyl ether. Analytical and Bioanalytical Chemistry 408, 2471–2483. https://doi.org/10.1007/s00216-016-9344-z

Smoluch, M., Grasso, G., Suder, P., Silberring, J. (Eds.), 2019. Mass spectrometry: an applied approach, Second edition. Wiley series on mass spectrometry. Wiley, Hoboken, New Jersey.

Snyder, L.R., Kirkland, J.J., Dolan, J.W., 2010. Introduction to modern liquid chromatography, Third edition. Wiley, Hoboken, New Jersey.

Solhaug, A., Eriksen, G.S., Holme, J.A., 2016. Mechanisms of Action and Toxicity of the Mycotoxin Alternariol: A Review. Basic & Clinical Pharmacology & Toxicology 119, 533–539. https://doi.org/10.1111/bcpt.12635

Solhaug, A., Vines, L. L., Ivanova, L., Spilsberg, B., Holme, J. A., Pestka, J., Collins, A., Eriksen, G. S., 2012. Mechanisms involved in alternariol-induced cell cycle arrest. Mutation Research/Fundamental and Molecular Mechanisms of Mutagenesis, 738-739, 1–11. doi:10.1016/j.mrfmmm.2012.09.001

Soukup, S.T., Kohn, B.N., Pfeiffer, E., Geisen, R., Metzler, M., Bunzel, M., Kulling, S.E., 2016. Sulfoglucosides as Novel Modified Forms of the Mycotoxins Alternariol and Alternariol Monomethyl Ether. Journal of Agricultural and Food Chemistry 64, 8892–8901. https://doi.org/10.1021/acs.jafc.6b03120

Stypuła-Trębas, S., Minta, M., Radko, L., Jedziniak, P., Posyniak, A., 2017. Nonsteroidal mycotoxin alternariol is a full androgen agonist in the yeast reporter androgen bioassay. Environmental Toxicology and Pharmacology 55, 208–211. https://doi.org/10.1016/j.etap.2017.08.036

Taevernier, L., Wynendaele, E., De Vreese, L., Burvenich, C., De Spiegeleer, B., 2016. The mycotoxin definition reconsidered towards fungal cyclic depsipeptides. Journal of Environmental Science and Health, Part C 34, 114–135. https://doi.org/10.1080/10590501.2016.1164561

Thermo Fisher Scientific, https://www.thermofisher.com/hu/en/home/technical-resources/media-formulation.187.html, accessed online, 25/6/2021.

Thomma, B.P.H.J., 2003. *Alternaria* spp.: from general saprophyte to specific parasite: *Alternaria*. Molecular Plant Pathology 4, 225–236. https://doi.org/10.1046/j.1364-3703.2003.00173.x

Tiessen, C., Ellmer, D., Mikula, H., Pahlke, G., Warth, B., Gehrke, H., Zimmermann, K., Heiss, E., Fröhlich, J., Marko, D., 2017. Impact of phase I metabolism on uptake, oxidative stress and genotoxicity of the emerging mycotoxin alternariol and its monomethyl ether in esophageal cells. Archives of Toxicology 91, 1213–1226. https://doi.org/10.1007/s00204-016-1801-0

Tiessen, C., Fehr, M., Schwarz, C., Baechler, S., Domnanich, K., Böttler, U., Pahlke, G., Marko, D., 2013. Modulation of the cellular redox status by the *Alternaria* toxins alternariol and alternariol monomethyl ether. Toxicology Letters 216, 23–30. https://doi.org/10.1016/j.toxlet.2012.11.005

Tolosa, L., Gómez-Lechón, M.J., Pérez-Cataldo, G., Castell, J.V., Donato, M.T., 2013. HepG2 cells simultaneously expressing five P450 enzymes for the screening of hepatotoxicity: identification of bioactivable drugs and the potential mechanism of toxicity involved. Archives of Toxicology 87, 1115–1127. https://doi.org/10.1007/s00204-013-1012-x

Traub, E., 1975. Observations on “Late onset disease” and Tumor Incidence in Different Strains of Laboratory Mice infected Congenitally with LCM Virus: I. Experiments with Random-bred NMRI Mice. Zentralblatt für Veterinärmedizin Reihe B 22, 764–782. https://doi.org/10.1111/j.1439-0450.1975.tb00643.x

Tswett, M., 1906. Physikalisch-chemische Studien über das Chlorophyll. Die Adsorptionen [Physical-chemical studies of chlorophyll. Adsorption]. Berichte der Deutschen Botanischen Gesellschaft. 24, 316–323. doi:10.1111/j.1438-8677.1906.tb06524.x

Tuszynski, G.P., Murphy, A., 1990. Spectrophotometric quantitation of anchorage-dependent cell numbers using the bicinchoninic acid protein assay reagent. Analytical Biochemistry 184, 189–191. https://doi.org/10.1016/0003-2697(90)90032-5

Vashist, S.K., Luong, J.H.T., 2018. Bioanalytical Requirements and Regulatory Guidelines for Immunoassays, in: Handbook of Immunoassay Technologies. Elsevier, pp. 81–95. https://doi.org/10.1016/B978-0-12-811762-0.00004-9

Vejdovszky, K., Hahn, K., Braun, D., Warth, B., Marko, D., 2017. Synergistic estrogenic effects of *Fusarium* and *Alternaria* mycotoxins *in vitro*. Archives of Toxicology 91, 1447–1460. https://doi.org/10.1007/s00204-016-1795-7

Vinken, M., Rogiers, V. (Eds.), 2015. Protocols in *in vitro* hepatocyte research, Methods in molecular biology. Humana Press, New York.

Wilkening, S., Stahl, F., Bader, A., 2003. Comparison of primary human hepatocytes and hepatoma cell line HepG2 with regard to their biotransformation properties. Drug Metabolism & Disposition 31, 1035–1042. https://doi.org/10.1124/dmd.31.8.1035

Williams, R.T., 1974. Inter-Species Variations in the Metabolism of Xenobiotics. Biochemical Society Transactions 2, 359–377. https://doi.org/10.1042/bst0020359

Williams, T.I., Weil, H., 1952. Definition of Chromatography. Nature 170, 503–503. https://doi.org/10.1038/170503b0

Yan, Z., Feng, C., Jin, X., Liu, D., Hong, Y., Qiao, Y., Bai, Y., Moon, H.-B., Qadeer, A., Wu, F., 2021. *In vitro* metabolic kinetics of cresyl diphenyl phosphate (CDP) in liver microsomes of crucian carp (*Carassius carassius*). Environmental Pollution 274, 116586. https://doi.org/10.1016/j.envpol.2021.116586

d'Yvoire, M.B., Prieto, P., Blaauboer, B.J., Bois, F.Y., Boobis, A., Brochot, C., Coecke, S., Freidig, A., Gundert-Remy, U., Hartung, T., Jacobs, M.N., Lavé, T., Leahy, D.E., Lennernäs, H., Loizou, G.D., Meek, B., Pease, C., Rowland, M., Spendiff, M., Yang, J., Zeilmaker, M., 2007. Physiologically-based Kinetic Modelling (PBK Modelling): Meeting the 3Rs Agenda: The Report and Recommendations of ECVAM Workshop 63 a. Alternatives to Laboratory Animals 35, 661–671. https://doi.org/10.1177/026119290703500606

Zhuang, X., Lu, C., 2016. PBPK modeling and simulation in drug research and development. Acta Pharmaceutica Sinica B 6, 430–440. https://doi.org/10.1016/j.apsb.2016.04.004

List of figures

List of tables

List of equations

Abbreviations

ACN	acetonitrile
ADV-HepG2	upgraded HepG2 cells co-transfected with adenoviral vectors
AME	alternariol monomethyl ether
ANOVA	analysis of variance
AOH	alternariol
APCI	atmospheric pressure chemical ionisation
APP	control after protein precipitation
BCA	bicinchoninic acid
BPP	control before protein precipitation
c	concentration
CYP450s	cytochromes P450 (enzyme superfamily, functioning as monooxygenases)
DAD	diode-array detector
DMSO	dimethyl sulphoxide
EC	evaporation control
EDTA	ethylenediamine tetraacetic acid
EFSA	European Food Safety Authority
ER	oestrogen receptor
ESI	electrospray ionisation
FBS	foetal bovine serum
GC	gas chromatography
HAc	acetic acid
H2AX	H2A histone family member X (a type of histone protein)
HBM	human biomonitoring
HLM	human liver microsomes
HPLC	high-performance liquid chromatography
IC_{50}	half-maximal inhibitory concentration
i. d.	inner diameter (LC columns)
LC	liquid chromatograph(y)
LLOQ	lower limit of quantification
LM	liver microsomes
LOD	limit of detection
LOQ	limit of quantification
LSD	least significant difference test
MeOH	methanol
mRNA	messenger ribonucleic acid
MS	mass spectrometry/mass spectrometer
MS/MS	tandem mass spectrometry
m/*z*	mass-to-charge ratio
NADPH	nicotinamide adenine dinucleotide phosphate

NMRI	Naval Medical Research Institute
PBS	phosphate-buffered saline
PBTK modelling	physiologically based toxicokinetic modelling
P/S	penicillin-streptomycin
Q	(single) quadrupole
QqQ	triple quadrupole
RIPA buffer	radioimmunoprecipitation assay buffer
ROS	reactive oxygen species
RP	reversed-phase (chromatography)
RPMI 1640	Roswell Park Memorial Institute 1640 medium
RSD (%)	relative standard deviation
SC	solvent control
SD	standard deviation
S/N	signal-to-noise ratio
SRM	selected reaction monitoring
TC	tissue culture
TOF	time of flight
TTC	threshold of toxicological concern
UDPGA	uridine-diphosphate-glucuronic acid
UGT	uridine diphosphoglucuronosyl transferase
UHPLC	ultra-high-performance liquid chromatography
ULOQ	upper limit of quantification
UV	ultraviolet (detector)
V	volume

Appendix
I. Incubation plans of HepG2 cells

PBS	PBS	PBS	PBS	PBS	PBS	PBS	PBS	PBS	PBS	PBS	PBS
PBS	AOH FBS 15 min	AOH FBS 15 min	AOH FBS 1440 min	AOH FBS 1440 min	AOH no FBS 300 min	AOH no FBS 300 min	AME FBS 120 min	AME FBS 120 min	AME no FBS 90 min	AME no FBS 90 min	PBS
PBS	AOH FBS 30 min	AOH FBS 30 min	AOH no FBS 15 min	AOH no FBS 15 min	AOH no FBS 1440 min	AOH no FBS 1440 min	AME FBS 300 min	AME FBS 300 min	AME no FBS 120 min	AME no FBS 120 min	PBS
PBS	AOH FBS 60 min	AOH FBS 60 min	AOH no FBS 30 min	AOH no FBS 30 min	AME FBS 15 min	AME FBS 15 min	AME FBS 1440 min	AME FBS 1440 min	AME no FBS 300 min	AME no FBS 300 min	PBS
PBS	AOH FBS 90 min	AOH FBS 90 min	AOH no FBS 60 min	AOH no FBS 60 min	AME FBS 30 min	AME FBS 30 min	AME no FBS 15 min	AME no FBS 15 min	AME no FBS 1440 min	AME no FBS 1440 min	PBS
PBS	AOH FBS 120 min	AOH FBS 120 min	AOH no FBS 90 min	AOH no FBS 90 min	AME FBS 60 min	AME FBS 60 min	AME no FBS 30 min	AME no FBS 30 min	SC FBS 1440 min	SC FBS 1440 min	PBS
PBS	AOH FBS 300 min	AOH FBS 300 min	AOH no FBS 120 min	AOH no FBS 120 min	AME FBS 90 min	AME FBS 90 min	AME no FBS 60 min	AME no FBS 60 min	SC no FBS 1440 min	SC no FBS 1440 min	PBS
PBS	PBS	PBS	PBS	PBS	PBS	PBS	PBS	PBS	PBS	PBS	PBS

Figure A1: Incubation plan of 96-well plate for the incubation of HepG2 cells with AOH and AME – preliminary studies

PBS	PBS	PBS	PBS	PBS	PBS	PBS	PBS	PBS	PBS	PBS	PBS
PBS	**AOH FBS 4 h**	**AOH FBS 4 h**	**AOH FBS 4 h**	**AOH FBS 8 h**	**AOH FBS 8 h**	**AOH FBS 8 h**	**EC AOH FBS 10 h**	AOH FBS 14 h	AOH FBS 14 h	AOH FBS 14 h	PBS
PBS	**AOH no FBS 4 h**	**AOH no FBS 4 h**	**AOH no FBS 4 h**	**AOH no FBS 8 h**	**AOH no FBS 8 h**	**AOH no FBS 8 h**	**EC AOH FBS 10 h**	AOH no FBS 14 h	AOH no FBS 14 h	AOH no FBS 14 h	PBS
PBS	**AOH FBS 6 h**	**AOH FBS 6 h**	**AOH FBS 6 h**	**AOH FBS 10 h**	**AOH FBS 10 h**	**AOH FBS 10 h**	**EC AOH FBS 10 h**	AOH FBS 16 h	AOH FBS 16 h	AOH FBS 16 h	PBS
PBS	**AOH no FBS 6 h**	**AOH no FBS 6 h**	**AOH no FBS 6 h**	**AOH no FBS 10 h**	**AOH no FBS 10 h**	**AOH no FBS 10 h**	**EC AOH no FBS 10 h**	AOH no FBS 16 h	AOH no FBS 16 h	AOH no FBS 16 h	PBS
PBS	BPP AOH FBS 18 h	BPP AOH no FBS 18 h	APP AOH FBS 18 h	APP AOH no FBS 18 h	SC FBS 18 h	SC no FBS 18 h	**EC AOH no FBS 10 h**	AOH FBS 18 h	AOH FBS 18 h	AOH FBS 18 h	PBS
PBS	BPP AOH FBS 18 h	BPP AOH no FBS 18 h	APP AOH FBS 18 h	APP AOH no FBS 18 h	SC FBS 18 h	SC no FBS 18 h	**EC AOH no FBS 10 h**	AOH no FBS 18 h	AOH no FBS 18 h	AOH no FBS 18 h	PBS
PBS	BPP AOH FBS 18 h	BPP AOH no FBS 18 h	APP AOH FBS 18 h	APP AOH no FBS 18 h	SC FBS 18 h	SC no FBS 18 h	PBS	PBS	PBS	PBS	PBS

Figure A2: Incubation plan of 96-well plate for the incubation of HepG2 cells with AOH – first biological replicate

PBS	PBS	PBS	PBS	PBS	PBS	PBS	PBS	PBS	PBS	PBS	PBS
PBS	**AME FBS 4 h**	**AME FBS 4 h**	**AME FBS 4 h**	**AME FBS 8 h**	**AME FBS 8 h**	**AME FBS 8 h**	**EC AME FBS 10 h**	AME FBS 14 h	AME FBS 14 h	AME FBS 14 h	PBS
PBS	**AME no FBS 4 h**	**AME no FBS 4 h**	**AME no FBS 4 h**	**AME no FBS 8 h**	**AME no FBS 8 h**	**AME no FBS 8 h**	**EC AME FBS 10 h**	AME no FBS 14 h	AME no FBS 14 h	AME no FBS 14 h	PBS
PBS	**AME FBS 6 h**	**AME FBS 6 h**	**AME FBS 6 h**	**AME FBS 10 h**	**AME FBS 10 h**	**AME FBS 10 h**	**EC AME FBS 10 h**	AME FBS 16 h	AME FBS 16 h	AME FBS 16 h	PBS
PBS	**AME no FBS 6 h**	**AME no FBS 6 h**	**AME no FBS 6 h**	**AME no FBS 10 h**	**AME no FBS 10 h**	**AME no FBS 10 h**	**EC AME no FBS 10 h**	AME no FBS 16 h	AME no FBS 16 h	AME no FBS 16 h	PBS
PBS	BPP AME FBS 18 h	BPP AME no FBS 18 h	APP AME FBS 18 h	APP AME no FBS 18 h	SC FBS 18 h	SC no FBS 18 h	**EC AME no FBS 10 h**	AME FBS 18 h	AME FBS 18 h	AME FBS 18 h	PBS
PBS	BPP AME FBS 18 h	BPP AME no FBS 18 h	APP AME FBS 18 h	APP AME no FBS 18 h	SC FBS 18 h	SC no FBS 18 h	**EC AME no FBS 10 h**	AME no FBS 18 h	AME no FBS 18 h	AME no FBS 18 h	PBS
PBS	BPP AME FBS 18 h	BPP AME no FBS 18 h	APP AME FBS 18 h	APP AME no FBS 18 h	SC FBS 18 h	SC no FBS 18 h	PBS	PBS	PBS	PBS	PBS

Figure A3: Incubation plan of 96-well plate for the incubation of HepG2 cells with AME – first biological replicate

PBS	PBS	PBS	PBS	PBS	PBS	PBS	PBS	PBS	PBS	PBS	PBS
PBS	AOH FBS 14 h	AOH FBS 14 h	AOH FBS 14 h	AOH FBS 16 h	AOH FBS 16 h	AOH FBS 16 h	BPP AOH FBS 18 h	**AOH FBS 6 h**	**AOH FBS 6 h**	**AOH FBS 6 h**	PBS
PBS	AOH no FBS 14 h	AOH no FBS 14 h	AOH no FBS 14 h	AOH no FBS 16 h	AOH no FBS 16 h	AOH no FBS 16 h	BPP AOH FBS 18 h	**AOH no FBS 6 h**	**AOH no FBS 6 h**	**AOH no FBS 6 h**	PBS
PBS	AOH FBS 18 h	AOH FBS 18 h	AOH FBS 18 h	**AOH FBS 4 h**	**AOH FBS 4 h**	**AOH FBS 4 h**	BPP AOH FBS 18 h	**AOH FBS 8 h**	**AOH FBS 8 h**	**AOH FBS 8 h**	PBS
PBS	AOH no FBS 18 h	AOH no FBS 18 h	AOH no FBS 18 h	**AOH no FBS 4 h**	**AOH no FBS 4 h**	**AOH no FBS 4 h**	BPP AOH no FBS 18 h	**AOH no FBS 8 h**	**AOH no FBS 8 h**	**AOH no FBS 8 h**	PBS
PBS	APP AOH FBS 18 h	APP AOH no FBS 18 h	SC FBS 18 h	SC no FBS 18 h	**EC AOH FBS 8 h**	**EC AOH no FBS 8 h**	BPP AOH no FBS 18 h	**AOH FBS 10 h**	**AOH FBS 10 h**	**AOH FBS 10 h**	PBS
PBS	APP AOH FBS 18 h	APP AOH no FBS 18 h	SC FBS 18 h	SC no FBS 18 h	**EC AOH FBS 8 h**	**EC AOH no FBS 8 h**	BPP AOH no FBS 18 h	**AOH no FBS 10 h**	**AOH no FBS 10 h**	**AOH no FBS 10 h**	PBS
PBS	APP AOH FBS 18 h	APP AOH no FBS 18 h	SC FBS 18 h	SC no FBS 18 h	**EC AOH FBS 8 h**	**EC AOH no FBS 8 h**	PBS	PBS	PBS	PBS	PBS

Figure A4: Incubation plan of 96-well plate for the incubation of HepG2 cells with AOH – second biological replicate

PBS	PBS	PBS	PBS	PBS	PBS	PBS	PBS	PBS	PBS	PBS	PBS
PBS	AME FBS 14 h	AME FBS 14 h	AME FBS 14 h	AME FBS 16 h	AME FBS 16 h	AME FBS 16 h	BPP AME FBS 18 h	**AME FBS 6 h**	**AME FBS 6 h**	**AME FBS 6 h**	PBS
PBS	AME no FBS 14 h	AME no FBS 14 h	AME no FBS 14 h	AME no FBS 16 h	AME no FBS 16 h	AME no FBS 16 h	BPP AME FBS 18 h	**AME no FBS 6 h**	**AME no FBS 6 h**	**AME no FBS 6 h**	PBS
PBS	AME FBS 18 h	AME FBS 18 h	AME FBS 18 h	**AME FBS 4 h**	**AME FBS 4 h**	**AME FBS 4 h**	BPP AME FBS 18 h	**AME FBS 8 h**	**AME FBS 8 h**	**AME FBS 8 h**	PBS
PBS	AME no FBS 18 h	AME no FBS 18 h	AME no FBS 18 h	**AME no FBS 4 h**	**AME no FBS 4 h**	**AME no FBS 4 h**	BPP AME no FBS 18 h	**AME no FBS 8 h**	**AME no FBS 8 h**	**AME no FBS 8 h**	PBS
PBS	APP AME FBS 18 h	APP AME no FBS 18 h	SC FBS 18 h	SC no FBS 18 h	**EC AME FBS 8 h**	**EC AME no FBS 8 h**	BPP AME no FBS 18 h	**AME FBS 10 h**	**AME FBS 10 h**	**AME FBS 10 h**	PBS
PBS	APP AME FBS 18 h	APP AME no FBS 18 h	SC FBS 18 h	SC no FBS 18 h	**EC AME FBS 8 h**	**EC AME no FBS 8 h**	BPP AME no FBS 18 h	**AME no FBS 10 h**	**AME no FBS 10 h**	**AME no FBS 10 h**	PBS
PBS	APP AME FBS 18 h	APP AME no FBS 18 h	SC FBS 18 h	SC no FBS 18 h	**EC AME FBS 8 h**	**EC AME no FBS 8 h**	PBS	PBS	PBS	PBS	PBS

Figure A5: Incubation plan of 96-well plate for the incubation of HepG2 cells with AME – second biological replicate

PBS	PBS	PBS	PBS	PBS	PBS	PBS	PBS	PBS	PBS	PBS	PBS
PBS	**AOH FBS 10 h**	**AOH FBS 10 h**	**AOH FBS 10 h**	BPP AOH FBS 18 h	SC FBS 18 h	APP AOH FBS 18 h	AOH FBS 18 h	**AOH FBS 4 h**	**AOH FBS 4 h**	**AOH FBS 4 h**	PBS
PBS	**AOH no FBS 10 h**	**AOH no FBS 10 h**	**AOH no FBS 10 h**	BPP AOH FBS 18 h	SC FBS 18 h	APP AOH FBS 18 h	AOH FBS 18 h	**AOH no FBS 4 h**	**AOH no FBS 4 h**	**AOH no FBS 4 h**	PBS
PBS	AOH FBS 14 h	AOH FBS 14 h	AOH FBS 14 h	BPP AOH FBS 18 h	SC FBS 18 h	APP AOH FBS 18 h	AOH FBS 18 h	**AOH FBS 6 h**	**AOH FBS 6 h**	**AOH FBS 6 h**	PBS
PBS	AOH no FBS 14 h	AOH no FBS 14 h	AOH no FBS 14 h	BPP AOH no FBS 18 h	SC no FBS 18 h	APP AOH no FBS 18 h	AOH no FBS 18 h	**AOH no FBS 6 h**	**AOH no FBS 6 h**	**AOH no FBS 6 h**	PBS
PBS	AOH FBS 16 h	AOH FBS 16 h	AOH FBS 16 h	BPP AOH no FBS 18 h	SC no FBS 18 h	APP AOH no FBS 18 h	AOH no FBS 18 h	**AOH FBS 8 h**	**AOH FBS 8 h**	**AOH FBS 8 h**	PBS
PBS	AOH no FBS 16 h	AOH no FBS 16 h	AOH no FBS 16 h	BPP AOH no FBS 18 h	SC no FBS 18 h	APP AOH no FBS 18 h	AOH no FBS 18 h	**AOH no FBS 8 h**	**AOH no FBS 8 h**	**AOH no FBS 8 h**	PBS
PBS	**EC AOH FBS 8 h**	**EC AOH FBS 8 h**	**EC AOH FBS 8 h**	**EC AOH no FBS 8 h**	**EC AOH no FBS 8 h**	**EC AOH no FBS 8 h**	PBS	PBS	PBS	PBS	PBS

Figure A6: Incubation plan of 96-well plate for the incubation of HepG2 cells with AOH – third biological replicate

PBS	PBS	PBS	PBS	PBS	PBS	PBS	PBS	PBS	PBS	PBS	PBS
PBS	**AME FBS 10 h**	**AME FBS 10 h**	**AME FBS 10 h**	BPP AME FBS 18 h	SC FBS 18 h	APP AME FBS 18 h	AME FBS 18 h	**AME FBS 4 h**	**AME FBS 4 h**	**AME FBS 4 h**	PBS
PBS	**AME no FBS 10 h**	**AME no FBS 10 h**	**AME no FBS 10 h**	BPP AME FBS 18 h	SC FBS 18 h	APP AME FBS 18 h	AME FBS 18 h	**AME no FBS 4 h**	**AME no FBS 4 h**	**AME no FBS 4 h**	PBS
PBS	AME FBS 14 h	AME FBS 14 h	AME FBS 14 h	BPP AME FBS 18 h	SC FBS 18 h	APP AME FBS 18 h	AME FBS 18 h	**AME FBS 6 h**	**AME FBS 6 h**	**AME FBS 6 h**	PBS
PBS	AME no FBS 14 h	AME no FBS 14 h	AME no FBS 14 h	BPP AME no FBS 18 h	SC no FBS 18 h	APP AME no FBS 18 h	AME no FBS 18 h	**AME no FBS 6 h**	**AME no FBS 6 h**	**AME no FBS 6 h**	PBS
PBS	AME FBS 16 h	AME FBS 16 h	AME FBS 16 h	BPP AME no FBS 18 h	SC no FBS 18 h	APP AME no FBS 18 h	AME no FBS 18 h	**AME FBS 8 h**	**AME FBS 8 h**	**AME FBS 8 h**	PBS
PBS	AME no FBS 16 h	AME no FBS 16 h	AME no FBS 16 h	BPP AME no FBS 18 h	SC no FBS 18 h	APP AME no FBS 18 h	AME no FBS 18 h	**AME no FBS 8 h**	**AME no FBS 8 h**	**AME no FBS 8 h**	PBS
PBS	**EC AME FBS 8 h**	**EC AME FBS 8 h**	**EC AME FBS 8 h**	**EC AME no FBS 8 h**	**EC AME no FBS 8 h**	**EC AME no FBS 8 h**	PBS	PBS	PBS	PBS	PBS

Figure A7: Incubation plan of 96-well plate for the incubation of HepG2 cells with AME – third biological replicate

II. *In vitro* metabolism rates of AOH and AME following 10 minutes incubation with liver microsomes from different species

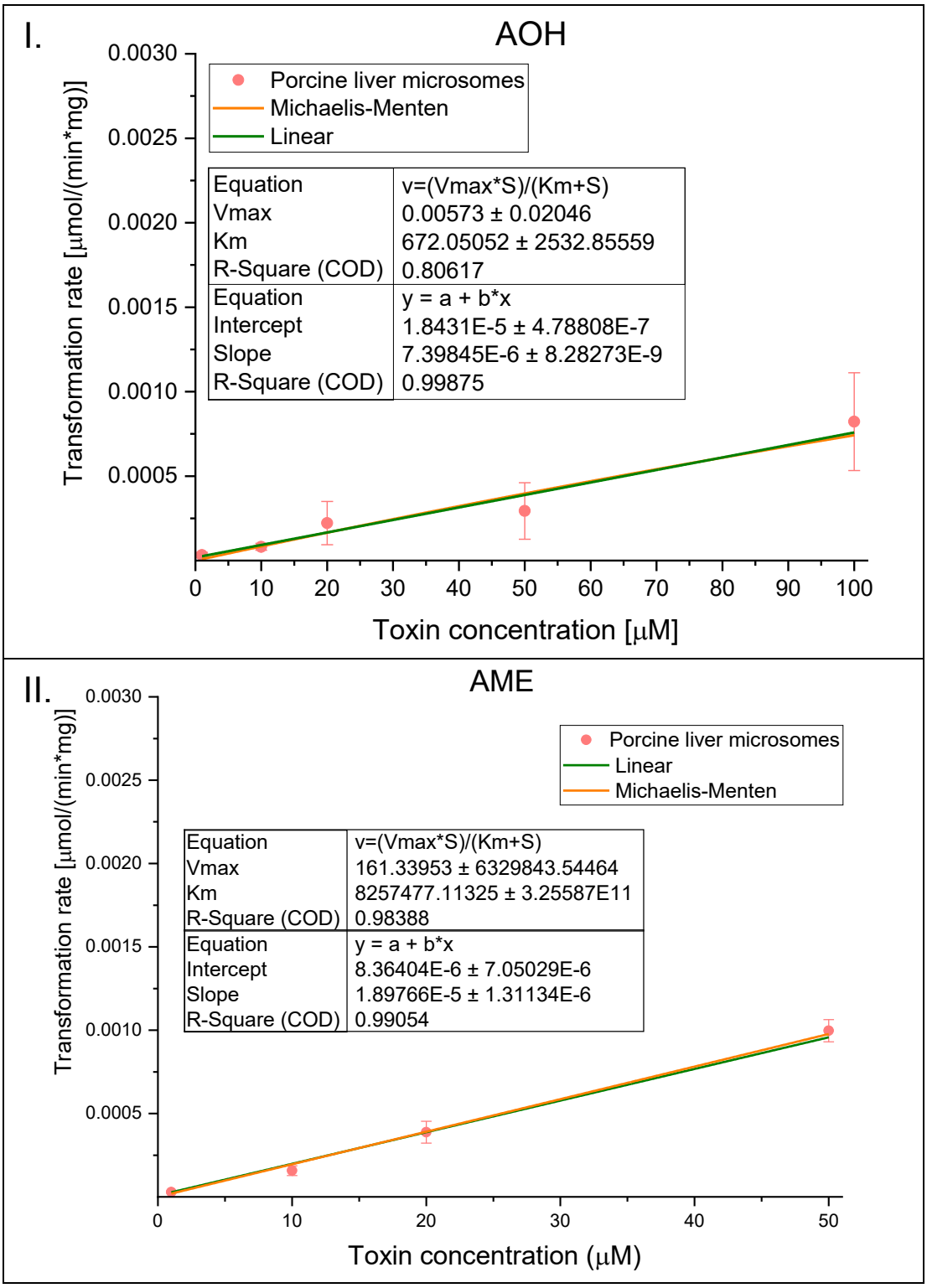

Figure A8: Transformation rate in the second batch of porcine liver microsomes after the incubation with AOH and AME for 10 minutes. The data illustrates the transformation rate values of AOH (Graph I.) or AME (Graph II.) after 10 minutes of incubation, as a function of the nominal initial toxin concentration. The values are normalised to the protein content of the metabolising microsomes, based on the results of the BCA assay. Each data point represents the average of 3-6 technical replicates ± standard deviation. The results of one biological replicate are shown. All of the depicted data points were used for curve and linear fitting.

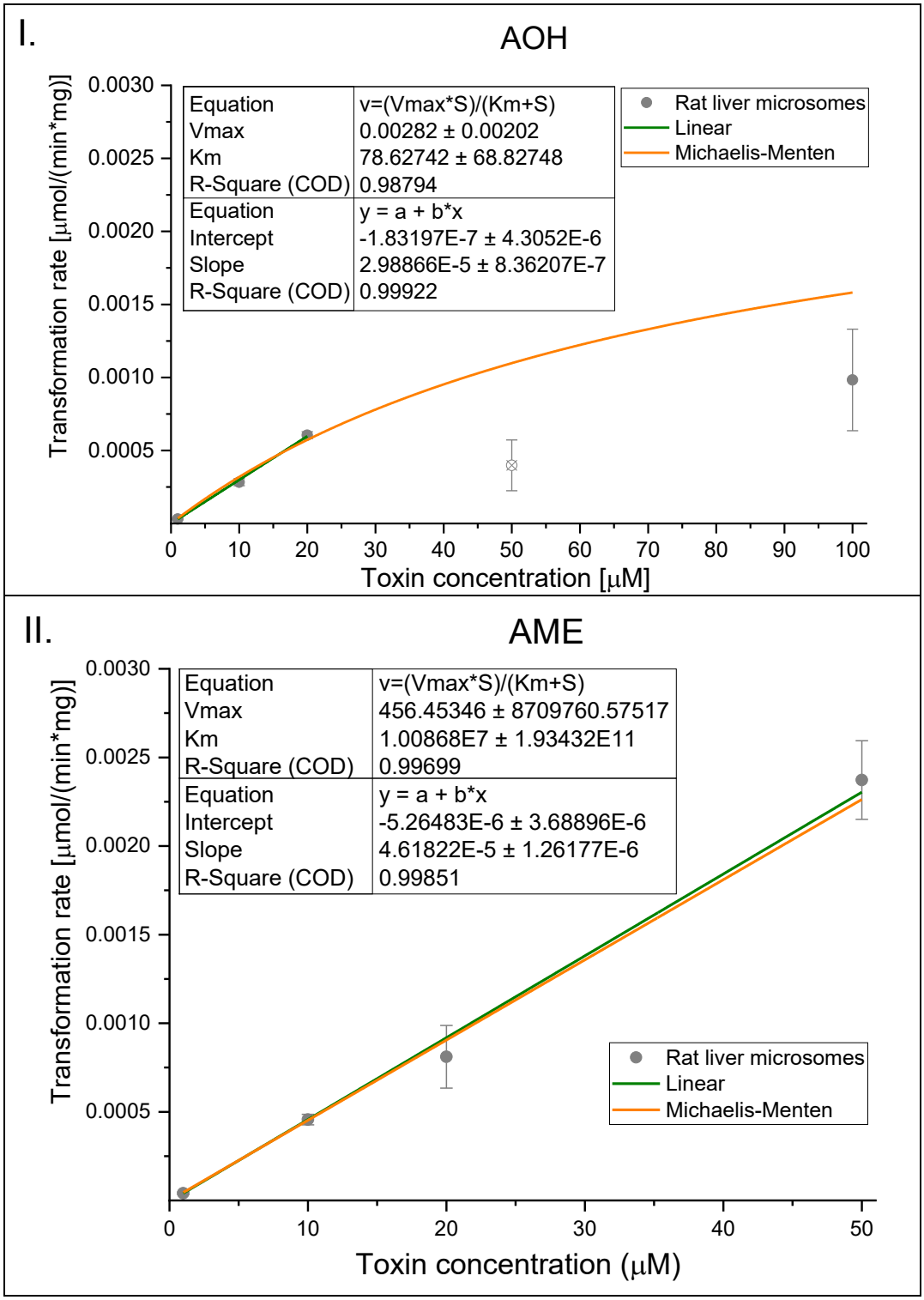

Figure A9: Transformation rate in pooled rat liver microsomes after the incubation with AOH and AME for 10 minutes. The data illustrates the transformation rate values of AOH (Graph I.) or AME (Graph II.) after 10 minutes of incubation, as a function of the nominal initial toxin concentration. The values are normalised to the protein content of the metabolising microsomes, based on information provided by the manufacturer. Each data point represents the average of 4-7 technical replicates ± standard deviation. In the case of AOH, the first three data points were used for linear regression and four of five data points were used for fitting the Michaelis-Menten curve, by excluding the data points by the concentration of 50 µM AOH. In the case of AME, all of the depicted data points were used for both of the curve fittings (Graph II.)

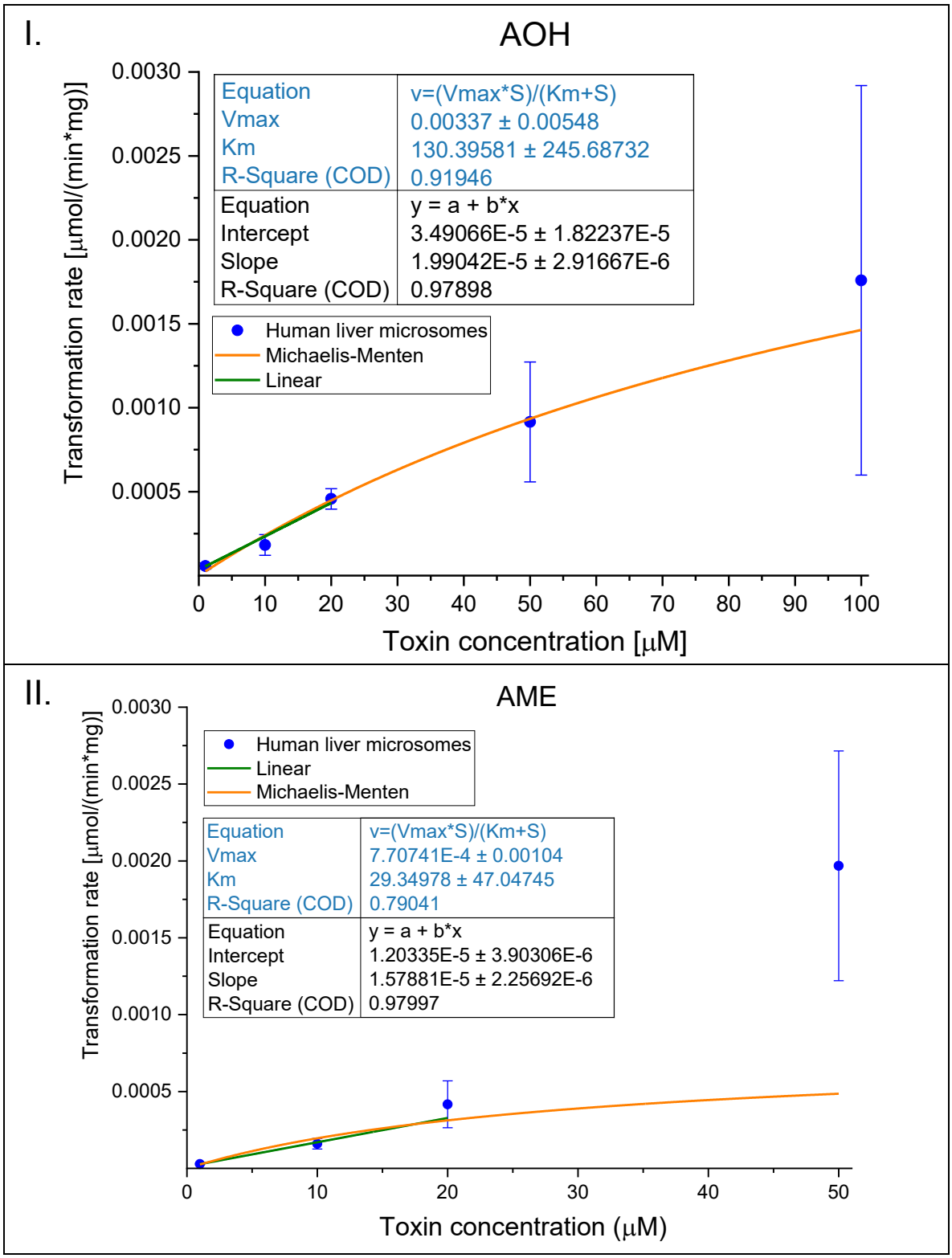

Figure A10: Transformation rate in pooled human liver microsomes after the incubation with AOH and AME for 10 minutes. The data illustrates the transformation rate values of AOH (Graph I.) or AME (Graph II.) after 10 minutes of incubation, as a function of the nominal initial toxin concentration. The values are normalised to the protein content of the metabolising microsomes, based on information provided by the manufacturer. Each data point represents the average of 4-5 technical replicates ± standard deviation. For both AOH and AME, the first three data points were used for linear regression and all data points were used for fitting the Michaelis-Menten curve.

III. HR-MS measurements

Table A1: Transition list containing the investigated analytes in the data evaluation of the HR-MS measurements

Detected pseudo-molecular ion	Compound name	Compound mass	Charge
$[M-H]^-$	Alternariol	257.046	-1
$[M-H]^-$	Hydroxy-alternariol	273.040	-1
$[M-H]^-$	Dihydroxy-alternariol	289.035	-1
$[M-H]^-$	Alternariol-sulphate	337.002	-1
$[M-H]^-$	Alternariol-disulphate	416.959	-1
$[M-H]^-$	Alternariol-glucuronide	433.078	-1
$[M-H]^-$	Alternariol-bis-glucuronide	609.110	-1
$[M-H]^-$	Alternariol-sulphate-glucuronide	513.035	-1
$[M-H]^-$	Methyl-alternariol	271.061	-1
$[M-H]^-$	Acetyl-alternariol	299.056	-1
$[M-H]^-$	Glutathione adduct of AOH	546.118	-1
$[M-H]^-$	Cysteinylglycine adduct of AOH	415.060	-1
$[M-H]^-$	Cysteine adduct of AOH	374.070	-1
$[M-H]^-$	Mercapturic acid adduct of AOH	401.057	-1
$[M+HCOO]^-$	Alternariol	303.051	-1
$[M+HCOO]^-$	Hydroxy-alternariol	319.046	-1
$[M+HCOO]^-$	Dihydroxy-alternariol	335.041	-1
$[M+HCOO]^-$	Alternariol-sulphate	383.008	-1
$[M+HCOO]^-$	Alternariol-disulphate	462.965	-1
$[M+HCOO]^-$	Alternariol-glucuronide	479.083	-1
$[M+HCOO]^-$	Alternariol-bis-glucuronide	655.116	-1
$[M+HCOO]^-$	Alternariol-sulphate-glucuronide	559.040	-1
$[M+HCOO]^-$	Methyl-alternariol	317.066	-1
$[M+HCOO]^-$	Acetyl-alternariol	345.061	-1
$[M+HCOO]^-$	Glutathione adduct of AOH	592.124	-1
$[M+HCOO]^-$	Cysteinylglycine adduct of AOH	461.066	-1
$[M+HCOO]^-$	Cysteine adduct of AOH	420.075	-1
$[M+HCOO]^-$	Mercapturic acid adduct of AOH	447.062	-1
$[M+H]^+$	Alternariol	259.060	1
$[M+H]^+$	Hydroxy-alternariol	275.055	1
$[M+H]^+$	Dihydroxy-alternariol	291.050	1
$[M+H]^+$	Alternariol-sulphate	339.017	1
$[M+H]^+$	Alternariol-disulphate	418.974	1
$[M+H]^+$	Alternariol-glucuronide	435.092	1
$[M+H]^+$	Alternariol-bis-glucuronide	611.125	1
$[M+H]^+$	Alternariol-sulphate-glucuronide	515.049	1
$[M+H]^+$	Methyl-alternariol	273.075	1
$[M+H]^+$	Acetyl-alternariol	301.070	1
$[M+H]^+$	Glutathione adduct of AOH	548.133	1

$[M+H]^+$	Cysteinylglycine adduct of AOH	417.075	1
$[M+H]^+$	Cysteine adduct of AOH	376.084	1
$[M+H]^+$	Mercapturic acid adduct of AOH	403.071	1
$[M+NH_4]^+$	Alternariol	276.087	1
$[M+NH_4]^+$	Hydroxy-alternariol	292.082	1
$[M+NH_4]^+$	Dihydroxy-alternariol	308.076	1
$[M+NH_4]^+$	Alternariol-sulphate	356.043	1
$[M+NH_4]^+$	Alternariol-disulphate	436.001	1
$[M+NH_4]^+$	Alternariol-glucuronide	452.119	1
$[M+NH_4]^+$	Alternariol-bis-glucuronide	628.151	1
$[M+NH_4]^+$	Alternariol-sulphate-glucuronide	532.076	1
$[M+NH_4]^+$	Methyl-alternariol	290.102	1
$[M+NH_4]^+$	Acetyl-alternariol	318.097	1
$[M+NH_4]^+$	Glutathione adduct of AOH	565.159	1
$[M+NH_4]^+$	Cysteinylglycine adduct of AOH	434.101	1
$[M+NH_4]^+$	Cysteine adduct of AOH	393.111	1
$[M+NH_4]^+$	Mercapturic acid adduct of AOH	420.098	1
$[M+Na]^+$	Alternariol	281.042	1
$[M+Na]^+$	Hydroxy-alternariol	297.037	1
$[M+Na]^+$	Dihydroxy-alternariol	313.032	1
$[M+Na]^+$	Alternariol-sulphate	360.999	1
$[M+Na]^+$	Alternariol-disulphate	440.956	1
$[M+Na]^+$	Alternariol-glucuronide	457.074	1
$[M+Na]^+$	Alternariol-bis-glucuronide	633.107	1
$[M+Na]^+$	Alternariol-sulphate-glucuronide	537.031	1
$[M+Na]^+$	Methyl-alternariol	295.057	1
$[M+Na]^+$	Acetyl-alternariol	323.052	1
$[M+Na]^+$	Glutathione adduct of AOH	570.115	1
$[M+Na]^+$	Cysteinylglycine adduct of AOH	439.057	1
$[M+Na]^+$	Cysteine adduct of AOH	398.066	1
$[M+Na]^+$	Mercapturic acid adduct of AOH	425.053	1
$[M+K]^+$	Alternariol	297.016	1
$[M+K]^+$	Hydroxy-alternariol	313.011	1
$[M+K]^+$	Dihydroxy-alternariol	329.006	1
$[M+K]^+$	Alternariol-sulphate	376.973	1
$[M+K]^+$	Alternariol-disulphate	456.930	1
$[M+K]^+$	Alternariol-glucuronide	473.048	1
$[M+K]^+$	Alternariol-bis-glucuronide	649.080	1
$[M+K]^+$	Alternariol-sulphate-glucuronide	553.005	1
$[M+K]^+$	Methyl-alternariol	311.031	1
$[M+K]^+$	Acetyl-alternariol	339.026	1
$[M+K]^+$	Glutathione adduct of AOH	586.088	1
$[M+K]^+$	Cysteinylglycine adduct of AOH	455.030	1
$[M+K]^+$	Cysteine adduct of AOH	414.040	1

$[M+K]^+$	Mercapturic acid adduct of AOH	441.0270	1
$[M+H]^+$	"AOH-S-Cys" (Juan-García *et al*., 2016)	415.000	1
$[M+H]^+$	"AOH+Asp" (Juan-García *et al*., 2016)	391.100	1
$[M+H]^+$	"AOH+Pro+2H" (Juan-García *et al*., 2016)	370.900	1
$[M+H]^+$	"AOH+Gly+2H" (Juan-García *et al*., 2016)	335.000	1
$[M-H]^-$	Alternariol monomethyl ether	271.061	-1
$[M-H]^-$	Hydroxy-alternariol monomethyl ether	287.056	-1
$[M-H]^-$	Dihydroxy-alternariol monomethyl ether	303.051	-1
$[M-H]^-$	Alternariol monomethyl ether-sulphate	351.018	-1
$[M-H]^-$	Alternariol monomethyl ether-disulphate	430.975	-1
$[M-H]^-$	Alternariol monomethyl ether-glucuronide	447.093	-1
$[M-H]^-$	Alternariol monomethyl ether-bis-glucuronide	623.126	-1
$[M-H]^-$	Alternariol monomethyl ether-sulphate-glucuronide	527.050	-1
$[M-H]^-$	Methyl-alternariol monomethyl ether	285.076	-1
$[M-H]^-$	Acetyl-alternariol monomethyl ether	313.071	-1
$[M-H]^-$	Glutathione adduct of AME	560.134	-1
$[M-H]^-$	Cysteinylglycine adduct of AME	429.076	-1
$[M-H]^-$	Cysteine adduct of AME	388.085	-1
$[M-H]^-$	Mercapturic acid adduct of AME	415.073	-1
$[M+HCOO]^-$	Alternariol monomethyl ether	317.066	-1
$[M+HCOO]^-$	Hydroxy-alternariol monomethyl ether	333.061	-1
$[M+HCOO]^-$	Dihydroxy-alternariol monomethyl ether	349.056	-1
$[M+HCOO]^-$	Alternariol monomethyl ether-sulphate	397.023	-1
$[M+HCOO]^-$	Alternariol monomethyl ether-disulphate	476.981	-1
$[M+HCOO]^-$	Alternariol monomethyl ether-glucuronide	493.099	-1
$[M+HCOO]^-$	Alternariol monomethyl ether-bis-glucuronide	669.131	-1
$[M+HCOO]^-$	Alternariol monomethyl ether-sulphate-glucuronide	573.056	-1
$[M+HCOO]^-$	Methyl-alternariol monomethyl ether	331.082	-1
$[M+HCOO]^-$	Acetyl-alternariol monomethyl ether	359.077	-1
$[M+HCOO]^-$	Glutathione adduct of AME	606.139	-1
$[M+HCOO]^-$	Cysteinylglycine adduct of AME	475.081	-1
$[M+HCOO]^-$	Cysteine adduct of AME	434.091	-1
$[M+HCOO]^-$	Mercapturic acid adduct of AME	461.078	-1
$[M+H]^+$	Alternariol monomethyl ether	273.075	1
$[M+H]^+$	Hydroxy-alternariol monomethyl ether	289.070	1
$[M+H]^+$	Dihydroxy-alternariol monomethyl ether	305.065	1
$[M+H]^+$	Alternariol monomethyl ether-sulphate	353.033	1
$[M+H]^+$	Alternariol monomethyl ether-disulphate	432.990	1
$[M+H]^+$	Alternariol monomethyl ether-glucuronide	449.108	1
$[M+H]^+$	Alternariol monomethyl ether-bis-glucuronide	625.140	1
$[M+H]^+$	Alternariol monomethyl ether-sulphate-glucuronide	529.065	1
$[M+H]^+$	Methyl-alternariol monomethyl ether	287.091	1
$[M+H]^+$	Acetyl-alternariol monomethyl ether	315.086	1

$[M+H]^+$	Glutathione adduct of AME	562.148	1
$[M+H]^+$	Cysteinylglycine adduct of AME	431.090	1
$[M+H]^+$	Cysteine adduct of AME	390.100	1
$[M+H]^+$	Mercapturic acid adduct of AME	417.087	1
$[M+NH_4]^+$	Alternariol monomethyl ether	290.102	1
$[M+NH_4]^+$	Hydroxy-alternariol monomethyl ether	306.097	1
$[M+NH_4]^+$	Dihydroxy-alternariol monomethyl ether	322.092	1
$[M+NH_4]^+$	Alternariol monomethyl ether-sulphate	370.059	1
$[M+NH_4]^+$	Alternariol monomethyl ether-disulphate	450.016	1
$[M+NH_4]^+$	Alternariol monomethyl ether-glucuronide	466.134	1
$[M+NH_4]^+$	Alternariol monomethyl ether-bis-glucuronide	642.167	1
$[M+NH_4]^+$	Alternariol monomethyl ether-sulphate-glucuronide	546.092	1
$[M+NH_4]^+$	Methyl-alternariol monomethyl ether	304.118	1
$[M+NH_4]^+$	Acetyl-alternariol monomethyl ether	332.112	1
$[M+NH_4]^+$	Glutathione adduct of AME	579.175	1
$[M+NH_4]^+$	Cysteinylglycine adduct of AME	448.117	1
$[M+NH_4]^+$	Cysteine adduct of AME	407.127	1
$[M+NH_4]^+$	Mercapturic acid adduct of AME	434.114	1
$[M+Na]^+$	Alternariol monomethyl ether	295.057	1
$[M+Na]^+$	Hydroxy-alternariol monomethyl ether	311.052	1
$[M+Na]^+$	Dihydroxy-alternariol monomethyl ether	327.047	1
$[M+Na]^+$	Alternariol monomethyl ether-sulphate	375.015	1
$[M+Na]^+$	Alternariol monomethyl ether-disulphate	454.972	1
$[M+Na]^+$	Alternariol monomethyl ether-glucuronide	471.090	1
$[M+Na]^+$	Alternariol monomethyl ether-bis-glucuronide	647.122	1
$[M+Na]^+$	Alternariol monomethyl ether-sulphate-glucuronide	551.047	1
$[M+Na]^+$	Methyl-alternariol monomethyl ether	309.073	1
$[M+Na]^+$	Acetyl-alternariol monomethyl ether	337.068	1
$[M+Na]^+$	Glutathione adduct of AME	584.130	1
$[M+Na]^+$	Cysteinylglycine adduct of AME	453.072	1
$[M+Na]^+$	Cysteine adduct of AME	412.082	1
$[M+Na]^+$	Mercapturic acid adduct of AME	439.069	1
$[M+K]^+$	Alternariol monomethyl ether	311.031	1
$[M+K]^+$	Hydroxy-alternariol monomethyl ether	327.026	1
$[M+K]^+$	Dihydroxy-alternariol monomethyl ether	343.021	1
$[M+K]^+$	Alternariol monomethyl ether-sulphate	390.988	1
$[M+K]^+$	Alternariol monomethyl ether-disulphate	470.946	1
$[M+K]^+$	Alternariol monomethyl ether-glucuronide	487.064	1
$[M+K]^+$	Alternariol monomethyl ether-bis-glucuronide	663.096	1
$[M+K]^+$	Alternariol monomethyl ether-sulphate-glucuronide	567.021	1
$[M+K]^+$	Methyl-alternariol monomethyl ether	325.047	1
$[M+K]^+$	Acetyl-alternariol monomethyl ether	353.042	1

$[M+K]^+$	Glutathione adduct of AME	600.104	1
$[M+K]^+$	Cysteinylglycine adduct of AME	469.046	1
$[M+K]^+$	Cysteine adduct of AME	428.056	1
$[M+K]^+$	Mercapturic acid adduct of AME	455.043	1
$[M]^+$	Alternariol	258.052	1
$[M]^+$	Hydroxy-alternariol	274.047	1
$[M]^+$	Dihydroxy-alternariol	290.042	1
$[M]^+$	Alternariol-sulphate	338.009	1
$[M]^+$	Alternariol-disulphate	417.966	1
$[M]^+$	Alternariol-glucuronide	434.084	1
$[M]^+$	Alternariol-bis-glucuronide	610.117	1
$[M]^+$	Alternariol-sulphate-glucuronide	514.042	1
$[M]^+$	Methyl-alternariol	272.068	1
$[M]^+$	Acetyl-alternariol	300.062	1
$[M]^+$	Glutathione adduct of AOH	547.125	1
$[M]^+$	Cysteinylglycine adduct of AOH	416.067	1
$[M]^+$	Cysteine adduct of AOH	375.077	1
$[M]^+$	Mercapturic acid adduct of AOH	402.064	1
$[M]^+$	Alternariol monomethyl ether	272.068	1
$[M]^+$	Hydroxy-alternariol monomethyl ether	288.062	1
$[M]^+$	Dihydroxy-alternariol monomethyl ether	304.057	1
$[M]^+$	Alternariol monomethyl ether-sulphate	352.025	1
$[M]^+$	Alternariol monomethyl ether-disulphate	431.982	1
$[M]^+$	Alternariol monomethyl ether-glucuronide	448.100	1
$[M]^+$	Alternariol monomethyl ether-bis-glucuronide	624.132	1
$[M]^+$	Alternariol monomethyl ether-sulphate-glucuronide	528.057	1
$[M]^+$	Methyl-alternariol monomethyl ether	286.083	1
$[M]^+$	Acetyl-alternariol monomethyl ether	314.078	1
$[M]^+$	Glutathione adduct of AME	561.140	1
$[M]^+$	Cysteinylglycine adduct of AME	430.082	1
$[M]^+$	Cysteine adduct of AME	389.092	1
$[M]^+$	Mercapturic acid adduct of AME	416.079	1